5-2016

Design, Modeling and Control of a Thermal Management System for Hybrid Electric Vehicles

Xinran (William) Tao
Clemson University, xinrant@g.clemson.edu

Design, Modeling and Control of a Thermal Management System for Hybrid Electric Vehicles

---

A Dissertation
Presented to
the Graduate School of
Clemson University

In Partial Fulfillment
of the Requirements for the Degree
Doctor of Philosophy
Mechanical Engineering

---

by
Xinran (William) Tao
May 2016

Accepted by:
Dr. John R. Wagner, Committee Chair
Dr. Richard S. Miller
Dr. Todd Schweisinger
Dr. Ardalan Vahidi

Abstract

Hybrid electric vehicle (HEV) technology has evolved in the last two decades to become economically feasible for mass produced automobiles. With the integration of a lithium battery pack and electric motors, HEVs offer a significantly higher fuel efficiency than traditional vehicles that are driven solely by an internal combustion engine. However, the additional HEV components also introduce new challenges for the powertrain thermal management system design. In addition to the common internal combustion engine, the battery pack, the generator(s), as well as the electric motor(s) are now widely applied in the HEVs and have become new heat sources, and they also require proper thermal management.

Conventional cooling systems have been typically equipped with a belt driven water pump and radiator fan, as well as other mechanical actuators such as a thermostat valve. The operation of these components is generally determined by the engine speed. This open-loop cooling strategy has a low efficiency and suffers the risk of over-cooling the coolant and components within the system. In advanced thermal management systems, the mechanical elements are upgraded by computer controlled actuators including a servo-motor driven pump, variable speed fans, a smart thermostat, and an electric motor driven compressor. These electrified actuators offer the opportunity to improve temperature tracking and reduce parasitic losses.

This dissertation investigates a HEV powertrain thermal management system

featuring computer controlled cooling system actuators. A suite of mathematical models have been created to describe the thermal behavior of the HEV powertrain components. Model based controllers were developed for the vehicle's cooling systems including the battery pack, electric motors, and internal combustion engine. Optimal control theory has been applied to determine the ideal battery cooling air temperature and the desired heat removal rate on the e-motor cooling surface. A model predictive controller(MPC) was developed to regulate the refrigerant compressor and track the battery cooling air temperature. A series of Lyapunov-based nonlinear controllers have been implemented to regulate the coolant pumps and radiator fans in the cooling systems for the engine and e-motors.

Representative numerical results are presented and discussed. Overall, the proposed control strategies have demonstrated the effectiveness in improving both the temperature tracking performance and the cooling system power consumption reduction. The peak temperature error in the selected A123 battery core can be tracked within 0.25 $^{\circ}C$ of the target; a 50% reduction of the vapor compression system energy consumption can be obtained by properly designing the cooling air flow structure. Similarly, the cooling system of HEV electric motors shows that the machine internal peak temperature can be tracked to the target value with a maximum error of 3.9 $^{\circ}C$ and an average error of 0.13 $^{\circ}C$. A 70% to 81% cooling system energy consumption reduction can be achieved comparing to classical controller, maintaining a similar level of hotspot temperature stabilization under different driving cycles. The proposed optimal nonlinear controller tracks the engine coolant temperature with an average error of 0.35 $^{\circ}C$ and at least 13% reduction in engine cooling power. Further, a close analysis on the cooling system energy consumption reduction has been conducted with a heat exchanger simulation tool established for cooling system design optimization.

This research has developed the basis for the holistic control of HEV powertrain thermal management systems by including a suite of model based nonlinear controllers to simultaneously regulate the cooling actuators for the battery pack, e-motors, and conventional internal combustion engine. Numerical studies have been conducted with a high fidelity HEV model under real life driving cycles to demonstrate the advantages of introducing advanced control theory into multi-mode vehicle drive systems.

Dedication

This dissertation is dedicated to my parents.

Acknowledgements

My graduate study in Clemson has been an amazing experience, during which I have received lots of help from many remarkable people. No words could sufficiently express my appreciation while I want to say thank you to every one of them.

First and foremost, I am lucky to have Dr. John R. Wagner as my advisor. Dr. Wagner has generously offered me his encouragement, research insights, a tremendous amount of patience, as well as innumerable hours of hard working, to guide me though every difficulty in my academic life. For the past five years, he has been treating me not only as a student but rather more like a family member. It is impossible for me to finish my graduate study without Dr. Wagner's continuous support, invaluable inspiration, and most importantly, consistent confidence in me, for which I shall give my deepest gratitude to him.

I wish to extend my sincere gratitude to my committee members, who are more than generous with their expertise and precious time. Thanks to Dr. Ardalan Vahidi, who has also been the professor lecturing all my graduate level control theory related courses and preparing me with a solid background of controller design for my research. Thanks to Dr. Todd Schweisinger, and Dr. Richard S. Miller for agreeing to serve on my committee and providing the valuable feedbacks and suggestions to finish this dissertation.

I've enjoyed and learned a lot from the 3-year-long collaborative research with

Professor Zoran Filipi, Professor Heath Hofmann, Dr. Kan Zhou, Dr. Andrej Ivanco, and Xueyu Zhang. I'm grateful to them for their brilliant contributions in our study on the overall HEV powertrain optimization. I also would like to thank all my student colleagues, Tianwei (Thomas) Wang, Julio C. R. Gonzalez, Gibran Ali, Dr. Tim Freeman, Dr. Joshua Finn, Dr. Ryan Schkoda, Mansel Oliver, Sheng (Mike) Fu, Yogendra Yadav, Junkui (Allen) Huang and Zaker Syed for making our lab such an enjoyable and stimulating environment to study in. My thankfulness goes to my good friends Ying Yu, Yu Zhao, Qifan He, Shuaishuai Liu, Wei Li, Zhiyuan Ma, and Jun Lan, for all the wonderful time we spent together.

Finally, I am forever indebted to my parents, for their support, understanding and unconditional love throughout my life.

Table of Contents

List of Tables

List of Figures

Nomenclature

$\mathbf{A}$	Thermal model matrix
A	Area $\left(m^2\right)$
Ah	Battery nominal capacity $(Amp \bullet hour)$
$\mathbf{B}$	Thermal model matrix
c_p	Specific heat $\left(\frac{J}{kg^\circ C}\right)$
C	Heat capacity $\left(\frac{J}{^\circ C}\right)$, Electric capacity (F)
$\mathbf{C}$	Thermal model matrix
dP	Pressure increase (Pa)
D	Diameter (m)
Dis	Pump displacement (mL)
$\mathbf{D}$	Specific heat matrix
$e, \hat{e}$	Control error $(^\circ C)$
E	Energy consumption (kJ), Nominal voltage $(Volt)$
F	Controller Feedback gain
h	Heat transfer coefficient
H	Cooling surface heat flux $\left(W/m^2\right)$ $\left(\frac{Watt}{^\circ C}\right)$
Hc	Feedforward gain matrix
i	Control volume index
I	Electric current (Amp)
J	Cost function
k	Thermal conductivity $\left(\frac{Watt}{m^\circ C}\right)$
K	Positive controller gain, Coolant valve position
$\mathbf{K}$	Thermal conductivity matrix
$\dot{m}$	Mass flow rate $\left(\frac{kg}{sec}\right)$
M	Mass (kg), Positive weighting matrices
n	Number of radiator control volumes
N	Rotational speed (RPM)
Nu	Nusselt number
Pr	Prandtl numbers
q	Heat flux $\left(\frac{Watt}{m^2}\right)$
$\overrightarrow{q}$	Heat flux vector
Q	Heat flow rate $(Watt)$, Matrix solved by the Riccati equation

r	Pump-fan speed ratio
R	Thermal resistance $\left(\frac{^\circ C}{Watt}\right)$, Electric resistance ($\Omega$), Positive weighting matrix
$\mathscr{R}$	Set of real numbers
Re	Reynolds number
s	Step-response mode matrix element
S, S_0	Step-response mode matrix
SL	Battery distance (mm)
SOC	Battery state of charge
ST	Battery distance (mm)
t	Time (sec)
T	Temperature ($^\circ C$), Temperature states
$\overrightarrow{t}$	E-motor temperature nodes
ΔT_m	Log mean temperature difference ($^\circ C$)
$\overrightarrow{t}$	Temperature state vector
u	Controller input
$\tilde{u}$	Optimal magnitude of the input
U	Input vector
V	Lyapunov cost function, Voltage ($Volt$), Flow velocity $\left(\frac{m}{sec}\right)$
$\mathbf{V}$	System eigenvector matrix
w	Mean temperature measurement error ($^\circ C$)
x, X	State space model state vector
α	Battery model constant
y	Thermal model output
Y	Step-response model output prediction array
$\tilde{Y}$	Corrected step-response model output prediction array
Δu	MPC input instant change
ΔU	MPC input instant change array
β	Battery model constant, Step-response model constant
γ	Battery model constant
ω	AC system compressor speed (RPM)
ρ	Density $\left(\frac{kg}{m^3}\right)$
μ	Dynamic viscosity($Pa \bullet sec$)
∞	Infinity

Subscripts

$_{air}$	Air
$_{amb}$	Ambient environment
$_b$	Battery
$_B$	Temperature band
$_c$	Cold coolant

cap	Electric capacitor
$core$	Battery core
d	Desired value, Dynamic eigenmode
e	Engine, electric source
f	Cooling fluid
fan	Radiator fan
$flow$	Flow channel
h	Hot coolant
hot	Motor hot spot
H	Heat flow rate
i	Time instant index
I	Integral
m	E-motor
max	Maximum value
min	Minimum value
o	Outlet point
p	Pressure drop
$pipe$	Coolant pipe
$pump$	Coolant pump
P	Proportional
Q	Heat removal
r	Reference value, Rotor
rad	Radiator
s	Estimated value, Static eignmode
ss	Steady state
k	Battery column index
s	Battery surface, Stator
u	Cooling surface
v	Engine coolant valve
w	Coolant water
$wall$	Radiator coolant wall
x	Design variable
0	Initial variable

Superscripts

$\hat{}$	Estimated value
$\tilde{}$	Estimation error, Magnitude range, Corrected value
$\rightarrow$	Vector
$\bar{}$	Average value

Chapter 1

Introduction

The transportation industry consumes over 25% of the world's energy usage and is responsible for a considerable share of the global CO_2 emissions due to fossil fuel combustion. With the growing number of ground vehicles around the world, significant fuel economy improvements are required to stabilize and eventually reduce greenhouse gas emissions. To achieve higher fuel efficiency, hybrid electric vehicle (HEV) technology has been introduced in the late 1970's (Nairobi and Kenya, 2009). In addition to the conventional internal combustion engine, hybrid electric vehicle powertrains are characterized by a secondary electric energy storage device (e.g., batteries) and electric propulsion motors. In most instances, an electric generator is coupled to the gasoline or diesel engine to produce power. These technology upgrades allow an obvious improvement in fuel economy but also complicate the powertrain structure and make the HEV cooling task more difficult. This dissertation is focused on the investigation of thermal management control strategies for a heavy duty military HEV powertrain.

1.1 Background

For the last two decades, vehicle emission control has drawn increasing attention from governments, environment protection organizations, and automobile manufactures. Nowadays, high efficiency, low emission, operation safety, and cabin comfort have become the top objectives sought by the automobile industry. To achieve these objectives, new techniques and devices are continuously introduced and integrated into the design of the vehicles. Some of that include high level power management, battery material test and battery life improvements, electric motor modelling and size scaling, as well as smart thermal management systems.

It is reported that the road transportation sector is responsible for 23% of the global CO_2 emissions from fossil fuel combustion, following electric and heat generation which contributes 42%. The remaining 35% of the CO_2 emission is attributed to residential, industry, and other sectors (IEA, 2014). With the expected tripling of the number of light duty vehicles in the coming years and a resulting doubling of CO_2 emissions, unprecedented attention has been focused on improving vehicle fuel economy (Wambsganss, 1999). Different countries around the world are introducing increasingly stringent emission standards for automotive manufacturers to achieve greenhouse gas reductions. For example, the European Union released a mandatory emission reduction target for new cars of 130 grams of CO_2 per kilometre (g/km) by 2015. The policy relating to achieving this target has been in effect since 2012. An updated emission target is set at 95 g/km for 2021. This requires a reduction of 18% and 40%, respectively when compared against the 2007 fleet average of 158.7 g/km (Policy, 2015). China and the United States together contribute over one third of the global greenhouse gas emissions. In November 2014, the United States and China released a joint announcement on climate change and clean energy cooperation. The

two countries agreed to cut net greenhouse gas emissions between 26% to 28% from the 2005 level by the year 2025 (Whitehouse, 2014).

To meet the increasingly tough greenhouse gas emission standards, vehicle manufactures have developed powertrain designs for higher fuel efficiency. With this background, new structure of vehicle powertrain design equipped with secondary propulsion motors and energy storage devices were eventually introduced into the industry.

1.2 Hybrid Electric Vehicle Technology

Conventionally, a vehicle's propulsion system is driven by an internal combustion engine (ICE). A standard ICE based powertrain has two main components: the engine, and the transmission gear box. The overall propulsion system performance, especially the fuel economy, is highly dependent on the engine's efficiency. Meanwhile, the internal combustion engine, either gasoline or diesel, needs to work within a proper temperature range to remain reliable and efficient. However, the conventional ICE powertrain suffers some obvious drawbacks in fuel conservation. For example, a large portion of the combustion energy is wasted when the engine operates at idle speed without crankshaft load. Further, the energy lost during braking cannot be recovered. Due to their high power density, developed manufacturing techniques, and great energy density of fossil fuel, ICE driven vehicles are still widely used in daily life.

There are a number of proposed solutions to maximize the fuel economy of ICE powered vehicles. One of the most intuitive methods is to restore the energy that has been wasted by the powertrain. Hybrid electric vehicles (HEV) maintain the advantage of high energy density from the conventional ICE driven vehicles, and

introduces a secondary energy storage device into the propulsion system which makes energy regeneration possible. Researchers started studies on hybrid electric vehicles back in the 1970's. HEVs became available on the global market in 1997. During the last two decades, significant developments have been achieved in HEV industry. New battery materials, advanced e-motor designs and the evolution of real time control system have all contributed to the successes realized. Fig. 1.1 shows the number of HEVs that have been produced by different areas around the world (IEA, 2014).

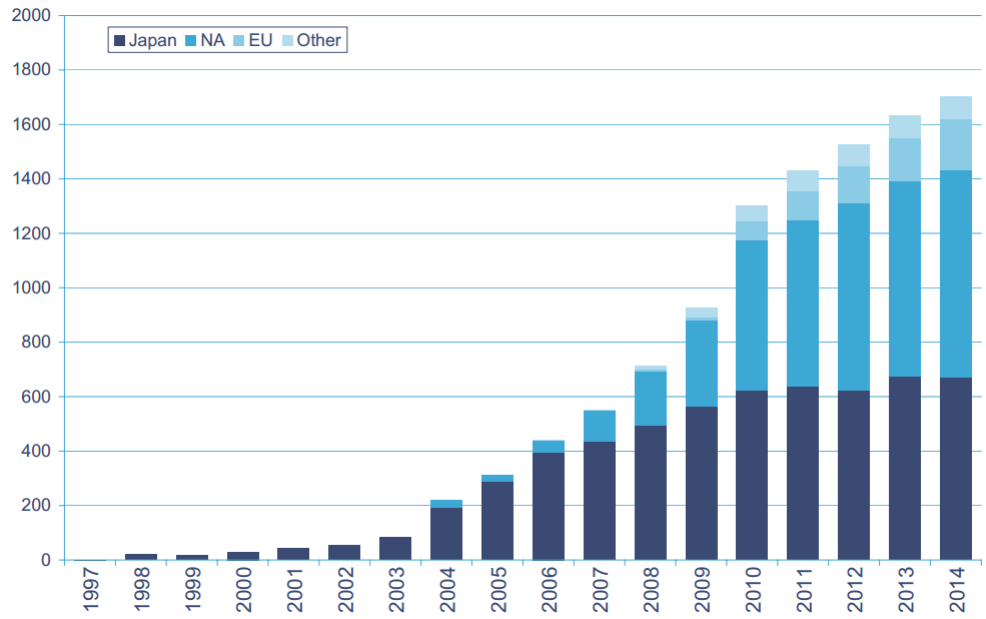

Figure 1.1: Global Hybrid Vehicle Assembly (thousands) by Region 1997 - 2014 (IEA, 2014), Where NA is North America and EU is European Union

Unlike ICE propelled vehicles, a typical HEV powertrain is characterized by two power sources. The vehicle combines an engine and an electric motor, with battery pack, to enable energy regeneration and shutting down during idle conditions and braking. Two typical HEV powertrain architectures are shown in Fig. 1.2. The parallel hybrid, in which both of the prime movers operate on the same drive shaft, allows the two propulsion sources to drive the vehicle individually or simultaneously.

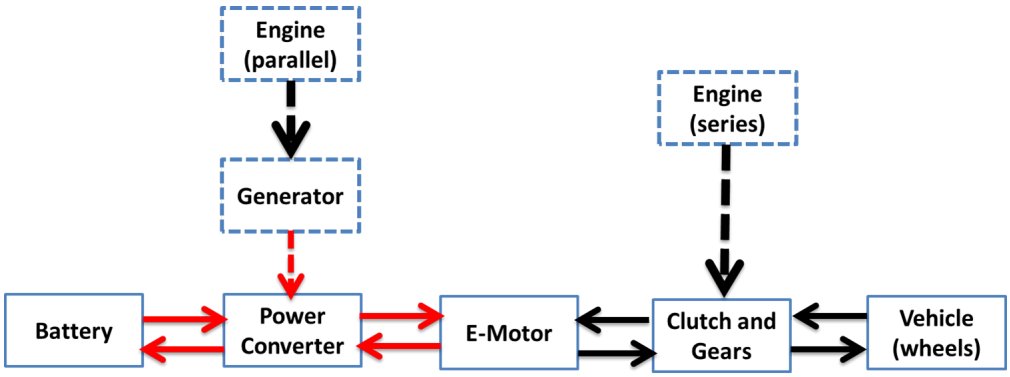

Figure 1.2: HEV Powertrain Architectures: (left) Parallel Hybrid and (right) Series Hybrid. Black Arrows: Mechanical Power; Red Arrows: Electrical Power

The series hybrid, in which the electric motors alone drive the vehicle, permits the electricity to be supplied either by a battery or by an engine-driven generator. Fig. 1.3 compares the energy flow in a ICE driven vehicle with a HEV(Demirdöven and Deutch, 2004). It can be observed that HEV achieves higher fuel efficiency through utilizing the energy lost during engine idle stop, brake regeneration, and ensuring the ideal operation range for the engine.

Despite the fact that an HEV is potentially 10% to 30% heavier in weight than an ICE driven vehicle (Guzzella and Sciarretta, 2007) due to the added battery pack, the HEV technique is still very meaningful and considered the favourable solution of the future vehicle powertrain designs for the following reasons. First of all, HEV technology enables power regeneration by applying the reversible secondary power source and energy storage device. Secondly, HEV design permits a high level powertrain management optimization approach which ensures the engine operation within the "sweet spot" range. Lastly, HEV offers the potential of engine downsize and even shut-down to achieve "zero emission" (Zhang et al., 2014a).

Most of the components in the HEV powertrain will generate a considerable amount of heat during driving cycles. The electrified powertrain elements are quite

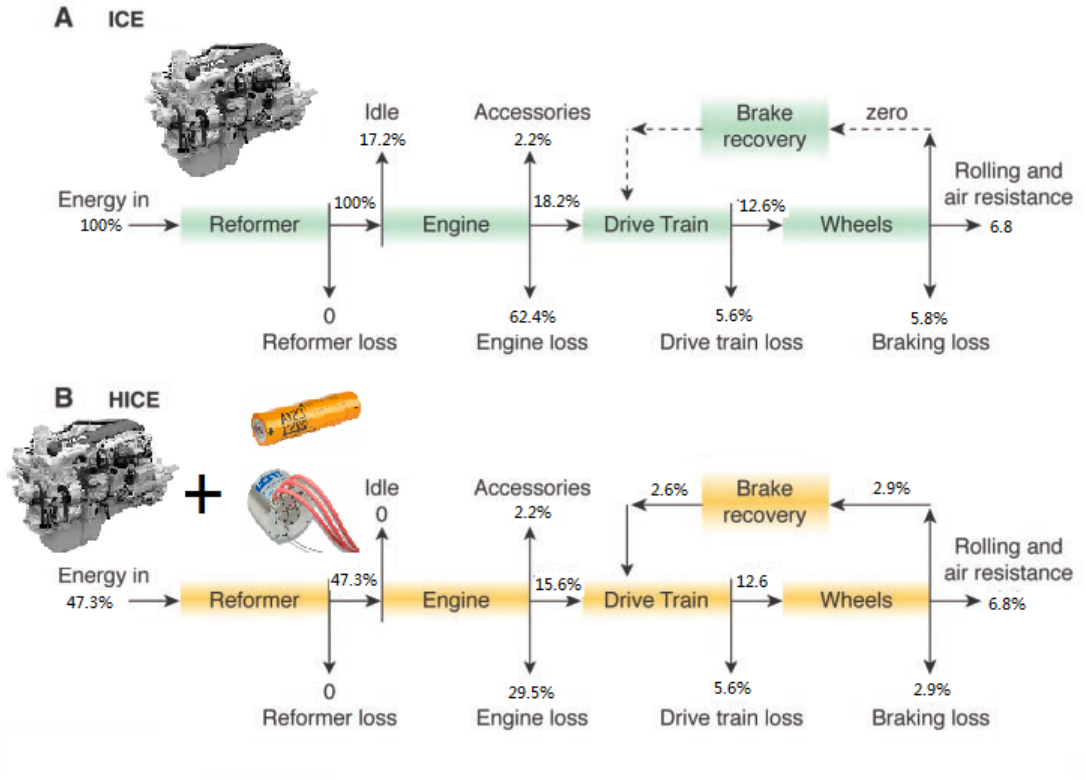

Figure 1.3: Normalized Energy Flow for Various Vehicle configurations (Same Effective Wheel Propulsion = 12.6). (A) Baseline ICE powertrain, the Conventional Internal Combustion, Spark Ignition Engine, Input Energy = 100; (B) HEV, a Hybrid Vehicle with e-motors and Parallel Powertrain which Eliminates Idling Loss and Captures some energy of braking, Input Energy = 47.3 (Demirdöven and Deutch, 2004)

vulnerable in overheated environments. On the other hand, the auxiliary energy loss caused by the thermal management system accessories contributes to the fuel consumption. Given the importance of high fuel efficiency, a reliable, high efficiency thermal management system is necessary. This dissertation proposes a thermal management system featuring electrified actuators and advanced control unit for HEV propulsion components to guarantee their proper performance, safe operation, high efficiency output, and finally, a long usage life cycle.

1.3 Powertrain Thermal Management

Powertain thermal management has been a lasting challenge in the automotive industry. Traditional engine cooling systems are equipped with a belt driven coolant pump and a clutched cooling air fan. Their operation speeds are determined by the engine crankshaft. Due to this dependency on the engine operation, it is noticeable that the conventional cooling system functionality is not optimized for the overall thermal management performance with its open-loop control structure. For example, this dependency on the engine speed will result in a small coolant flow at low engine speeds and high loading conditions of the engine, which is usually a driving condition associate with large heat generation rates comparing to the idle speed condition. Additionally, in the traditional engine cooling system, the coolant flow rate is regulated by a thermostat valve to prevent the engine from overheating or being overcooled. This coolant flow rate regulation design, based on mechanical actuators is very inefficient. A large amount of fuel energy is wasted due to parasitic losses of the unnecessary cooling activities.

The cooling system for the internal combustion engine has been studied for years. Researchers have conducted analytical studies on the cooling system by introducing the numerical modelling of the system (PricewaterhouseCoopers, 2007) (Park and Jung, 2008). To improve the performance of the engine cooling system, Saxena *at. al* (Saxena et al., 2010) applied a HEV cooling system simulation to evaluate the cooling circuit transients for a given driving cycle. Recently, the replacement of the traditional thermal management system actuators with a variable speed pump and a electric flow control valve provides the opportunity for an optimal control of the coolant flow rate and better coolant temperature tracking (Choi et al., 2007). A smart thermostat valve shows enhanced coolant flow control performance by Wagner

et al. (Wagner et al., 2003). Advanced controller design has been implemented into the engine cooling system by Salah *et al.* (Salah et al., 2008) and they demonstrated a significant improvement in coolant temperature tracking for the engine cooling system. The electrified computer controlled actuators offer the possibility to track coolant temperature at a very high level of accuracy. However, the existing thermal management strategies can hardly achieve the accurate controlling of the engine piston wall temperatures during different thermal loading conditions.

1.4 Problem Statement

The goal of this dissertation is to seek a systematic approach to design a hybrid electric vehicle (HEV) powertrain thermal management system featuring computer controlled cooling actuators. Thermal management design for HEV powertrain faces two main problems that require careful consideration. First, the components in HEV powertrain operate at different temperatures, which means they all need individual cooling strategies designed specifically for the unique ideal temperature range. Second, the complexity of the HEV powertrain results in large cooling loads and thermal management system power consumption. How to minimize this auxiliary energy loss is a key question addressed in this dissertation.

The thermal management system of a HEV is more complicated when compared to a conventional ICE driven vehicle. In addition to stabilizing the engine coolant temperature within a proper range, other electronic accessories in the powertrain also require a comprehensive designed thermal management strategy. The electric components have different requirements of the operational temperature range for safety and high efficiency performance, which vastly increase the difficulty of the powertrain thermal management tasks. For example, the battery pack needs to be

maintained with a very narrow margin of temperature range to keep the proper internal electro-chemical reaction stable output. Although operation under high temperature will reduce battery internal resistance and joule loss, overheated environments endanger the battery safety with high risks of thermal runaway and explosion. Previous studies show that the life cycle of a Li-ion battery is influenced by its operation temperature. The battery life drops dramatically when the battery is operated at temperatures higher than 60 $^{\circ}C$ or lower than 10 $^{\circ}C$ (Lam et al., 2000)(Bhatti, 1997). This temperature range is much lower than the typical ICE operation temperature. Thus the battery pack requires its own thermal management unit separated from ICE cooling cycle.

In addition to different target temperature ranges for the battery pack, e-motor and engine, the increased cooling load may be considerable. The fuel consumption contributed by the cooling system power loss is a portion that needs to be carefully reduced to improve the overall fuel economy. In this dissertation, the proposed cooling system design for HEV powertrains aims to minimize the overall cooling power consumption by applying advanced numerical modelling methods and control theories to optimize the cooling actuators operation.

The HEV powertrain thermal management system will accommodate the heat removal task for all the heat source components in the battery pack, the electric motors and the internal combustion engine.

1.5 Research Approach and Objectives

This dissertation proposes a thermal management system design for HEV powertrains, highlighted by the integration and control of electro-mechanical actuators. The objectives of this dissertation can be summarized as follows:

1: Develop synchronous supervisory control unit which simultaneously regulates the temperatures inside the battery pack, e-motor, and the IC engine through real time monitoring by a series of mathematical thermal models with a selected level of sophistication corresponding to the temperature tracking accuracy requirement.

2: Minimize power consumption through the nonlinear controlled management and optimized operation of the distributed cooling system actuators (coolant pumps, refrigerant compressor, cooling air fans) while satisfying heat rejection requirements.

3: Develop a numerical simulation tool for the heat exchanger size scaling and controller design purposes.

A suite of mathematical models with different level of sophistication are created for the powertrain heat generating elements by considering the balance of the fidelity importance and the calculation cost in respect to the real time control purpose. For battery pack thermal management, a lumped parameter electro-thermal battery cell model is implemented. The cooling air is provided by an vapor compression system modelled in a commercial software package AMESim. An optimal controller is developed for calculating the ideal cooling air temperature. The vapour compression system compressor is regulated by a model predictive controller for cooling air temperature tracking.

The thermal management system for the e-motors is designed based on a reduced-order thermal model developed at the University of Michigan. A linear optimal controller is introduced to calculated the ideal heat removal rate from each motor and a nonliear tracking controller is established to regulate the electric motors cooling cycle operation.

For the sake of completeness, the control strategy design for the conventional internal combustion engine cooling system temperature stabilization and power reduction will also be covered in the future work. The dissertation also looks into the thermal management performance and its effect on the fuel economy of a Mine Resistant Ambush Protected All Terrain Vehicle (M-ATV). The vehicle simulation is built up in MATLab/Simulink environment and a detailed thermal management system model is implemented into the simulation using the commercial software package AMESim. The structure of the high fidelity heavy duty military purpose vehicle simulation is shown in Fig. 1.4.

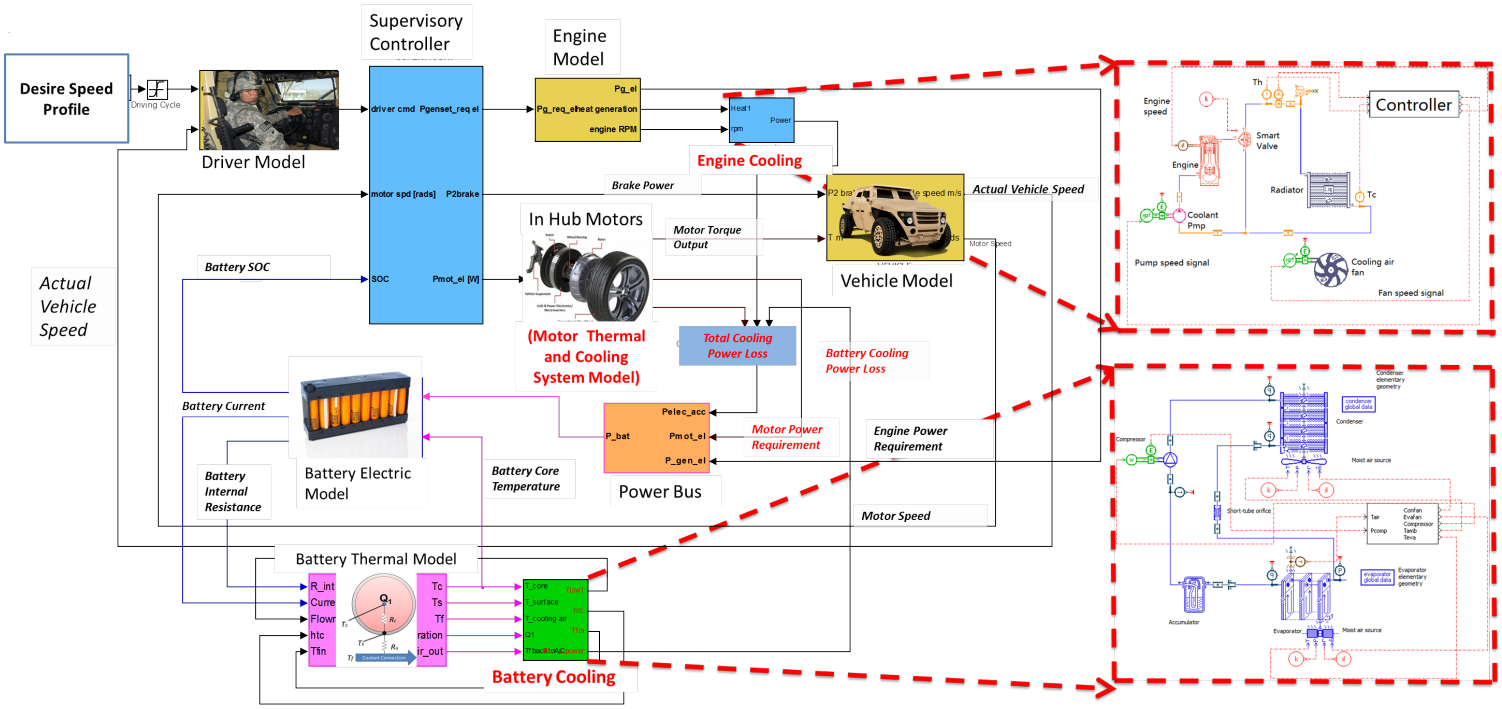

Figure 1.4: MRAP All Terrain Vehicle (M-ATV) Model built under AMESim-Simulink Co-Simulation

The research project has been conducted in collaboration with the Clemson University International Center for Automotive Research (CU-ICAR) and University of Michigan Electric Engineering Department as shown in Fig. 1.5. Together, the team is investigating a new concept and systematic method of heavy duty military purpose hybrid electric vehicle powertrain design with consideration of cooling system power consumption. The research will be carried on to the ICE cooling system controller design and heat exchanger size scaling optimization tool. Numerical case studies will be conducted to demonstrate the improvements in the HEV powertrain thermal management system performance on vehicle level simulation. The results to date demonstrate the significant advantages in both temperature tracking and energy conservation in comparison to traditional methods.

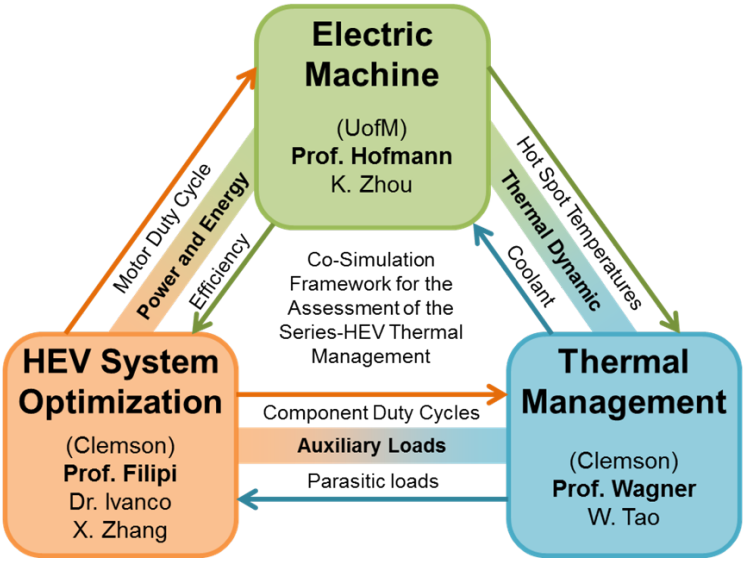

Figure 1.5: Collaborative Research Investigation of HEV Powertrain Design

1.6 Dissertation Organization

This dissertation is organized into six chapters. Chapter 1 gives the background introduction of this study. Chapter 2 introduces an overall concept of the holistic control strategy designed for the HEV powertrain thermal management system. Chapter 3 discusses in detail the modelling and controller development for a HEV battery pack thermal management system, focussing on the ideal cooling air temperature and mass flow rate derivation for the battery core temperature stabilization, under an urban assault driving cycle. Chapter 4 will demonstrate a model predictive controller designed for the vapour compression system to obtain the battery pack cooling air at a prescribed ideal temperature. Chapter 5 covers the study on a cooling system designed for the electric motors, based on a reduce-ordered FEA e-motor thermal model. Chapter 6 present a simultaneous fan, pump and valve control strategy designed for the conventional internal combustion engine thermal management system. Chapter 7 contains the conclusions of the dissertation and recommendation of the future work.

Chapter 2

Hybrid Electric Vehicle Thermal Management System - Nonlinear Controller Design

The components in a hybrid electric vehicle (HEV) powertrain include the battery pack, an internal combustion engine, and the electric machines such as motors and possibly a generator. These components generate a considerable amount of heat during driving cycles. A robust thermal management system with advanced controller, designed for temperature tracking, is required for vehicle safety and energy efficiency. this chapter examines the integration of advanced control algorithms to a HEV powertrain cooling system featuring an electric-mechanical compressor, coolant pump, three radiators, and heat exchanger and radiator fans. Mathematical models are developed to numerically describe the thermal behaviour of these powertrain elements. A series of controllers are designed to effectively manage the battery pack, electric motors, and the internal combustion engine temperatures. These controllers regulate the refrigerant compressor, coolant pump, and cooling fans to minimize the

temperature fluctuations while reducing the overall cooling system power consumption. Simulation results for assault and convoy escort driving cycles are presented to show that the controllers meet the powertrain heat removal requirements. The battery core temperature can be tracked to within 0.8 $^{\circ}C$ of the target value, the internal (stator) temperature of electric motors can be maintained within 1.1 $^{\circ}C$ of the desired value. The coolant temperature at engine's outlet exhibited a 0.4 $^{\circ}C$ error range from the prescribed target value of 90 $^{\circ}C$. The overall auxiliary power consumption of the cooling system is reduced by 45% when compared to a conventional cooling control method.

2.1 Introduction

The development of hybrid electric vehicles (HEV) has required increasingly complex powertrain designs and advanced control systems to optimize the consumption of available energy. A number of different energy sources and storage devices exist in modern ground vehicles tracks which can offer new challenges to the thermal management system's design. Compared to the internal combustion engine (ICE) in a traditional powertrain, the battery package and the electrical machines in the HEV powertrains are more vulnerable in overheated environments. The Li-ion battery cells that commonly applied in HEVs are sensitive to temperature changes. Consequently, their performance will be significantly reduced if the internal chemical reaction cannot proceed in a proper temperature range. Long time operation under overheated conditions will also decrease the battery cycle life. In more severe conditions, the battery cells may catch on fire or explode if the heat accumulated. The heat generation during continuously battery charging/discharging must be effectively removed to guarantee the battery pack performance and longevity. Similarly, the electrical motors produce

heat due to the conduction and core losses and also requires a proper thermal management system. Finally, the internal combustion engine remains a crucial power source, as well as a heat source, in HEV powertrains. An improved thermal management system should remove the waste heat from these components to maintain their prescribed working temperatures while reducing the auxiliary cooling actuators power consumption.

Previous studies have investigated overall cooling system architectures for conventional and hybrid vehicles plus their affect on the cooling system power consumption (Park and Jung, 2010). Salah *et al.* (Salah et al., 2008)(Salah et al., 2010) applied the nonlinear control theory to advanced thermal management system design for the internal combustion engine cooling fan and demonstrated the improvements in temperature tracking and power efficiency. Cho *et al.* (Cho et al., 2007) explored the benefit of a controllable electric pump in a truck engine cooling system. The study results showed a significant reduction in the pump power consumption and possible heat exchanger downsize. Shams- Zahraei *et al.*(Shams-Zahraei et al., 2012) presented a hybrid vehicle energy management system incorporating an engine thermal management method which offers the global optimal battery charge and discharge . A high level powertrain management optimization was completed using a dynamic programming method by Zhang *et al.* (Zhang et al., 2014a). They considered the influence of battery cooling auxiliary losses and increased the overall fuel economy. However, limited work has been focused on the development of holistic control algorithms for the entire HEV powertrain thermal management system. This chapter evaluates the performance of a computer controlled thermal management system equipped with model based controllers. A set of thermal models of the heat generating components in the HEV powertrain are developed. Different approaches of modelling have been chosen with consideration of practical applications, computational cost, and real-time

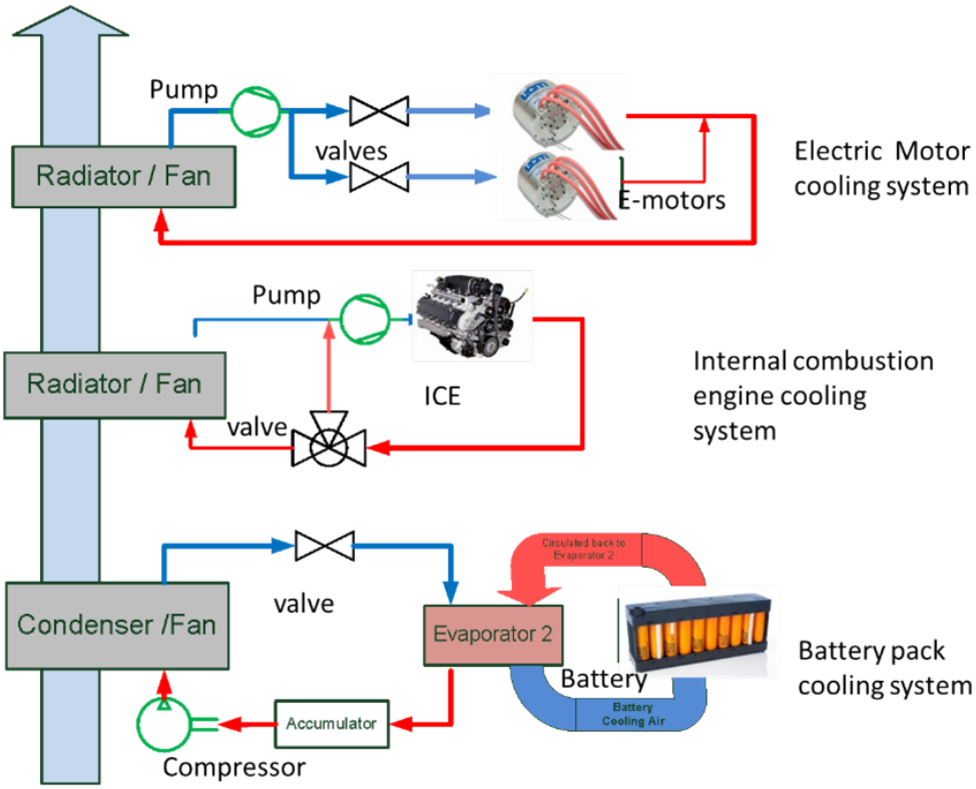

Figure 2.1: Hybrid Electric Vehicle Powertrain Thermal Management System

controller design. Advanced control theories are introduced to track the reference temperatures, minimize the temperature fluctuations, improve the cooling fluids regulation process, and reduce the cooling power consumption. The proposed thermal management system structure is shown in Fig. 2.1. The reminder of this chapter is organized as follows. The cooling system main components, including the battery pack, e-machines, and internal combustion engine, will be introduced with a series of mathematical models in Section 2.2 to establish a basis for controller design. A suite of controllers will be developed in Section 2.3. Section 2.4 presents the numerical results of simulations under different driving cycles and cooling conditions. Section 2.5 concludes this chapter.

2.2 A Hybrid Electric Vehicle Cooling System Mathematical Model

The proposed thermal management aims to address the heat removal task for main components in the HEV powertrain, including the battery pack, electric motors and the internal combustion engine. The battery pack in this study is equipped with an air conditioning system for active air cooling. The electric motors and internal combustion engine are cooled by circulated coolant. The thermal models of each components are introduced in this section.

2.2.1 Battery Pack Thermal Model

In this study, a battery pack consisting of 360 AHR32113 cells is cooled with an air conditioning (AC) system. The AC system includes a radiator, a evaporator, a cooling air fan, and a refrigerant compressor. The AC system provides cooling air for circulation through the battery pack and back to the evaporator. For controller design purposes, in this work, a lumped-parameter thermal model (Forgez et al., 2010) is applied to simulate the transit change in the cylindrical battery cells in terms of the core temperature, T_{core}, and surface temperature, T_s.

$$C_{core}\frac{dT_{core}}{dt} = \left(\frac{T_s - T_{core}}{R_{core}}\right) + Q_b \tag{2.1}$$

$$C_s\frac{dT_s}{dt} = \left(\frac{T_f - T_s}{R_u}\right) - \left(\frac{T_s - T_{core}}{R_{core}}\right) \tag{2.2}$$

where C_{core} and C_s are the heat capacity of the battery core and the battery surface, respectively. The thermal resistance, R_{core}, between the battery core and the battery

surface, is assumed to be a constant value. The thermal resistance between the battery surface and the cooling air, R_u, is obtained based on the convective heat transfer coefficient on the battery surface and convective transfer area. Lin *et al.* (Lin et al., 2011) proposed a parametrization method to estimate C_{core} , C_s, R_e, and R_{core}. The heat generation, Q_b , is approximately equal to the concentrated Joule loss in the battery. The detailed battery electrical sub-model is reported in (Tao and Wagner, 2014) to analytically obtain the heat generated by the Joule loss from the input battery current. Finally, the cooling air temperature dynamic change while flowing across the battery bank is written as

$$C_f \frac{dT_{f,k}}{dt} = \dot{m}_{air} c_{p,air} \left(T_{f,k-1} - T_{f,k} \right) + \frac{T_s - T_{f,k}}{R_u} \tag{2.3}$$

where R_u is the thermal resistance at the battery surface. The parameter C_f is the heat capacity of the air surrounding one battery column, $c_{p,air}$ is the specific heat of air under atmosphere pressure, and the subscript k is the column index. A larger k means that the column is positioned further away from the air inlet port. The cooling air temperature that passes the $k-th$ column, $T_{f,k}$, denotes the outlet cooling air temperature at the $k-th$ column. The battery cell thermal model structure is offered in Fig. 2.2.

In the AC system, the most power consuming actuator is the refrigerant compressor because it provide a pressure rise in the refrigerant path. The variable speed refrigerant compressor can be controlled to adjust the cooling air temperature. Due to the highly nonlinear thermal dynamics and phase change, a detailed simulation of the AC system is too sophisticated and not necessary for controller design purpose. An AC system model has been built in AMESim.

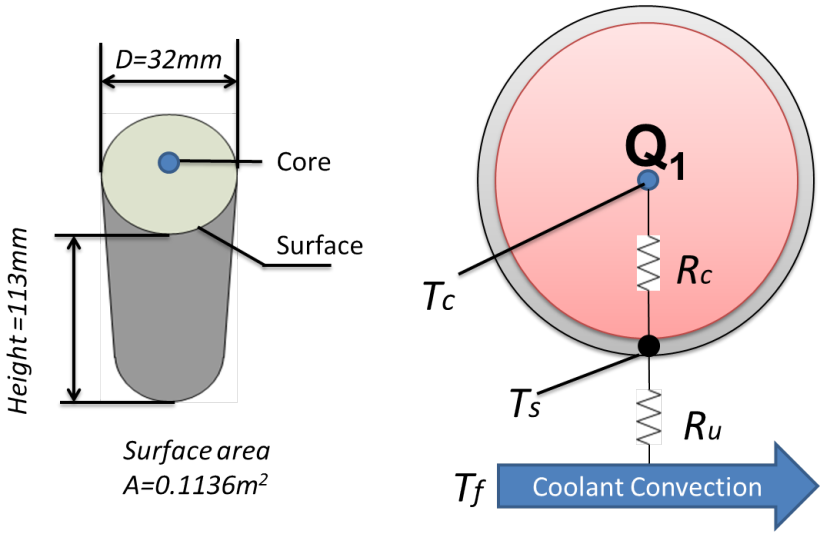

Figure 2.2: Single Cell Thermal Model with Three Temperature States - Battery Core, T_{core}, Battery Surface, T_s, and Cooling Air, T_f.

2.2.2 Engine Thermal Model

The internal combustion engine is the primary power source of the vehicle. It converts approximately one third of the fuel's chemical energy into propulsion power and other third is taken away by the exhausted waste gas. The rest of the combustion energy is directed into waste heat that needs to be removed by the cooling system. The traditional engine cooling system consists of a belt driven coolant pump, a clutched radiator fan, and a wax thermostat. In this study, these components are upgraded with servomotor actuators. The mechanical coolant pump and radiator fan are replaced by computer controlled pump and fans.

The transit thermal performance of the engine cooling system can be described by the following equations for the dynamic temperatures change in the engine, coolant and cooling air

$$C_e \frac{\mathrm{d}T_e}{\mathrm{d}t} = Q_e - h_e\left(T_e - T_h\right) \tag{2.4}$$

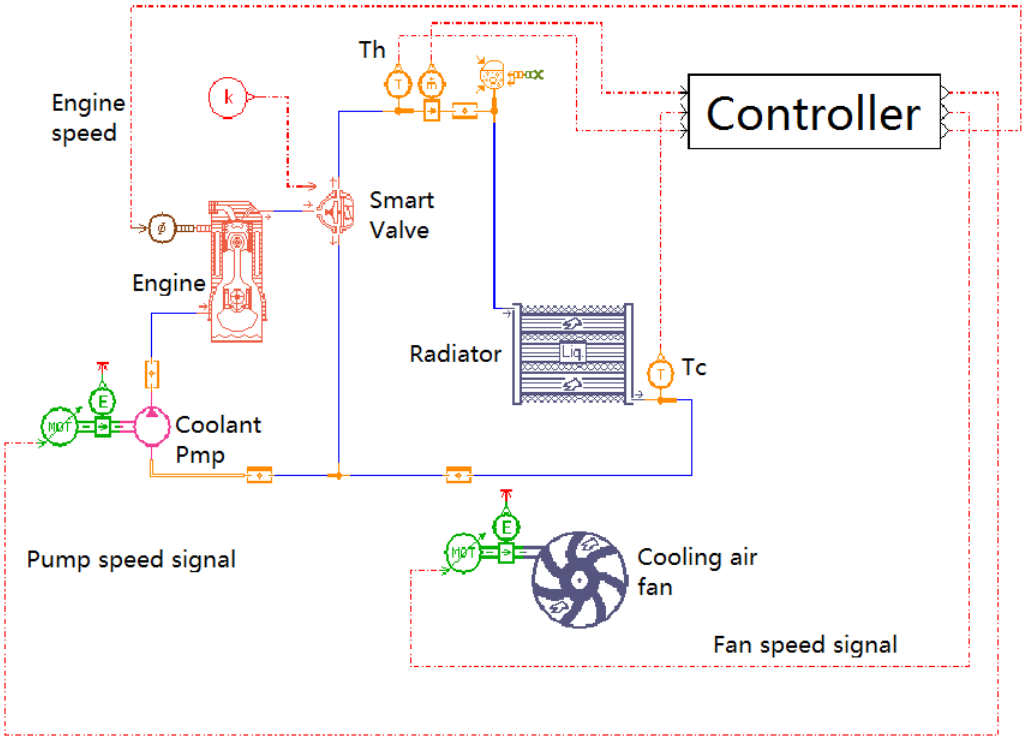

Figure 2.3: Internal Combustion Engine Thermal Management System Featuring a Variable Speed Coolant Pump and a Cooling Air Fan (Constructed in AMESim)

$$M_{w,e}c_{p,w}\frac{\mathrm{d}T_h}{\mathrm{d}t} = h_e\left(T_e - T_c\right) + \dot{m}_w c_{p,w}\left(T_c - T_h\right) \tag{2.5}$$

$$M_{w,rad}c_{p,w}\frac{\mathrm{d}T_c}{\mathrm{d}t} = h_r\left(T_{amb} - T_h\right) + \dot{m}_w c_{p,w}\left(T_h - T_c\right) \tag{2.6}$$

$$M_{air,rad}c_{p,air}\frac{\mathrm{d}T_{air,o}}{\mathrm{d}t} = h_r\left(T_h - T_{amb}\right) + \dot{m}_{air} c_{p,air}\left(T_{amb} - T_{air,o}\right) \tag{2.7}$$

where C_e is the equivalent thermal capacity of the engine block. The parameter $M_{w,e}$ and $M_{w,rad}$ are the coolant mass in the engine and radiator, $M_{air,rad}$ is air mass stored in the radiator. $c_{p,w}$ is the specific heat of coolant water. The variables T_e, T_h, T_c and $T_{air,o}$ denote engine temperature, coolant water temperature at engine

outlet, coolant water temperature at radiator outlet, and air temperature at radiator outlet respectively. Lastly, h_e is the equivalent heat transfer coefficient in the engine, which is also a function of the coolant mass flow rate, $\dot{m}_w$. The engine cooling system structure is shown in Fig. 2.3.

2.2.3 Electric Motor Thermal Model

The electric motor is another critical element of the HEV powertrain. Its propulsion output is constrained by the temperature limits. Real time thermal management with knowledge of the machine's internal temperature is very helpful for improving the machine operation safety and determining the torque/power capability at any time instant during a driving cycle. A Lumped-parameter thermal model has been introduced to capture the thermal performance of the electric machine (El-Refaie et al., 2004). The mathematical descriptions execute very fast but are not capable of demonstrating the temperature distribution inside the machine. For accurately estimating the electric machine's internal temperature, a finite element based thermal model has also been developed (Zhou et al., 2011). Unfortunately, the full order FEA thermal models for electric machine with complicated geometry is computationally too burdensome for a real time controller design. In this study, a reduced order 3D finite element based dynamic thermal models of a electric machine is chosen to explore a new concept of thermal control.

The partial differential equation of thermal conduction is given as

$$d\frac{\mathrm{d}T}{\mathrm{d}t} - k \bigtriangledown^2 T = q \tag{2.8}$$

where T is the continuum temperature, k and d are the motor thermal conductivity and specific heat respectively. q denotes the heat flux. The above equation can be

written in discrete form by finite element analysis techniques.

$$\mathbf{D}\,\dot{\overrightarrow{t}} - \mathbf{K}\,\overrightarrow{t} = \overrightarrow{q} \tag{2.9}$$

where $\overrightarrow{t}$ is the nodal temperature vector of the finite element mesh, **K** is the finite element matrices which corresponds to thermal conductivity, and **D** is the finite element matrix which corresponds to specific heat. The vector $\overrightarrow{q}$ corresponds to the excitation of the thermal model, including heat transfer on cooling surface, friction and windage losses, conduction and core losses. With a change of basis and model order reduction, this FEA model may be finalized into a state-space form models corresponding to the stator and rotor, respectively.

$$\dot{\overrightarrow{x}}_s = \mathbf{A}_s\,\overrightarrow{x}_s + \mathbf{B}_s\,\overrightarrow{q}_s \tag{2.10}$$

$$\overrightarrow{t}_s = \mathbf{V}_s\,\overrightarrow{x}_s \tag{2.11}$$

$$\dot{\overrightarrow{x}}_r = \mathbf{A}_r\,\overrightarrow{x}_r + \mathbf{B}_r\,\overrightarrow{q}_r \tag{2.12}$$

$$\overrightarrow{t}_r = \mathbf{V}_r\,\overrightarrow{x}_r \tag{2.13}$$

In these expressions, $\overrightarrow{t}_s$ and $\overrightarrow{t}_r$ are the temperature nodes of motor stator and motor rotor respectively. The model input is the heat flux vector $\overrightarrow{q}_s$ and $\overrightarrow{q}_r$. There's conduction heat transfer in the air gap between the stator inner surface and the rotor external surface. This heat flux can be calculated by determining the boundary temperatures and the effective conduction heat transfer coefficient in the

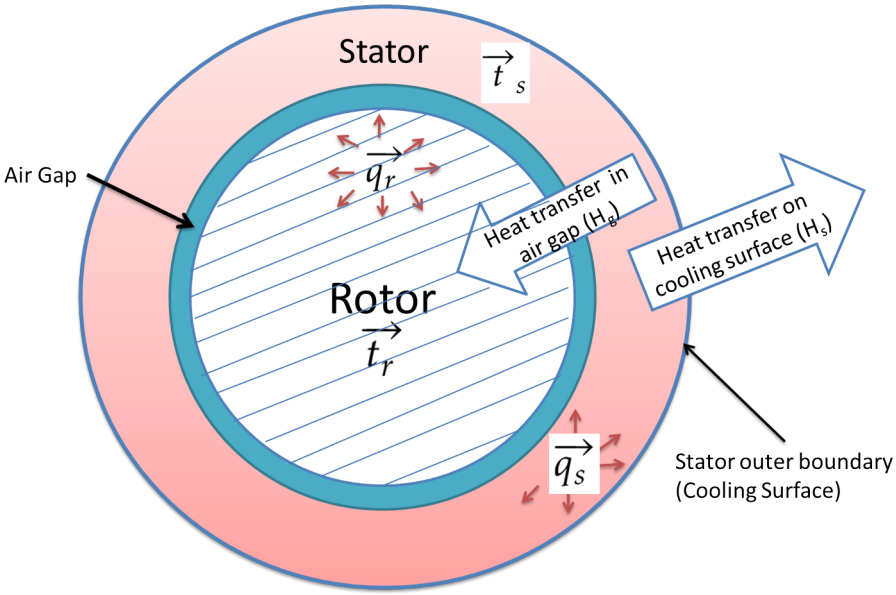

Figure 2.4: Electric Motor Thermal Model with Stator and Rotor plus the Accompanying Heat Transfer Effects

air gap, so the thermal model of the stator and rotor can be developed separately and coupled by heat transfer effect. The detailed procedures of the reduced-order three dimensional thermal model are reported in (Zhou et al., 2013). The thermal model of the electric motor with stator and rotor parts and the heat transfer behaviours are illustrated in Fig. 2.4.

The cooling surface heat flux is one of the element in the input vector $\overrightarrow{q}_s$, and is the only controllable input for the cooling system. To obtain the heat flux, the overall cooling surface heat transfer is calculated as

$$Q_s = min\left[h_m(T_{so} - T_c), (T_{so} - T_c)\dot{m}_w c_{p,w}\right] \tag{2.14}$$

where the heat transfer coefficient, h_m, is a function of the coolant mass flow rate $\dot{m}_w$. The electric motor cooling system model is built with the same approach as described in Eq. (2.6) and Eq. (2.7).

2.3 Thermal Control Algorithms

A series of controllers, designed using the thermal models for each powertrain element will be presented in this section. For the battery pack thermal management, the system aims to maintain the battery core temperature at a desired value for optimal performance. A nonlinear controller is developed for the engine cooling system operation to track the coolant temperature at the engine's outlet and to reduce the power consumption of the actuators. With the help of the high fidelity e-motor thermal model, a new cooling strategy concept is developed to maintain the hot spot temperature in the e-motor's stator by tracking an ideal heat removal rate on the cooling surface.

2.3.1 Battery Pack Cooling Control

To ensure the battery pack is properly working, the battery internal temperature, T_{core}, should be maintained at a desired value during the charging/discharging events. The battery thermal model establishes a basis for the controller designs. The cooling air mass flow rate is set to a constant value in this study, so the thermal resistance at the battery cell surface, R_s, is constant. The controller is designed to track the battery core temperature, T_{core}, to a prescribed reference value, $T_{core,r}$, by controlling the inlet cooling air temperature, $T_{f,in}$.

First, the thermal model can be written in a state space form as

$$\dot{X}_b = \mathbf{A}_b X_b + \mathbf{B}_b U_b \tag{2.15}$$

where $X_b = \left[T_{core}, T_s, T_f\right]$ and $U_b = [Q_b, T_{f,in}]$.

To track the battery core temperature with reasonable cooling air temperature

change, define a quadratic cost function as

$$J_b = \int_{t0}^{t1} \left\{ \left[X_b - X_{b,r} \right]^T R_1 \left[X_b - X_{b,r} \right] + U_b R_2 U_b \right\} dt \tag{2.16}$$

in which R_1 and R_2 are positive weighting matrices. Applying optimal control theory, the control law is defined with a feed forward term and a feedback term as

$$T_{f,in,d} = -F_0^{-1} X_b + H_c^{-1} X_{b,r} \tag{2.17}$$

The feedback gain and feed forward gain is defined as

$$F_0 = R_2^{-1} \mathbf{B}_b^T P \tag{2.18}$$

and

$$H_c = R_1 \left(\mathbf{A}_b - \mathbf{B}_b F_0 \right)^{-1} \mathbf{B}_b \tag{2.19}$$

where P is solved by a corresponding Riccati equation. Set $R_1 = [1,0,0;0,0,0;0,0,0]$ and $R_2 = [1,0;0,0.01]$ to reduce the battery core temperature error, $e_{core} = T_{core} - T_{core,r}$, by minimizing the cost function, J_b. Eq. (2.17) offers the ideal inlet cooling air temperature.

The cooling air is generated by an air conditioning (AC) system. The refrigerant compressor is the most power consuming part and its speed needs to be controlled to track the cooling air temperature at the prescribed value, $T_{f,in,d}$. In a previous study, a model predictive controller has been developed to regulate the compressor speed using a step-response model.

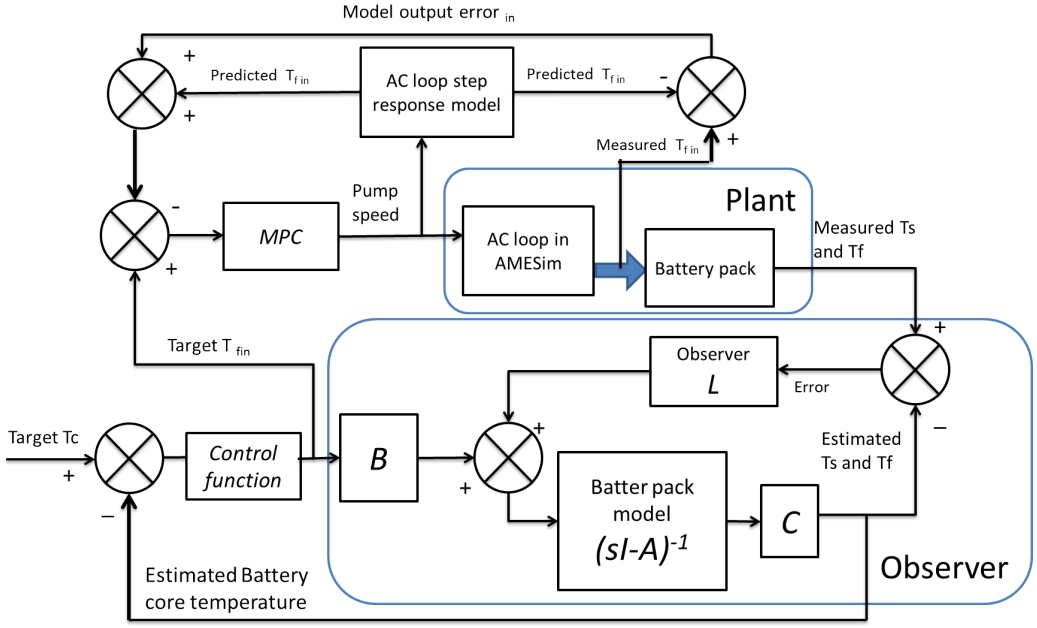

Figure 2.5: Controller Design for Battery Cooling System

The compressor speed is controlled as

$$\omega_t = \int \delta\omega_t \mathrm{d}t \tag{2.20}$$

where $\delta\omega_t$ is designed to minimize the error between the model predicted cooling air temperature and its desired value based on previous compressor speed input ω_{t-1}. The overall controller structure for the battery cooling system is shown in Fig. 2.5.

In a conventional battery cooling control system, a switch on/off control may be applied. The cooling system is triggered "on" when the battery temperature reaches the prescribed threshold, $T_{core,max}$, and switched "off" when the temperature is cooled down. The compressor operation in conventional method can be expressed as

$$\omega_t = \begin{cases} \omega_{max}; & \text{if } T_{core} \geq T_{core,max} \\ \omega_{min}; & \text{if } T_{core} \leq T_{core,min} \end{cases} \tag{2.21}$$

2.3.2 Engine Cooling Control

The internal combustion engine is the largest heat source in a vehicle. In this thermal management design for the internal combustion engine, a liquid-air cooling cycle is applied. The coolant pump and the cooling air fan are both electrically controlled. This provide the opportunity to improve the temperature tracking, optimize the coolant flow rate, and reduce the cooling power consumption. The thermal model of the engine cooling system described in Eq. (2.4) to Eq. (2.7) is applied to design a non-linear controller to stabilize the coolant temperature at the engine's outlet by regulating the coolant and cooling air flow rates. There are three assumptions made to facilitate the controller design process, (A1), The thermal valve is fully opened so that all the coolant at engine outlet will flow through the radiator. (A2), All the temperature states can be measured with available sensors and used as feedback signals in the control system. (A3), The radiator size is large enough to satisfy the heat removal requirement.

Set the desired coolant temperature at engine's outlet as $T_{h,d}$, and define the control error as the difference between the actual value $e_h = T_h - T_{h,d}$. A Lyapunov-based nonlinear controller can be designed to regulate the coolant mass flow rate and achieve the temperature tracking. The error dynamic can be written as

$$\dot{e}_h = \dot{T}_h - \dot{T}_{h,d} = \dot{T}_h \tag{2.22}$$

Referring to Eq. (2.5), the coolant mass flow rate control law can be derived using the following procedures

$$\dot{e}_h = \dot{T}_h - \dot{T}_{h,d} = \dot{T}_h \tag{2.23}$$

Define a Lyapunov cost function as

$$V_1 = \frac{1}{2}{e_h}^2 \tag{2.24}$$

so that

$$\dot{V}_1 = e_h \dot{e}_h = e_h \dot{T}_h \tag{2.25}$$

To eliminate the tracking error, define the mass flow rate control law as

$$\dot{m}_w = \frac{M_{w,e} c_{p,w} K_1 e_h + h_e (T_e - T_c)}{c_{p,w} (T_h - T_c)} \tag{2.26}$$

Now substitute flow rate into Eq. (2.5), so that the tracking error dynamic becomes

$$\dot{T}_h = -K_1 e_h \tag{2.27}$$

and Eq. (2.25) can be rewritten as

$$\dot{V}_1 = -K_1 e_h^2 \tag{2.28}$$

which indicates that the error $e_h \to 0$ with the proposed coolant mass flow rate.

The cooling air driven fan consumes a large amount of power and its speed needs to be controlled too. The cooling air mass flow rate control law is derived by tracking the coolant temperature at the radiator outlet (also the engine inlet), T_c, to a desired value, $T_{c,d}$, such that the heat taken away by the coolant flow is same to the heat transferred from the engine. The desired coolant temperature at the radiator outlet is defined as

$$T_{c,d} = \frac{-K_1 e_h M_{w,e} c_{p,w} - h_e (T_e - T_c)}{\dot{m}_w c_{p,w}} \tag{2.29}$$

To reduce the power consumption of the cooling air fan, it is reasonable to find the minimal cooling air mass flow rate required. With assumption A3, the heat exchanger size is large enough to allow the maximal possible heat transferred from the coolant to the air, and this means that the cooling air and the coolant temperatures are very close to each other when flow out from the radiator. So, the necessary cooling air mass flow rate can be derived by driving the cooling air temperature at the radiator outlet, $T_{air,o}$, to the prescribed coolant temperature at the engine inlet, $T_{c,d}$, which is calculated in Eq. (2.29).

Define another Lyapunov cost function as

$$V_2 = \frac{1}{2} {e_{air}}^2 \tag{2.30}$$

where $e_{air} = T_{air,o} - T_{c,d}$, so that

$$\dot{V_2} = e_{air}\dot{e_{air}} = e_{air}(\dot{T}_{air,o} - \dot{T}_{c,d}) \tag{2.31}$$

Refer to Eq. (2.7), the desired air mass flow rate control law is set as

$$\dot{m}_{air} = \frac{M_{air,r}c_{p,air}(-K_2 e_{air} + \dot{T}_{c,d}) - h_r\,(T_h - T_{amb})}{c_{p,air}(T_{amb} - T_{air,o})} \tag{2.32}$$

where K_2 is a positive constant, and the term $\dot{T}_{c,d}$ can be obtained from Eqs. (2.4), (2.5), (2.6) and measured coolant mass flow rate. Plug the prescribed air mass flow rate into Eq. (2.7), the dynamic change of the air temperature at radiator outlet can be expressed as

$$\dot{T}_{air,o} = -K_2 e_{air} + \dot{T}_{c,d} \tag{2.33}$$

By replacing the $\dot{T}_{air,o}$ term in the Eq. (2.31) by the Eq. (2.33), it can be seen

that the dynamic change of the error cost function V_2 becomes

$$\dot{V}_2 = -K_2 e_{air}^2 \tag{2.34}$$

which indicates that the proposed mass flow rate will eliminate the error e_{air}, given the heat exchanger size is large enough, the coolant water temperature at the radiator outlet is also converges to its desired value. Eq. (2.26) and Eq. (2.32) supply the control law of coolant mass flow rate for temperature tracking and minimal cooling air mass flow rate to meet the heat removal rate requirement.

2.3.3 Electric Motor Cooling Control

The state-space form of the thermal model enables the design of an optimal regulator with five inputs; only the third input state (conductive cooling heat transfer at e-motor surface) can be practically controlled. It is reasonable to take only the stator portion of the e-motor as the cooling subject since the heat source is located there and the hottest spots are always found in the stator. Thus, the optimal controller can be designed based on the state-space stator thermal model using matrices $\mathbf{A}s$, $\mathbf{B}s$, and $\mathbf{V}s$.

Generally, the stator thermal model shows that the highest temperature spots inside are those elements whose indexes are between 2 to 12 in the output vector, $\overrightarrow{t}_r$, which correspond to the positions near the windings. With this observed simulation results, the control objective can be reduced to only 10 elements by properly weighting matrices design. To develop an optimal controller to calculate the ideal heat removal requirement, define the cost function as

$$J_m = \int_{t0}^{t1} \left\{ [\overrightarrow{t}_s - \overrightarrow{t}_{s,r}]^T R_3 [\overrightarrow{t}_s - \overrightarrow{t}_{s,r}] + \tilde{q}_s^T R_4 \tilde{q}_s \right\} dt \tag{2.35}$$

where, R_3, and R_4 are positive symmetric weighting matrices. In this case, R_3 is designed to only stabilize the stator's highest internal temperature, the 2nd to 12th elements in model output vector $\overrightarrow{t}_s$, but not controlling the rest elements in the output vector. So the weighting matrices R_3 is written such that only the 2nd to 12th elements on its diagonal are large positive constants, and the value of the other diagonal elements are set to be zero. The term $\widetilde{q}_s = \overrightarrow{q}_s - \overrightarrow{q}_{s,0}$ defines the range of change of the heat flux, and $\overrightarrow{t}_{s,r}$ is the reference stator temperature vector.

The linear optimal control law for ideal heat flux on the cooling surface is derived as

$$\overrightarrow{q}_{s,d} = -F_1^{-1}\,\overrightarrow{x}_s + \overrightarrow{q}_{s,0} \tag{2.36}$$

The feedback and feed forward gain is defined as

$$F_1 = R_4^{-1}\mathbf{B}_s^T P_2 \tag{2.37}$$

and

$$\overrightarrow{q}_{s,0} = \mathbf{C}_s(R_3(\mathbf{A}_s - \mathbf{B}_s F_1)\mathbf{B}_s)^{-1}\,\overrightarrow{t}_{s,r} \tag{2.38}$$

where P_2 is solved as the non-negative-definite solution of the corresponding algebraic Riccati equation. The term $\overrightarrow{q}_{s,d}$ is the target input of the stator model: core loss; conduction loss; cooling heat flux; heat flux at machine end and heat flux at the air gap surface. Thus, the ideal heat removal rate at the machine cooling surface is identified by the third element in $\overrightarrow{q}_{s,d}$ obtained from Eq. (2.36) minimizing the prescribed cost function, J_2. To emphasize the important limitation that only the third input of this model is controllable, design the second weighting matrices in the

cost function as follows

$$R_4 = \begin{bmatrix} 5\times10^7 & 0 & 0 & 0 & 0 \\ 0 & 5\times10^7 & 0 & 0 & 0 \\ 0 & 0 & 1 & 0 & 0 \\ 0 & 0 & 0 & 5\times10^7 & 0 \\ 0 & 0 & 0 & 0 & 5\times10^7 \end{bmatrix} \tag{2.39}$$

In other words, the weighting coefficient of the third input is much smaller than the rest of the four uncontrolled inputs. To minimize the prescribed cost function, the regulator would address the feedback gain mainly on the third input. The large weighting coefficients for the rest of the inputs reduce the change range requirements of uncontrollable heat transfer.

The ideal heat removal flux on the motor surface, $\overrightarrow{q}_{s,d}$, obtained by the linear optimal regulator based on the motor thermal model is supplied to the cooling system control unit as a reference for tracking. A nonlinear tracking controller is developed to operate the coolant pump and fan speed for ideal heat removal rate tracking at the motor surface. The e-motor cooling system control structure is shown in Fig. 2.6.

Based on the heat transfer rate defined in Eq. (2.14), the heat removal rate tracking control error is defined as

$$e_Q = Q_{s,d} - min\left[h_m(T_{so} - T_c), (T_{so} - T_c)\dot{m}_c c_{p,w}\right] \tag{2.40}$$

where $Q_{s,d}$, is the desired cooling surface heat flow rate, which is the product of the ideal heat flux and the motor cooling surface area. The term h_m is the heat transfer coefficient expressed as a function of coolant mass flow rate. Now design a

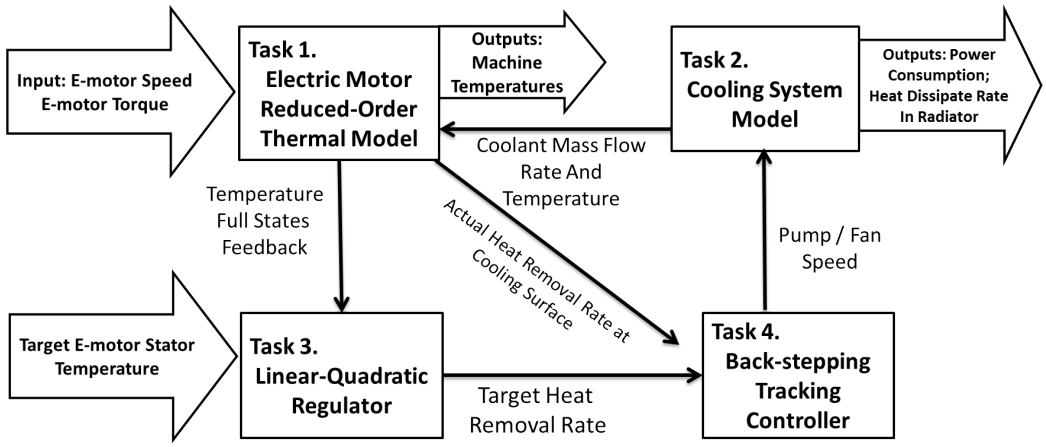

Figure 2.6: Controller Design for E-Motor Cooling System

cost function

$$V_3 = \frac{1}{2} e_H^2 \tag{2.41}$$

and its time derivative expressed as

$$\dot{V}_3 = e_Q(\dot{Q}_{s,d} - \dot{Q}_s) \tag{2.42}$$

The controller can be derived by formulating an ideal heat removal rate change as

$$\dot{Q}_s = \dot{Q}_{s,d} + K_3 e_Q \tag{2.43}$$

where K_3 is a positive constant. If one investigates the relationship between the heat removal rate and the coolant mass flow rate, then the heat transfer on the stator cooling surface follows the dynamic change rule as

$$\dot{Q}_s = (T_{so} - T_c)\frac{\partial h_m}{\partial \dot{m}_w}\frac{d\dot{m}_w}{dt} - h_m(\frac{\mathrm{d}T_c}{\mathrm{d}t}) \tag{2.44}$$

The ideal coolant mass flow rate in each motor is designed as

$$\frac{\mathrm{d}\dot{m}_w}{\mathrm{d}t} = \frac{\dot{Q}_{s,d} + K_3 e_Q - h_m \frac{\mathrm{d}T_c}{\mathrm{d}t}}{(T_{so} - T_c)\frac{\partial h_m}{\partial \dot{m}_w}} \tag{2.45}$$

so that the control law to obtain the coolant water mass flow rate is

$$\dot{m}_w = \int \frac{\dot{Q}_{s,d} + K_3 e_H - h_m \frac{\mathrm{d}T_c}{\mathrm{d}t}}{(T_{so} - T_c)\frac{\partial h_m}{\partial \dot{m}_w}} dt \tag{2.46}$$

By replacing the $\frac{\partial h_m}{\partial \dot{m}_w}$ term in Eq. (2.44) by Eq. (2.45)and Eq. (2.46), it can be obtained that $\dot{Q}_s = \dot{Q}_{s,d} + K_3 e_Q$. The dynamic change of the tracking error function $\dot{V}_3$ becomes

$$\dot{V}_3 = e_H(\dot{Q}_{s,d} - \dot{Q}_{s,d} - K_3 e_H) = -K_3 e_H^2 \tag{2.47}$$

and this proves that the proposed coolant mass flow rate in the Eq. (2.46) will achieve the $Q_{s,d}$ tracking.

In the e-motor cooling system, all four motors on-board are simultaneously cooled by the same radiator, as shown in Fig. 2.1. To reduce power waste in the radiator fan, the air flow rate may be optimized. To investigate the minimal air flow rate required, it is assumed that the heat removed by the cooling air flow from the radiator is the same as the heat removed from the motors by the coolant. So set the air mass flow rate proportional to the desired heat removal rate in the radiator, which is four times of the desired heat flux on the cooling surface for each e-motor. The radiator fan in the e-motor cooling cycle is operated such that

$$\dot{m}_{air} = \frac{4Q_{s,d}}{c_{p,air}(T_{air,o} - T_{amb})} \tag{2.48}$$

For comparison purpose, a classical PI controller is introduced to track the stator hotspot temperature and expressed as follows

$$\dot{m}_w = K_I \int R_3(\overrightarrow{t}_s - \overrightarrow{t}_{s,r})dt + K_P R_3(\overrightarrow{t}_s - \overrightarrow{t}_{s,r}) \tag{2.49}$$

For both e-motor cooling and the internal combustion engine cooling system, the mass flow rate of the coolant is proportional to the pump speed and the mass flow rate of the air is proportional to the fan speed. The power consumption rates of the fan and pump are simplified to be proportional to the cubic of the air mass flow rate and coolant mass flow rate, respectively. In the simulation, the cooling system power consumption requirement is provided by the AMESim fan/pump sub-model.

2.4 Numerical Results and Discussion of System Performance

To evaluate the proposed thermal management system, a numerical study is conducted on a series hybrid electric vehicle simulation. The hybrid electric vehicle model is developed with a MATLab/Simulink and AMESim co-simulation structure. The driver, supervisory controller, thermal management system controller, and the power system (include power pack, battery, e-motors, and powerbus) are developed with lookup data tables. The derived mathematical models are applied in the thermal management system simulation. The air conditioning system is modeled in AMESim; the cooling system is connected to the Simulink model using the AMESim-Simulink interface. The supervisory powertrain controller is programmed to optimize the power flow distribution in the system to ensure that the power output from the gen-set satisfies both the propulsion and cooling requirements. A Detailed introduction to

Table 2.1: Parameter Values and Simulation Specifications

Parameter	Value	Unit
C_{core}	268	$J/°C$
$c_{p,air}$	4090	$J/°C$
$c_{p,w}$	994	$J/°C$
C_s	18.8	$J/°C$
h_e	4000	$W/°C$
h_r	3500	$W/°C$
$M_{air,r}$	0.3	kg
$M_{w,e}$	2	kg
$M_{w,r}$	2	kg
R_c	1.266	$°C/W$
R_u	0.65	$°C/W$

Component	Specifications
Vehicle	Hybridized mid-size truck
Weight	14,000 kg
Engine	$7.2L$ Turbo-Diesel Engine: 330 kW
E-motors	Permanent Magnet: 4×95 kW
Battery Pack	Li-ion AHR32113 cells: 9 $kW \bullet h$

the series hybrid electric vehicle model is offered in (Zhang et al., 2014a). A summary of the thermal model parameters and the HEV simulation specifications are listed in the Table 2.1. An urban assault driving cycle and a convoy escort driving cycle are investigated in the study to evaluate the controller designs. The vehicle speed profile for both driving cycles is shown in Fig. 2.7. For each driving cycle, the battery current load profile is determined based on the vehicle speed profile and generated by the supervisory powertrain control unit.

For the purpose of comparisons, two different cooling system control methods are investigated. In Method 1, the powertrain thermal management system is oper-

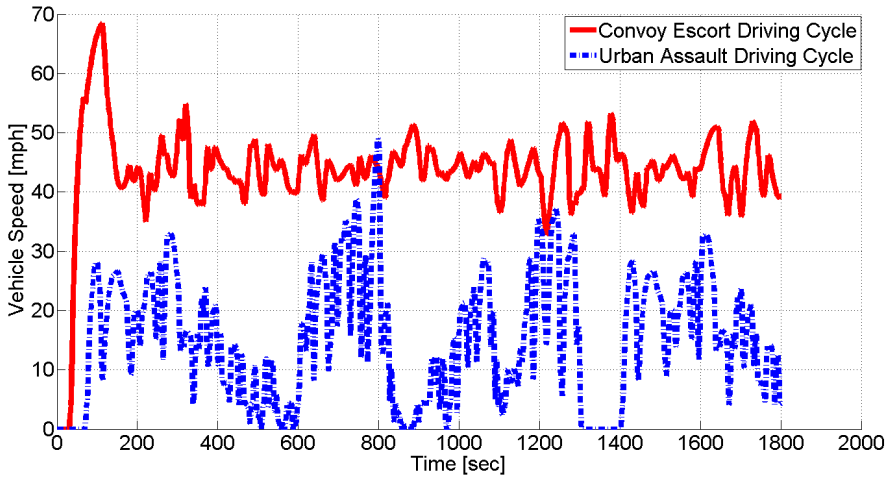

Figure 2.7: Vehicle Speed Profile for Urban Assault and Convoy Escort Driving Cycles

ated with the proposed controllers introduced in the Section 2.3. The target battery core temperature, $T_{core,r}$, is set as 30 $^{\circ}C$; the target engine coolant temperature at engine outlet, $T_{h,d}$, is 90 $^{\circ}C$ and the ideal e-motor internal hotspot temperature is set as 90 $^{\circ}C$. In Method 2, conventional thermal management control system is investigated with the same driving cycles. For the battery pack, the cooling system is operated by a on/off controller. When the battery core temperature reaches 30 $^{\circ}C$, the compressor in the air condition system is switched on and operates at its maximum speed, when the battery core is cooled under 29 $^{\circ}C$, the cooling system is switched off and the compressor operates at its minimum speed. The cooling air fan and the coolant pump in the engine cooling system is assumed to be driven by a belt, so their speeds are both proportional to the engine shaft speed. The e-motors cooling cycle is operated by a classical PI controller to regulated the stator internal hot spot temperature at target value of 90 $^{\circ}C$.

Eight tests were evaluated in the numerical simulation study. In Tests 2.1, 2.3, 2.5 and 2.7, the ambient temperature, T_{amb}, is set as 48 $^{\circ}C$. In the Tests 2.2, 2.4, 2.6 and 2.8, the ambient temperature is set as 25 $^{\circ}C$. In first four tests, the HEV

cooling system is operated with Method 1. In Tests 2.5 to 2.8, the cooling system is operated with Method 2. The temperature tracking performance in the battery core, the engine outlet coolant, and the e-motor stator hotspots will be investigated. The power consumption of the AC system compressor, the cooling air fans and coolant pumps for engine and e-motors are reported during the simulation. The driving cycle applied and the cooling method used in each test are listed in the Table 2.2.

Table 2.2: Numerical Study Test Conditions

Test	Cooling Algorithm	Driving Cycle	Surrounding Temperature [$°C$]
1	Method 1: Nonlinear Controllers	Urban Assault	48
2			25
3		Convoy Escort	48
4			25
5	Method 2: Conventional Controllers	Urban Assault	48
6			25
7		Convoy Escort	48
8			25

Fig. 2.8 shows the simulated battery and cooling air temperatures in Test 2.1. The battery core temperature is stabilized at 30 $°C$ with an average error of only 0.73 $°C$. In practical process, the weighting matrices R_1 and R_2 can be easily adjusted to reduce the cooling air temperature change range and compressor power consumption.

Table 2.3: Numerical Study Simulation Results

Test	Cooling System Actuators Power Consumption $[kJ]$					Mean Temperature Tracking Error $[°C]$		
	Engine Fan	Engine Pump	AC Compressor	E-motor Fan	E-motor Pump	Battery Core	Engine Coolant at Engine Outlet	E-motor Stator Hot Spot
2.1	4,554	1,350	701	10.3	3.0	0.73	0.4	2.3
2.2	1,109	284	193	1.7	0.6	0.8	0.7	1.9
2.3	11,260	3,293	745	36.4	10.6	0.7	0.4	1.2
2.4	2,725	696	201	10.2	2.9	0.7	0.75	1.1
2.5	6,420	1,6	650	14.3	4.17	1.1	7.88	2.8
2.6	6,420	1,6	370	5.1	1.46	1.3	N/A	2.8
2.7	12,360	3,120	632	15	4.6	1.1	4.1	1.3
2.8	12,360	3,120	360	9.1	2.62	1.1	N/A	1.3

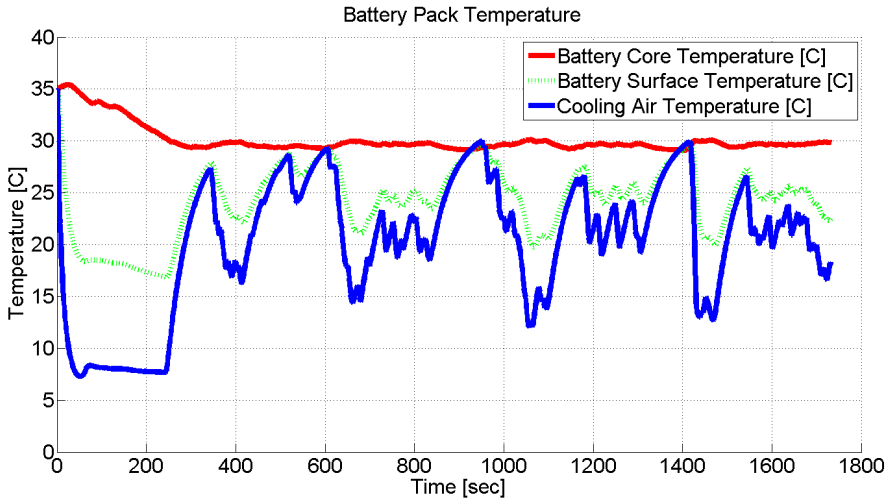

Figure 2.8: Test 2.1 - Battery and Cooling Air Temperatures for Urban Assault driving Cycle and Nonlinear Controllers

The engine and coolant temperatures simulated in Test 2.1 are displayed in Fig. 2.9. The coolant temperature at the engine outlet is maintained at target value of 90 $^{\circ}C$ with a small error of 0.4 $^{\circ}C$ and the temperature fluctuation in the engine itself is bellow 10 $^{\circ}C$.

The e-motors on the vehicle are heated by the conduction loss and core losses mainly in the stator, where the windings are located. Thus the cooling task focuses on the stator inner hotspots temperature tracking. Fig. 2.10 displays the simulation result of the electric motor cooling in Test 2.1. It can be observed that, the hotspot temperature inside the machine stator can be stabilized around the reference value. Meanwhile, the outer surface temperature only drops when the internal temperature is too high. The controller with full state feedback takes advantage of the temperature gradient from the heat generation points to the cooling surface which avoids the unnecessary cooling.

Fig. 2.11 presents the temperatures in battery package per Test 2.5. The battery core temperature in this test is also stabilized at target value with an average

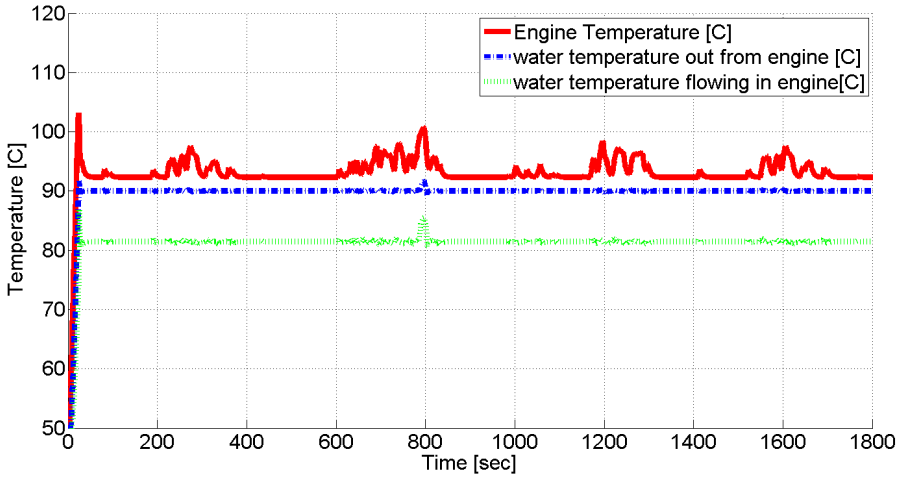

Figure 2.9: Test 2.1 - Engine and Coolant Temperatures for Urban Assault driving Cycle and Nonlinear Controllers

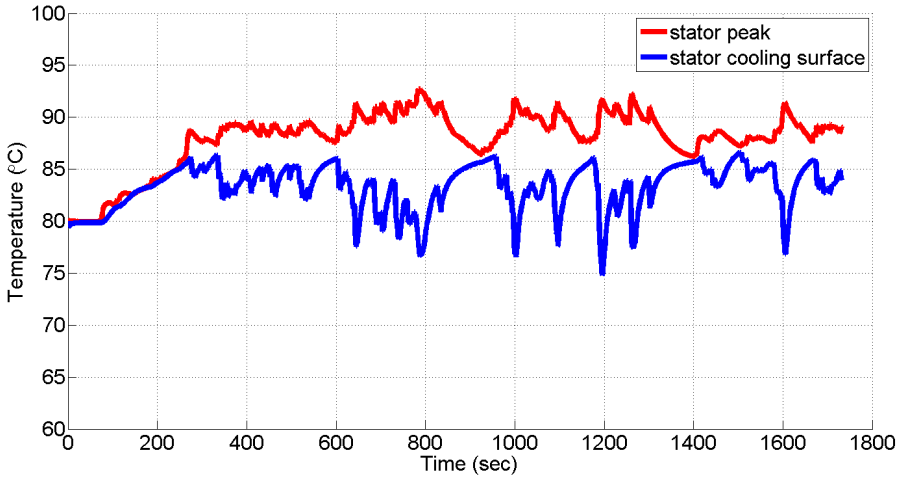

Figure 2.10: Test 2.1 - E-motor Temperatures for Urban Assault driving Cycle and Nonlinear Controllers

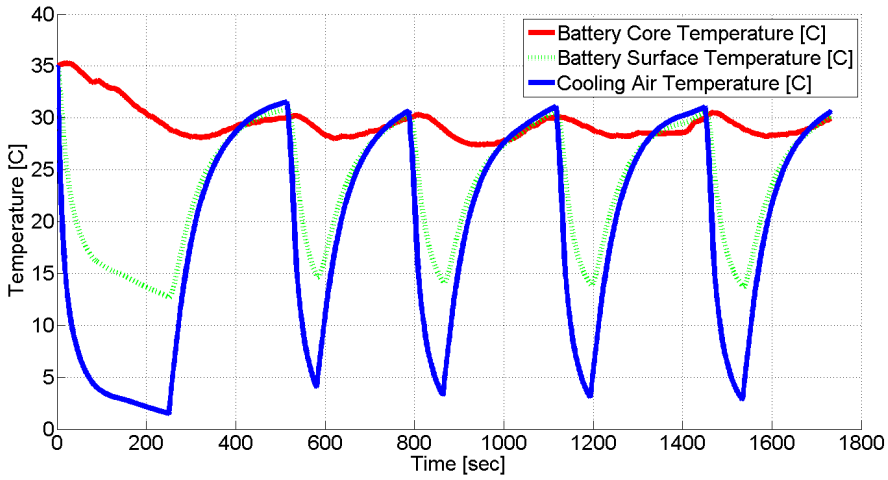

Figure 2.11: Test 2.5 - Battery and Cooling Air Temperatures for Urban Assault driving Cycle and Conventional Controllers

error of 1.13 $^{\circ}C$. The conventional on/off cooling strategy tends to consume larger power due to the constant speed of the compressor. The battery and the cooling air suffers a larger temperature fluctuation. In Test 2.5, the engine coolant pump and cooling air fan are both driven off the engine shaft. In this conventional open loop control, coolant temperature has no feedback for coolant pump regulation but only influences the opening of the coolant thermal valve. The unnecessary power consumed by the cooling system is very significant. Due to the fully opened valve (A3), during most of the driving cycle, it can be seen that the engine is over cooled. But when large heat generation occurs, the engine still suffers the risk of being overheated. In Test 2.5, the e-motors are cooled with a classical PI controller by tracking the stator's hotspot temperatures to the target value, 90 $^{\circ}C$. With only the stator hotspots temperature feedback, the simulation results show a large delay in temperature tracking. Both the hotspots and the cooling surface temperatures experience a large magnitude fluctuation.

Table 2.3 summarizes the temperature tracking errors and the power consump-

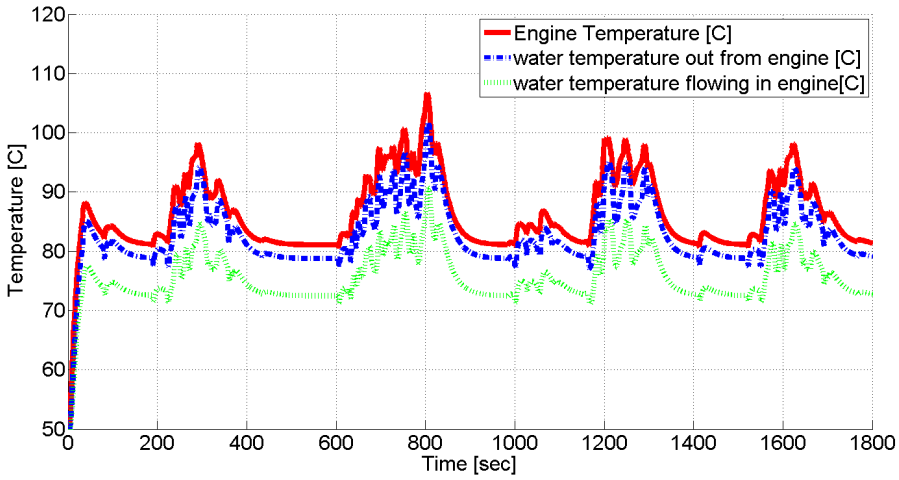

Figure 2.12: Test 2.5 - Engine and Coolant Temperatures for Urban Assault driving Cycle and Conventional Controllers

tion of the cooling system actuators for each test. In Method 2, the engine coolant pump and the fan speeds are directly coupled with the engine shaft. The open loop control method can hardly achieve coolant temperature tracking without the regulation of coolant valve opening. Once the speed ratio between the pump and the engine shaft is fixed for high ambient temperature condition, the engine will be overcooled in low temperature cases. Thus, the engine coolant temperature tracking errors for Tests 2.6 and 2.8 are not reported.

Comparing to the conventional cooling strategy, the proposed thermal management controllers provide excellent temperature tracking performance for cooling various subjects under different driving cycles and ambient temperatures. More importantly, the proposed cooling system control algorithm (Method 1 in Tests 2.1 to 2.4) offers an average 45% reduction in the total cooling power requirement compared to the conventional cooling methods (Method 2 in Tests 2.5 to 2.8).

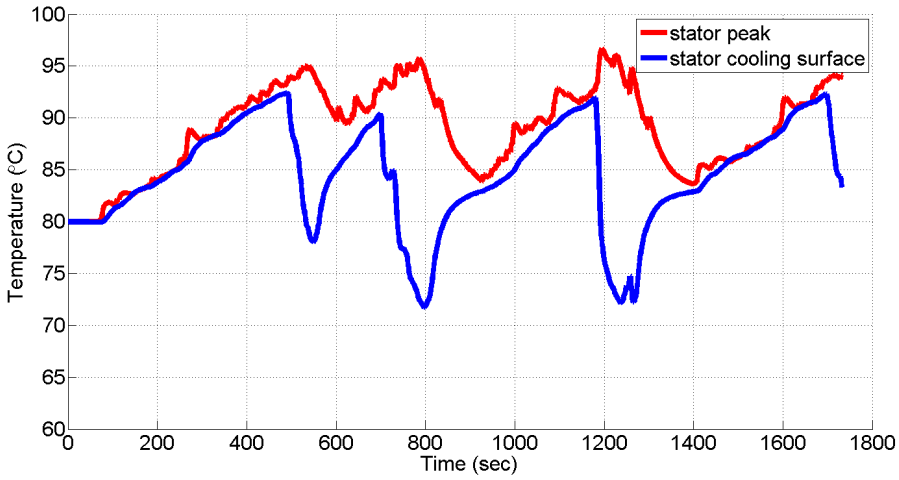

Figure 2.13: Test 2.5 - E-motor Temperature for Urban Assault Driving Cycle and Conventional Controllers

2.5 Summary

The thermal management system for the hybrid electric vehicle powertrains can be improved by applying mechatronic controlled, variable speed cooling system actuators. A series of thermal models for the heat generating components in a HEV powertain, including battery pack, internal combustion engine, and the electric motors, has been mathematically developed. Based on these thermal models, an optimal controller has been designed for the ideal battery cooling air calculation and a MPC controller is proposed for the air conditioning system compressor pump operation. A nonlinear control strategy was introduced for the engine coolant temperature stabilization while minimizing the system power consumption. The novel concept of e-motor thermal management was developed by taking advantage of a high fidelity 3D reduced ordered thermal model by determining a desired heat removal rate on the motor's cooling surface. Numerical simulations under prescribed driving cycles has demonstrated the advantages offered by the proposed control system in both temperature tracking and the power consumption reduction.

Chapter 3

Cooling Air Temperature and Mass Flow Rate Control for Hybrid Electric Vehicle Battery Thermal Management

Lithium-Ion (Li-ion) batteries are widely used in electric and hybrid electric vehicles for energy storage. However, a Li-ion battery's lifespan and performance is reduced if it's overheated during operation. To maintain the battery's temperature below established thresholds, the heat generated during charge/discharge must be removed and this requires an effective cooling system. This chapter introduces a battery thermal management system (BTMS) based on a dynamic thermal-electric model of a cylindrical battery. The heat generation rate estimated by this model helps to actively control the air mass flow rate. A nonlinear back-stepping controller and a linear optimal controller are developed to identify the ideal cooling air temperature which stabilizes the battery core temperature. The simulation of two different operating scenarios and three control strategies has been conducted. Simulation results indicate that the proposed controllers can stabilize the battery core temperature

with peak tracking errors smaller than 2.4 $^{\circ}C$ by regulating the cooling air temperature and mass flow rate. Overall the controllers developed for the battery thermal management system show improvements in both temperature tracking and cooling system power conservation, in comparison to the classical controller. The next step of this study is to integrate these elements into a holistic cooling configuration with AC system compressor control to minimize the cooling power consumption.

3.1 Introduction

The evolution of battery technology has prompted the replacement of the lead-acid and nickel-metal-batteries with Li-ion batteries. In current electric vehicles (EV) and hybrid electric vehicles (HEV), the Li-ion battery is widely chosen as an energy source due to its high power density and low self-discharge rate when not in use. For specific applications in EV/HEVs, the requirements of safety and reliability as well as long battery life should be taken into consideration. Thermal management is one of the most important tasks in battery management. Li-ion batteries generate a considerable amount of heat sourced from Joule losses during both the charge and the discharge phase. The volume of the battery package is usually very limited in vehicles, and the ventilating space for heat removal is small. Meanwhile, a Li-ion battery is very vulnerable in overheated environments during high C rate HEV operations. If the heat is accumulated in the battery package, the temperature exceeds certain limitations, which might lead to serious battery failure. Especially considering that high temperature will reduce the electric resistance at the battery electrode end, an even larger current might be resulted and leads to a higher heat generating rate. Therefore, the battery temperature should be strictly controlled within a narrow margin and avoid this kind of thermal runaway. Forced air or liquid cooling is required

in EV/HEVs' battery modules to effectively remove the heat.

Research on reliable battery thermal management system design focuses on several issues, including battery modeling, cooling structure design, and control algorithms. On the battery cell's level, finite element analysis (FEA) is one of the most applied methods in the battery thermal performance modeling. The FEA method is straightforward and provides accurate temperature prediction in different locations inside the battery package with various geometry and cooling structure (Yeow et al., 2012) (Karimi and Li, 2013). But it's too time-consuming for real time controller design. For the purpose of temperature stabilization control, high accuracy temperature prediction has been achieved using a very fast battery thermal modeling in state space form (Hu et al., 2011a). Forgez *et al.* (Forgez et al., 2010) introduced a lumped parameter thermal model of a cylindrical battery as the battery thermal behaviours were described by the dynamic change of battery core and surface temperatures.

On the battery module's level, a transient approach based on loosely coupled method was introduced to estimate temperature distribution within short simulation time in (Wang et al., 2011). Lin *et al.* (Lin et al., 2011) presented an online parametrization method and adaptive observer to estimate the cylindrical battery's core temperature and sensor deployment for overall temperature states observability. Discussions for maintaining uniformed battery module temperature also suggest cooling structure improvements (Duan and Naterer, 2010) (Sun et al., 2011) (Mahamud and Park, 2011) to regulate the cooling air flow path and assure the similar cooling condition for each battery cell. The thermal management system should be able to stabilize the battery temperature within a safe zone so that the battery bank won't be overheated during continuously high rate charging/ discharging and provide the overall optimal fuel efficiency without being switched off.

This study proposes an air cooling based battery thermal management system

which controls the temperature of the cooling air to stabilize the battery's internal temperature, applying a dynamic electrical-thermal coupled model of a cylindrical Li-ion battery and regulates the cooling air mass flow rate based on the estimated battery heat generation rate. The model simulates the battery power output, state-of-charge (SOC), heat generation and internal/surface temperatures change. The reminder of the paper is organized as follows. The modelling approach will be demonstrated in Section 3.2. A nonlinear back stepping controller and a linear optimal controller designed for inlet cooling air temperature control is introduced in Section 3.3. Simulations of two operating scenarios have been conducted, and the simulation result is discussed in Section 3.4. The conclusion of this chapter is contained in Section 3.5.

3.2 Mathematical Models

The battery's electrical and thermal behaviour interplay with each other and should both be considered in the battery cell modelling. A proper level of model complication is required for temperature control purposes. A microscopic battery model might be beneficial in analysing the electrochemical behaviour inside battery and gaining better understandings of the fundamentals governing the battery performance (Jayaraman et al., 2011) (Fang et al., 2010), but not necessary in controller designs for the battery thermal management system.

3.2.1 Electrical Model

In this study, the battery electrical behavior, represented by the Randles model (Guzzella and Sciarretta, 2007), is described by an equivalent circuit. The circuit contains an ideal power source, an internal resistance, and an equivalent RC network

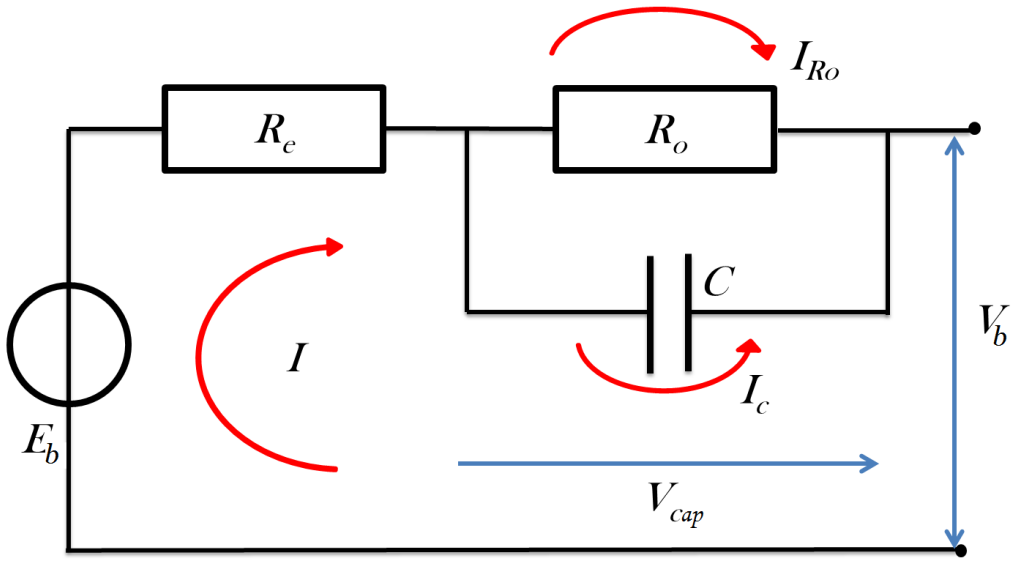

Figure 3.1: Randles Lumped Parameter Battery Model to Describe the Electrical System Transient.

shown as Fig. 3.1. The electric dynamic equations can be expressed as

$$\frac{\mathrm{d}V_{cap}}{\mathrm{d}t} = -\frac{V_{cap}}{R_o C} + \frac{1}{C} I \tag{3.1}$$

since

$$I - I_{R_o} + I_{cap} = \frac{V_{cap}}{R_o} + C\frac{\mathrm{d}V_{cap}}{\mathrm{d}t} \tag{3.2}$$

where I is the input current. The term V_{cap} denotes the voltage across the capacitor. The equivalent capacity, C, is a constant. The term is the current across the resistance R_o, and I is the current across the capacitor. The open circuit voltage, V_b, and the estimation of the state-of-charge (SOC) are the outputs of the electrical model. An online SOC estimation method was introduced in (Di Domenico et al., 2008). While the power distribution optimization and power train management are not the main topic of interests in this work, the SOC calculation in the simulation is simplified to a coulomb counting method, or $SOC = SOC_0 - \frac{1}{Ah}\int_{t_0}^{t} I\,(t)\,dt$. The term SOC_0 is the

initial battery state of charge, and Ah is the battery nominal energy capacity.

The internal electric resistances, R_e and R_o, are functions of the SOC, the battery core temperature, T_{core}, and the difference in the charge and discharge phases. In this study, the battery internal resistances of an AHR32113 Li-ion battery cell are approximated as

$$\begin{aligned} R_e &= \begin{cases} \alpha_1 - \beta_1 T_{core}; & \text{discharge} \\ \alpha_2 - \beta_2 T_{core}; & \text{charge} \end{cases} \\ R_o &= \begin{cases} \alpha_3 - \beta_3 T_{core} SOC; & \text{discharge} \\ \alpha_4 - \beta_4 T_{core} - \gamma SOC; & \text{charge} \end{cases} \end{aligned} \tag{3.3}$$

where $\alpha_i$andβ_i (for i=1, 2, ..., 4) and γ are the original resistance and influential coefficients. The values of these parameters are listed in the Table 3.1. The parametrizations given here are based on experimental battery characterization developed at Ohio State University, which have been modified to be representative of typical cylindrical batteries. The ideal power source, E_b, is also slightly influenced by the SOC and the temperature but assumed (A1) to be constant. Finally, the battery output voltage is obtained as

$$V_b = E_b - R_e I - V_e \tag{3.4}$$

3.2.2 Thermal Model

A lumped parameter thermal model is chosen for its effectiveness in representing dynamic changes of temperatures while not over computationally costing for real

time temperature control. The battery cell thermal model consists of three states: the battery core temperature, the battery surface temperature, and the temperature of the cooling air. The structure of the thermal model is shown in 3.2. The battery core thermal resistance, R_{core}, between T_{core} and T_s is a constant. The heat generation, Q_b, is approximated as the Joule loss, so that, with $I_{Ro} = \frac{V_{cap}}{R_o}$, the relationship becomes

$$Q_b = R_e I^2 + R_o I_{Ro}^2 \tag{3.5}$$

The lumped-parameter thermal model is a set of differential equations simulating the temperatures' transit change as

$$C_{core}\frac{\mathrm{d}T_{core}}{\mathrm{d}t} = \left(\frac{T_s - T_{core}}{R_{core}}\right) + Q_b \tag{3.6}$$

$$C_s\frac{\mathrm{d}T_s}{\mathrm{d}t} = \left(\frac{T_f - T_s}{R_u}\right) - \left(\frac{T_s - T_{core}}{R_{core}}\right) \tag{3.7}$$

The battery external thermal resistance, R_u, is determined by the convective heat transfer coefficient, h_b, at battery surface and it changes with the cooling fluid flow velocity. The average convective heat transfer coefficient for the entire batteries bundle can be analytically derived using heat transfer theory. The average Nusselt number for airflow across tube bundles composed in line layout is obtained as

$$Nu_D = 0.97 c Re_D^m Pr^{0.36}\left(\frac{Pr}{Pr_s}^{1/4}\right) \tag{3.8}$$

The Reynolds number,Re_D, may be expressed as

$$Re_D = \rho_{air} V_{max} D/\mu \tag{3.9}$$

The variable V_{max} is the maximum velocity of air flowing around the batteries and it's proportional to the cooling air mass flow rate, $\dot{m}_{air}$. The terms Pr and Pr_s are the Prandtl numbers of the cooling air evaluated at the cooling air and the cooling surface temperatures, respectively. The parameters c and m are factors determined by the distance between the battery cells and . The air density, ρ_{air}, the dynamic viscosity, μ, and the thermal conductivity, k_{air}, are related to the air temperature and considered constant in this work. When Re_D is larger than 2000, which satisfies most scenarios, the heat transfer coefficient h_b becomes

$$h_b = Nu_D \left(k_{air}/D\right) \tag{3.10}$$

When the cooling air flows across a row of battery cells, the cooling air is heated by the battery. The transit change of air temperature at the $k-th$ row of the cell is simulated as

$$C_{air}\frac{\mathrm{d}T_{f,k}}{\mathrm{d}t} = \frac{T_s - T_{f,k}}{R_u}\dot{m}_{air}c_{p,air}\left(T_{f,k-1} - T_{f,k}\right) \tag{3.11}$$

where the heat transfer resistance at the battery surface becomes $R_u = 1/\left(hA\right)$. The term A denotes the cooling surface area for each cell. The constant C_{air} is the heat capacity of the air stored inside the battery bank in the space surrounding one cell. Subscript k in Eq. (3.11) is the row index. A larger k means that the battery row is further away from the air inlet port. The cooling air temperature increases as it carries away the heat from the battery surface, hence, the larger k indicates higher cooling air temperatures. Eq. (3.11) described the temperature change of cooling air, which reflects the thermal performance of battery cells locates in different position. The temperature distribution across the whole battery bank should be as uniform as

possible. The temperature distribution uniformity can be improved by the cooling air flow path configuration design, the cooling surface optimization, and the compact geometry of the battery package (Damodaran et al., 2011)(Tran et al., 2014) (Park, 2013). The temperature change of the cooling air is the main factor leading to uneven temperature distribution across the battery bank (Xu and He, 2013).

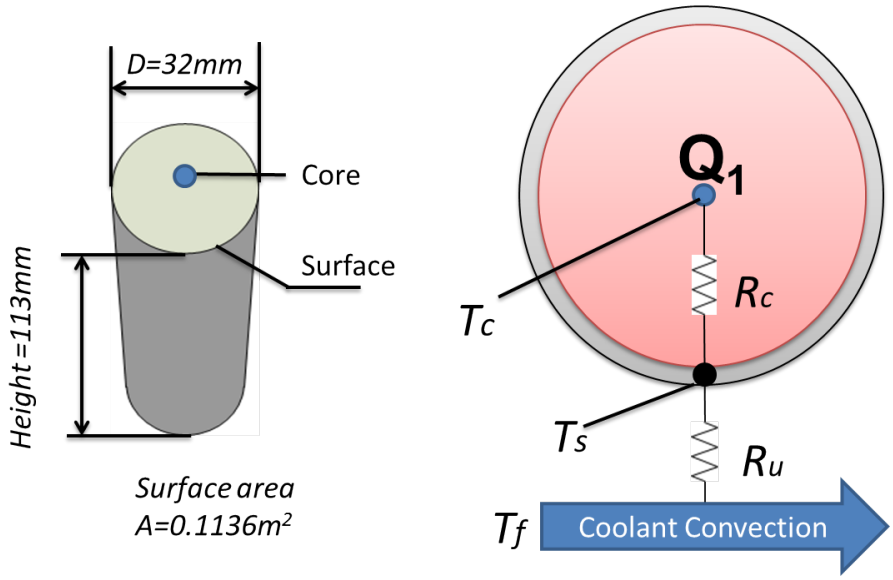

Figure 3.2: Single Battery Cell Thermal Model with Three Temperature States – Battery Core, T_{core}, Surface, T_s, and Cooling Air, T_f

Other than the temperature difference between the battery cells, large temperature gradients inside the battery cell also lead to non-uniformity in both the electrode reaction rates and the electrolyte concentration distributions (Gu and Wang, 2000). The layout of the battery cells influences the thermal resistance at the cooling surface, which also influences the prescribed temperature gradient. For the in-line layout, the battery cell distance can be denoted by SL and ST. The surface thermal resistance is mainly determined by the cooling air mass flow rate. With a given cooling air mass flow rate, smaller SL and ST provide a larger Reynolds number. Meanwhile, the closer the batteries are located to each other, higher pressure drops in the cooling air

flow will occur. Hence, a closer cell layout requires larger cooling air fan power. In this study, the battery pack consists of 240 AHR32113 cells. Each cell contains 14.6 $Watt \bullet hour$ of energy and its nominal discharging rate is 550 $Watts$. The batteries are evenly distributed in 12 power modules with 20 cells in each. In every module, 20 batteries layout in 10 columns and 2 rows. The cooling air is evenly routed into four streams and each stream of cooling air flows through three battery modules. Every three modules, including 60 battery cells, are cooled in one stream of cooling air.

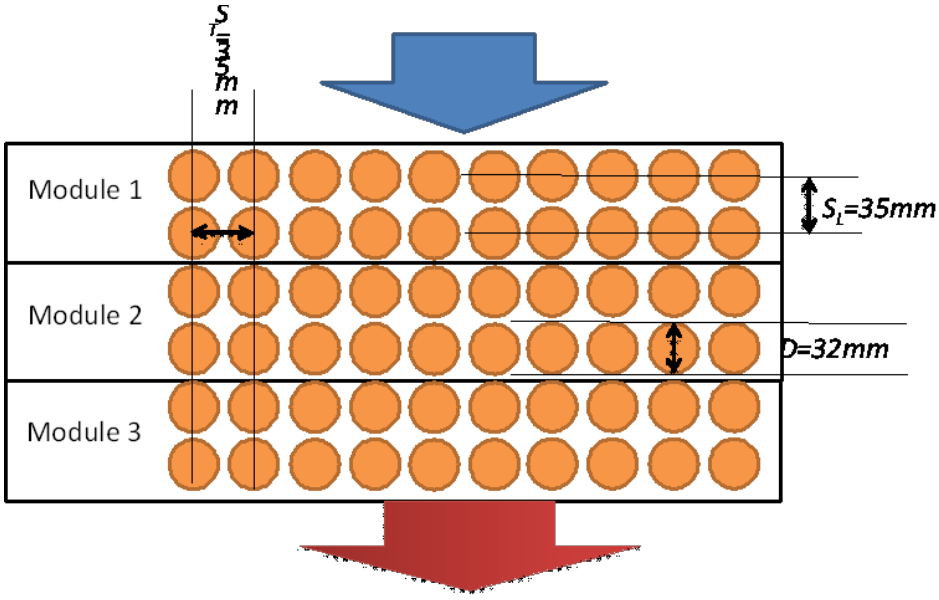

Figure 3.3: 60 Batteries in 3 Modules Layout in 10 Columns and 6 Rows along One Cooling Air Flow Path

With the symmetric layout of the battery cells and uniformed cooling air flow rate in each cooling fluid path, it's reasonable to assume (A2), that the cooling condition in every stream of cooling air is same. The cooling air flow and battery layout in the simulation is shown as Fig. 3.3. The manufacturing data and the simulation parameters of the thermal management system designed for AHR32112 package are listed in Table 3.1.

Table 3.1: Data Sheet for AHR32113 Cell and Thermal Model Parameters

Symbol	Value	Unit	Symbol	Value	Unit
A	0.01136	m_2	R_u	0.65	K/W
c	0.27	-	SOC_0	70%	-
C	1500	F	S_L	35	mm
C_{core}	148	J/K	S_T	35	mm
C_{air}	0.708	J/K	$T_{core,r}$	30	$°C$
$c_{p,air}$	993	$J/kg/°C$	Q_{avg}	0.94	kW
C_s	18.8	JK^{-1}	α_1, a_2	4e-3	-
D	32	mm	α_3	1.6e-3	-
E_b	3.3	V	α_4	8e-3	-
k	0.0258	W/mK	β_1	4.4e-5	-
K_I	-0.05	-	β_2	4.2e-5	-
K_p	-0.1	-	β_3	2.5e-5	-
m	0.63	-	β_4	2.5e-5	-
Pr	0.72	-	λ	3.6e-3	-
Pr_s	0.707	-	μ_{air}	14.82e-6	$Pa \bullet sec$
R_{core}	2.0	K/W	ρ_{air}	1.217	Kg/m^3

3.3 Controller Designs

The electrochemical reaction inside the battery core is largely influenced by temperature. The advanced thermal management system aims to stabilize battery internal temperature at reference value with minimum error. This section describes the procedures of calculating the mass flow rate and ideal temperature of the inlet cooling air. For optimal temperature calculation, three controllers are developed using a back stepping method, a linear optimal regulator method and the classical proportional integral approach. The estimated heat generating rate is applied to calculate the mass flow rate of the cooling air, which should be large enough to keep the temperature distribution across the battery bank uniform. The battery pack model is developed in MATLab/Simulink. The model structure is shown in Fig. 3.4. The inputs of the system are the battery load current and the cooling air. The thermal management actuators are the cooling air fan and the coolant compressor in the air

conditioning (AC) system. Thus the thermal management system can only regulate the mass flow rate and the inlet temperature of the cooling air. However, the heat generation determined by the input electrical current load can't be controlled.

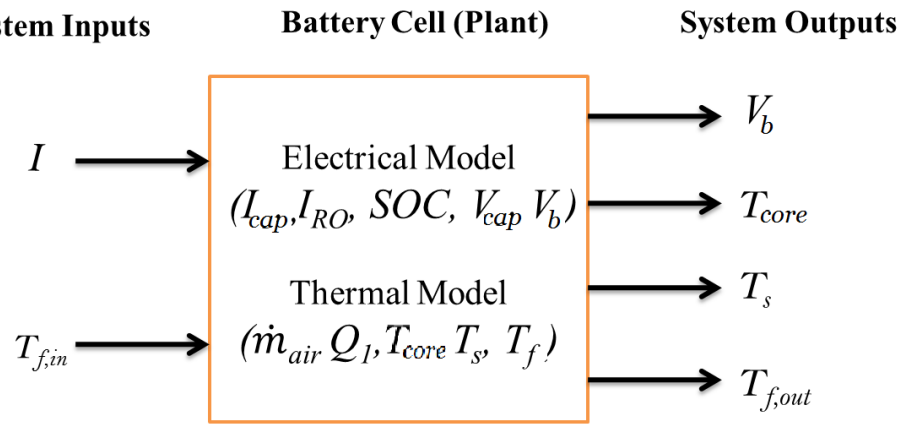

Figure 3.4: Battery Model Structure with System Inputs and Outputs

The temperature difference across the module is caused by the cooling air temperature change. The cooling air mass flow rate should be large enough so that the temperature change caused by the heat load is restricted to a reasonable small range. The cooling air mass flow rate of each stream is determined based on the relationship

$$\dot{m}_{air} = n_b Q_b \left[c_{p,air} \left(T_{f,o} - T_{f,in} \right) \right] \tag{3.12}$$

where and are the cooling air temperatures at the battery bank outlet and inlet. n_b is the number of battery cells cooled by this air flow, in this case 60. Specifically, assume (A3) that the heat carried away by the cooling air should be equal to the heat generated from the batteries. The term denotes the air temperature change after flowing across the battery bank which leads to uneven temperature distributions across the battery module. In this study the cooling air mass flow rate is controlled

such that. When the ambient temperature is high, it is difficult to achieve the battery core temperature stabilization by only controlling the cooling air mass flow rate (Zhang et al., 2014b). Given that the cooling air mass flow rate is large and provides a perfect heat transfer at the battery surface, the maximum possible heat removal rate limitation is

$$Q_{max} = n_b \left(T_{core} - T_f \right) / R_{core} \tag{3.13}$$

Other than the cooling air mass flow rate, the input cooling air temperature, $T_{f,in}$, should be controlled to insure that the heat removal rate, Q_{max}, can be large enough comparing to the heat generating rate, given the target core temperature and the internal thermal resistance R_{core} are constant. In this study, the controllers focus on achieving the ideal cooling air temperature. The AC system is applied to generate the cooling air. The ideal cooling air temperature is achieved by properly controlling the refrigerant compressor speed in the AC system. There are four assumptions imposed for the controller designs: (A4), All the temperature states, T_{core}, T_s, and T_f, can be measured with sensors. (A5), The heat generation rate, Q_b, can be estimated from the input current I. (A6), Battery cells in one row share the same cooling condition and cooling air temperature. (A7), Battery inner thermal resistance, R_{core}, is constant.

With the stated assumptions, the thermal performance can be described by a

single cell model. The battery model can be written in the state space form as

$$\begin{bmatrix} \frac{\mathrm{d}V_{cap}}{\mathrm{d}t} \\ \frac{\mathrm{d}T_{core}}{\mathrm{d}t} \\ \frac{\mathrm{d}T_s}{\mathrm{d}t} \\ \frac{\mathrm{d}T_f}{\mathrm{d}t} \end{bmatrix} = \begin{bmatrix} \frac{-1}{R_o C} & 0 & 0 & 0 \\ -\frac{2I}{R_o} & \frac{-1}{R_{core}C_{core}} & \frac{1}{R_{core}C_{core}} & 0 \\ 0 & \frac{1}{R_{core}C_s} & \frac{-1}{R_{core}C_s}+\frac{-1}{R_u C_s} & \frac{1}{R_u C_s} \\ 0 & 0 & \frac{1}{R_u C_{air}} & \frac{\left(-\dot{m}_{air}c_{p,air}-1\right)}{R_u C_{air}} \end{bmatrix} \begin{bmatrix} V_{cap} \\ T_{core} \\ T_s \\ T_{amb} \end{bmatrix} + \begin{bmatrix} 0 \\ 0 \\ 0 \\ \dot{m}_{air}c_{p,air} \end{bmatrix} T_{f,in} + \begin{bmatrix} \frac{I}{C} \\ \frac{1}{C}\left(\left(R_o+R_e\right)I^2 + C^2\left(\frac{\mathrm{d}V_{cap}}{\mathrm{d}t}\right)^2\right) \\ 0 \\ 0 \end{bmatrix} \tag{3.14}$$

3.3.1 Back Stepping Controller

Both the heat generation rate and the inlet cooling air temperature $T_{f,in}$, are the effective inputs that influence the battery core temperature. However, the heat generation rate can only be estimated by the model but not controllable by the thermal management system. Considering the nonlinear relationship between the current input, I and the temperature state, a cooling air temperature regulator with information of the system inputs, I and T_f,in using a Lyapunov-based nonlinear controller is designed for battery core temperature tracking, using the hand-crafted back stepping method (Salehi and Shahrokhi, 2009). Based on the electrical model and Eq. (3.5), the heat generating rate Q_b from battery core can be rewritten in the following form given the input current I as

$$Q_b = I^2\left(R_o+R_e\right) - 2CIR_o\frac{\mathrm{d}V_{cap}}{\mathrm{d}t} + C^2\left(\frac{\mathrm{d}V_{cap}}{\mathrm{d}t}\right)^2 R_o \tag{3.15}$$

where $\frac{\mathrm{d}V_{cap}}{\mathrm{d}t}$ is also derived as a function of I in Eq. (3.1). To quantify the battery core temperature stabilization performance, the tracking error is defined as

$$e_{core} = T_{core} - T_{core,r} \tag{3.16}$$

where $T_{core,r}$ is the desired value of T_{core}, and it is a constant. The time derivative of the tracking error based on Eq. (3.6) and Eq. (3.16) becomes

$$\frac{\mathrm{d}e_{core}}{\mathrm{d}t} = \frac{\mathrm{d}T_{core}}{\mathrm{d}t} = \frac{Q_b + (T_s - T_{core})/R_{core}}{C_{core}} \tag{3.17}$$

The controller design objective is to reduce the temperature tracking error, e_{core}. It is assumed that all the temperature states, T_{core}, T_s, and T_{air}, are measurable or can be estimated.

Define a positive definite function J_1 as

$$J_1 = \frac{e_{core}^2}{2} \tag{3.18}$$

The tracking error can be eliminated if the time derivative of J_1 is a negative definite function so that

$$\frac{\mathrm{d}J_1}{\mathrm{d}t} = e_{core}\frac{\mathrm{d}e_{core}}{\mathrm{d}t} = -k_1 e_{core}^2 \tag{3.19}$$

Along with Eq. (3.17), the desired temperature of battery surface, $T_{s,d}$, is solved as

$$T_{s,d} = T_{core} - Q_b R_{core} - k_1 e_{core} C_{core} R_{core} \tag{3.20}$$

The error between the actual surface temperature and its desired value, e_s,

can be defined as

$$e_s = T_s - T_{s,d}; e_s + T_{s,d} = T_s \tag{3.21}$$

By substituting T_s using Eq. (3.21), plug it in Eq. (3.17) and Eq. (3.19), the actual derivative of J_1 becomes $\frac{\mathrm{d}J_1}{\mathrm{d}t} = -k_1 e_{core}^2 + \frac{e_s}{R_{core}C_{core}} e_{core}$. To cancel out the positive term and eliminate the tracking error in the surface temperature state, define another positive definite function as

$$J_2 = \frac{1}{2} e_{core}^2 + \frac{1}{2} e_s^2 \tag{3.22}$$

Set the time derivative of L_2 as a negative definite function as

$$\begin{aligned} \frac{\mathrm{d}J_2}{\mathrm{d}t} &= e_{core}\frac{\mathrm{d}e_{core}}{\mathrm{d}t} + e_s\frac{\mathrm{d}e_s}{\mathrm{d}t} \\ &= -k_1 e_{T_{core}}^2 + \frac{e_s}{R_{core}C_{core}} e_{core} + e_s\frac{\mathrm{d}e_s}{\mathrm{d}t} = -k_1 e_{T_{core}}^2 - k_2 e_{T_s}^2 \end{aligned} \tag{3.23}$$

Based on the desired temperature of surface obtained in Eq. (3.20), the time derivative of e_s is written as

$$\frac{\mathrm{d}e_s}{\mathrm{d}t} = \frac{\mathrm{d}T_s}{\mathrm{d}t} - \frac{\mathrm{d}T_{core}}{\mathrm{d}t} + k_1 C_{core} R_{core} \frac{\mathrm{d}e_{core}}{\mathrm{d}t} + R_{core}\frac{\mathrm{d}Q_b}{\mathrm{d}t} \tag{3.24}$$

Combine Eq. (3.7), Eq. (3.23) and 3.24, so that the ideal cooling air temperature can be solved as

$$\begin{aligned} T_{f,in} = &\left(\frac{\mathrm{d}T_{core}}{\mathrm{d}t} - k_2 e_s e_s - k_1 \frac{\mathrm{d}e_{core}}{\mathrm{d}t} C_{core} R_{core} - \frac{e_{core}}{C_{core}R_{core}} \right) C_s R_u \\ &+ \frac{(T_s - T_{core})\, R_u}{R_{core}} + T_s \end{aligned} \tag{3.25}$$

The suggested input cooling air temperature in Eq. (3.25) stabilizes the battery core temperature by driving the error function J_2 to zero. It can be seen in

Section 3.4 that this controller designed with consideration of Q_b can successfully track $T_{core,r}$, but requires a large magnitude of input change.

3.3.2 Linear Optimal Controller

The system can be decoupled by replacing the input I with the heat generation rate, Q_b, derived from Eq. (3.5). The term Q_b is an uncontrollable disturbance. Because Q_b is determined by I and it can't be regulated by the thermal management system. By taking only the cooling air inlet temperature as the controllable input, the thermal model decoupled from the electrical model is rewritten in a linear state-space form as

$$\begin{bmatrix} \frac{\mathrm{d}T_{core}}{\mathrm{d}t} \\ \frac{\mathrm{d}T_s}{\mathrm{d}t} \\ \frac{\mathrm{d}T_f}{\mathrm{d}t} \end{bmatrix} = \begin{bmatrix} \frac{-1}{R_{core}C_{core}} & \frac{1}{R_{core}C_{core}} & 0 \\ \frac{1}{R_{core}C_s} & \left(\frac{-1}{R_{core}C_s} + \frac{-1}{R_uC_s}\right) & \frac{1}{R_uC_s} \\ 0 & \frac{1}{R_uC_{air}} & \frac{\left(-\dot{m}_{air}c_{p,air}-1\right)}{R_uC_{air}} \end{bmatrix} \begin{bmatrix} T_{core} \\ T_s \\ T_f \end{bmatrix} + \begin{bmatrix} \frac{1}{C_{core}} & 0 \\ 0 & 0 \\ 0 & \dot{m}_{air}c_{p,air} \end{bmatrix} \begin{bmatrix} Q_b \\ T_{f,in} \end{bmatrix} \tag{3.26}$$

where the state vector, X_b, and input, U_b, vectors are defined as $X_b = \left[T_{core}, T_s, T_f\right]^T$ and $U_b = \left[Q_b, T_{f,in}\right]^T$.

To avoid large magnitude input, the range of the inlet cooling air temperature should be restricted. An optimal controller is developed based on the thermal model to identify the ideal temperature of the cooling air at battery package inlet, $T_{f,in}$, by minimizing the function defined as

$$J_b = \int_{t0}^{t1} \left\{ \left[X_b - X_{b,r}\right]^T R_1 \left[X_b - X_{b,r}\right] + \tilde{U_b} R_2 \tilde{U_b} \right\} dt \tag{3.27}$$

where R_1, and R_2 are positive symmetric weighting matrices. A larger weighting coefficient would reduce the magnitude of the corresponding terms in the cost function. The objective state to be controlled is the battery core temperature, set $R_1 = [1,0,0;0,0,0;0,0,0]$ to reduce core temperature error. The variable $\tilde{U}_b$ is the magnitude of the inlet cooling air temperature change range. The first input of the thermal model, Q_b, is not regulated by the thermal management controller. The only controllable input is the inlet cooling air temperature, $T_{f,in}$. Design $R_2 = [1,0,0,0.01]$, the Q_b term in the cost function is applied a large weighting coefficient and the regulator mathematically restricted the ideal vary range of this uncontrollable input. With a smaller weighting coefficient on T_f, in term, the regulator essentially minimizes the cost function relying only on the second input of the system.

The optimal control law can be obtained by solving for the feedback controller gain matrix. The reference point, $T_{core,r}$, is not zero, and the linear optimal controller is written in the form

$$T_{f,in} = -F_0 X_b + H_c^{-1} X_{b,r} \tag{3.28}$$

in which

$$\begin{cases} H_c^{-1} = \left(R_1 \left(\mathbf{A}_b - \mathbf{B}_b F_0\right)^{-1} \mathbf{B}_b\right)^{-1} \\ F_0 = R_2^{-1} \mathbf{B}_b^T P; u_0 = H_c^{-1} X_{b,r} \\ T_{f,in} = -F_0 X_b + u_0 \end{cases} \tag{3.29}$$

where P is solved by an algebraic Riccati equation. The terms $\mathbf{A}_b$ and $\mathbf{B}_b$ are the matrices present in the state-space model per Eq. (3.26). The variable T_{air},in is the result of optimal inlet cooling air temperature obtained by calculating the feedback gain F_0 and feed forward gain H_c^{-1} in Eq. (3.28). The controller stabilizes the battery internal temperature by minimizing the cost function defined in Eq. (3.27).

Comparing to the back stepping controller introduced in last section, the op-

timal controller reduces the magnitude of ideal cooling air temperature range with a compensation term designed in the cost function, and thus it's more practical to be applied in AC system operation. The optimal controller takes advantage of the temperature gradient from battery core to battery surface and avoids unnecessary cooling. The controller design method is suitable for other battery models and cooling configurations. The thermal model can be replaced by more sophisticated ones such as FEA thermal model, in which case the size of the system matrix would be change but the design procedure is still valid.

3.3.3 Classical PI Controller

From historical perspective, control papers tend to evaluated various controller designs to demonstrate performance. The PI controller was chosen since it's widely used in the auto transfer industry to regulate temperature for electro mechanical systems. A classical proportional-integral (PI) controller is developed as

$$T_{f,in} = -K_P e_{core} + \int K_I e_{core} \mathrm{d}t \tag{3.30}$$

where e_{core} is the battery core temperature tracking error that defined in Eq. (3.16). The term K_I is the integral gain and K_P is the proportional gain defined using the PI tuner in Simulink and are both negative constants due to the way how e_{core} is defined.

3.4 Case Study - Numerical Results

Numerical simulations are conducted to validate the proposed thermal management control system designs. Eight tests with different electric current input

profile and cooling scenarios, as listed in Table 3.2, were implemented in the MATLab/Simulink and AMEsim simulations, for comparison.

Table 3.2: Simulation Scenarios for Tests 3.1 - 3.8

Case No.	Active Control	Input Current Load,I,(A)	Cooling Air Temp,$T_{f,in}$
3.1	Yes	30sin(0.01t)	Back Stepping Control
3.2	Yes		Optimal Control
3.3	No		Fixed; 25 $^{\circ}C$
3.4	Yes		PI Control
3.5	Yes	Urban Assault Drving Profile	Back Stepping Control
3.6	Yes		Optimal
3.7	No		Fixed; 25 $^{\circ}C$
3.8	Yes		PI Control

The back stepping controller designed in last section is implemented in Tests 3.1 and 3.5. The linear optimal controller is applied in Tests 3.2 and 3.6. A fixed cooling air temperature of 25 $^{\circ}C$ is offered in Tests 3.3 and 3.7. A classical PI controller is implemented with only battery core temperature feedback in Tests 3.4 and 3.8. When the cooling air flow rate is set as constant 0.27 kg/sec for all tests, the battery modules suffer an uneven temperature distribution. So in the Tests 3.2, 3.4, 3.6 and 3.8, the cooling air mass flow rate is applied as described in Eq. (3.12). The input of the simulation is the battery current load, I. In Tests 3.1 - 3.4, the input current is a sine wave with amplitude of 30 Amps. In Tests 3.5 to 3.8, the current load input to the battery model is from an urban assault profile. The current load profiles applied are shown in Fig. 3.5.

A vapour compression air conditioning (AC) system model, including an evaporator, a condenser, a electric coolant compressor with displacement of 100 ml, and a 20 mm diameter fan, was created in AMESim. In vapour compression systems, the power consumption required by the coolant compressor is generally larger than that of the cooling air fan motor since the compressor provides a pressure rise in the coolant

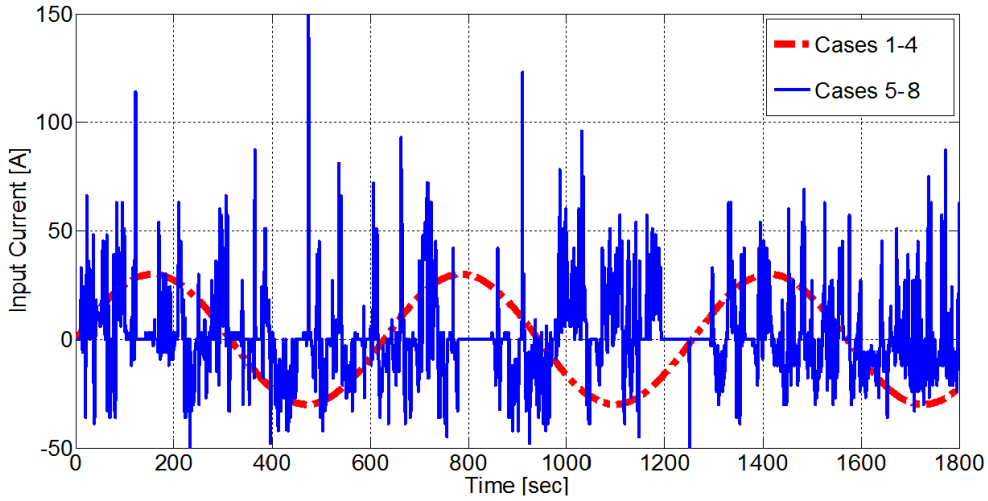

Figure 3.5: Input Current Profile for Tests 3.1 - 3.4 (Sine Wave), and for Tests 3.5 - 3.8 (Urban Assault)

flow path. In this study, only the power consumption of the coolant compressor is investigated, which is provided by the AMESim AC model. The total heat removal out from the battery module, Q_o, is obtained as a function of the temperature change in the cooling air and its mass flow rate as follows

$$Q_o = \int_0^t \dot{m}_{air} c_{p,air} \left(T_{f,o} - T_{f,in} \right) \mathrm{d}t \tag{3.31}$$

Four sets of data are investigated for the thermal management system performance evaluation. The simulation results of Tests 3.1 - 3.8 are listed in Table 3.3.

In Test 3.1, the input cooling air temperature is regulated by the back stepping controller. The simulated battery and cooling air temperatures are shown in Fig. 3.6. The battery core temperature tracking error is very small and stabilized around reference value well. The peak value of the tracking error is 0.62 $^{\circ}C$. In Test 3.2, the cooling air is sent into the battery bank at the ideal temperature calculated by

Table 3.3: Tests 3.1 - 3.8 Numerical Results

Test No.	Peak, Average Tracking error, max, average($^\circ C$)	Total Heat Removal, Q_o (kJ)	Peak Core Temperature Difference, $T_{core,6} - T_{core,1}$ $(^\circ C)$	Compressor Energy Consumption, $(kW \bullet hr)$
3.1	0.62,0.39	1,598	4.08	0.09
3.2	2.31, 0.85	1,484	3.44	0.08
3.3	12.54, 7.12	1,280	2.84	0.08
3.4	6.94,,0.01	1,328	4.12	0.10
3.5	0.84,,0.2	1,703	4.43	N/A
3.6	2.43,,0.67	1,628	3.91	0.10
3.7	8.27,,4.97	1452	3.24	0.04
3.8	3.52,,-0.53	1,650	3.52	0.11

the linear optimal controller. The error between the battery core temperature and its target value of 30 $^\circ C$ is smaller than 2.31 $^\circ C$.

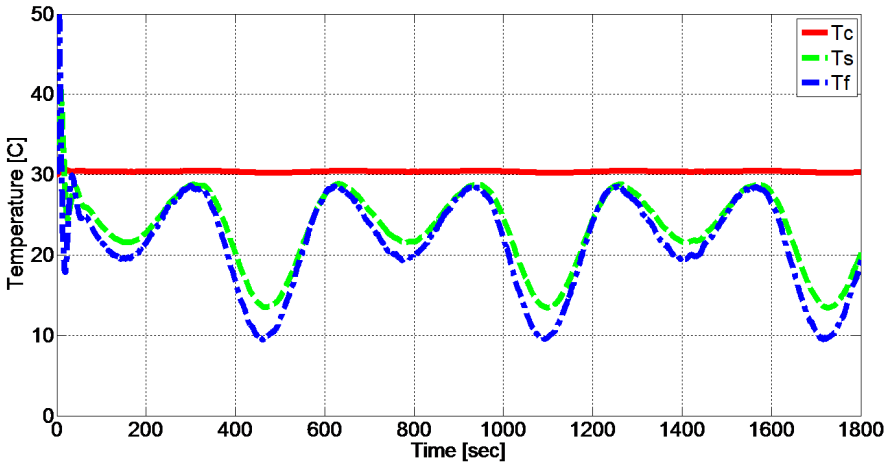

Figure 3.6: Test 3.1 - Battery Core, Battery Surface, and Cooling Air Temperatures Verse Time with Back Stepping Controller.

In Test 3.3, the cooling air temperature is fixed at 25 $^\circ C$. The first column of the battery and cooling air temperatures is shown in Fig. 3.7. With a fixed inlet cooling air temperature, the battery core temperature is hardly stabilized around the target value of 30 $^\circ C$. The tracking error reaches 12.54 $^\circ C$ and keeps increasing

at the end of the simulation. The heat removal, Q_o, in Test 3.1 is 24.8% larger than the total heat removal in this test which proves that active controlled cooling air temperature benefits the heat dissipated inside the battery modules. Comparing with Test 3.3, results of Tests 3.1 and 3.2 shows that the cooling air temperature control is an effective method in battery internal temperature stabilization. In Test 3.4, a classical PI controller is implemented and the battery core temperature is stabilized around the reference value but with a large tracking error. The energy consumed by the cooling system is larger than Tests 3.1 and 3.2.

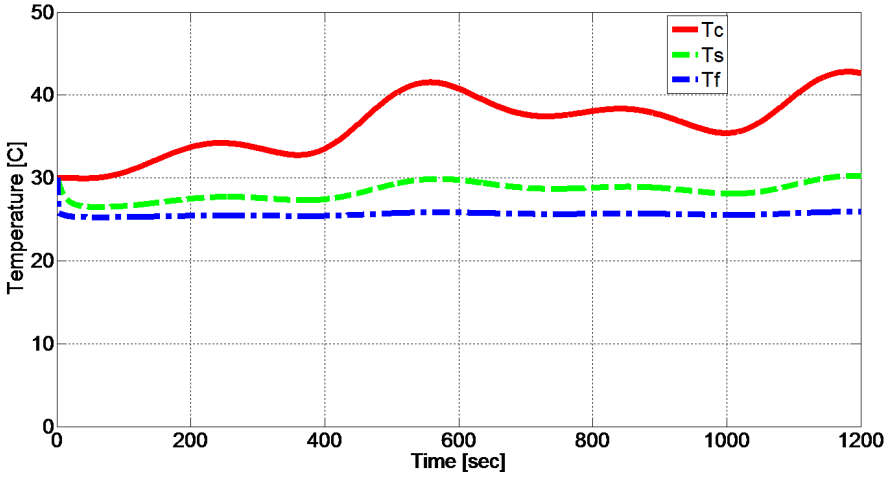

Figure 3.7: Test 3.3 - Battery Core, Battery Surface and Cooling Air Temperatures Vases Time with Fixed Cooling Temperature.

In Test 3.5, the current load applied on the battery pack is an urban assault profile per Fig. 3.5. The nonlinear back stepping controller is implemented; however the controller responds to the input current and heat generating rate. With the applied current profile of urban assault cycle, the ideal cooling air temperature changes drastically and not likely achieved by the AC system so the power consumption of the coolant compressor was not reported. The simulated result indicates that the battery internal temperature can be accurately stabilized at the target value by the back

stepping controller, assuming that the inlet cooling air temperature can be accurately tracked by the AC system. The simulated peak tracking error is 0.84 $^{\circ}C$.

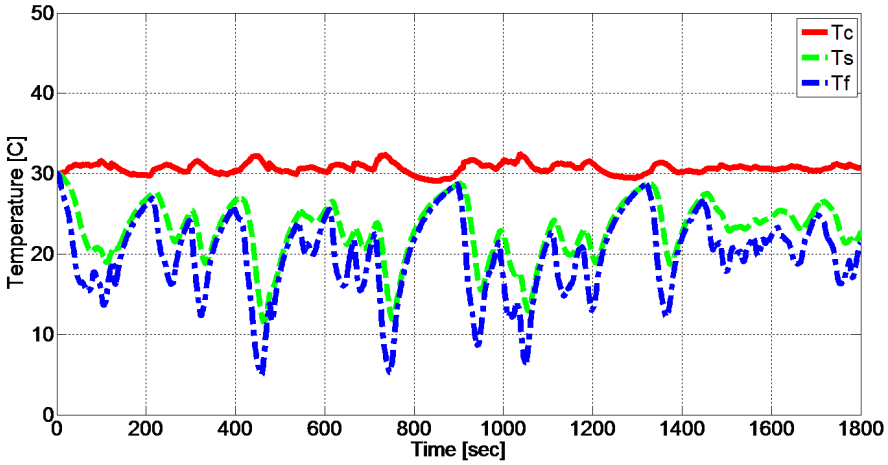

Figure 3.8: Test 3.6 - Battery Core, Surface, and Cooling Air Temperatures Verse Time with Linear Optimal Controller

In Test 3.6, the cooling air temperature is obtained for the optimal controller. The simulation results in Fig. 3.8 indicate that the internal battery temperature under the urban assault current load profile can be controlled with an error of 2.43 $^{\circ}C$. The total cooling air mass flow rate across the battery package is actively controlled using Eq. (3.12) based on the estimation of heat generation. The mass flow rate of the cooling air in the Test 3.6 is shown is the Fig. 3.9.

The cooling air temperature at the battery module inlet is fixed at 25 $^{\circ}C$ in Test 3.7. The results indicate that the battery internal temperature is not accurately tracked with a fixed temperature cooling air since the peak battery core temperature tracking error is 8.27 $^{\circ}C$ off the target value.

In Test 3.8, the input cooling air temperature is derived from a classical PI controller with the tracking error of the battery core temperature feedback. The simulated battery and cooling air temperatures are shown in Fig. 3.10. With the

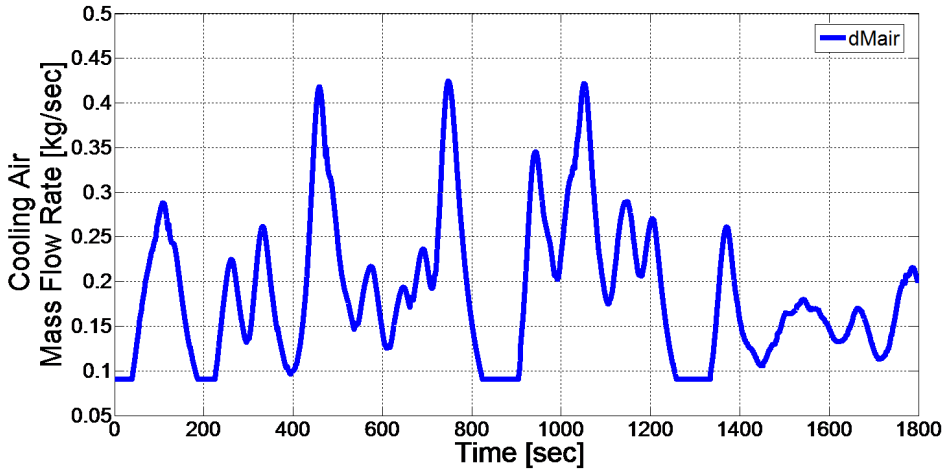

Figure 3.9: Test 3.6 - Cooling Air Mass Flow Rate Verse Time with Linear Optimal Controller

active control of the cooling air temperature, T_{air}, the battery core temperature is gradually stabilized around the target value after a relatively longer time. The heat removal is 1650 kJ but the energy consumed in the refrigerant compressor is 0.11 $kW \bullet hr$, and is higher than that in Test 3.6, which is 0.1 $kW \bullet hr$.

The numerical simulation results validate the proposed thermal management methods introduced in Section 3.2.1. With larger energy consumed by compressor in AC system comparing to that when the cooling air temperature is fixed at 25 $^{\circ}C$, the heat removal rate and battery internal temperature stabilization are significantly improved by actively controlling the cooling air temperature. It is clear that the cooling air temperature is a key variable to be controlled for battery core temperature tracking. The nonlinear back-stepping controller and linear optimal controller are designed to find the ideal inlet cooling air temperature. Both methods can stabilize the battery core temperature at target value within a small error. Comparing with a classical PI controller, the linear optimal controller offers better performance in both temperature stabilization and AC system power conservation.

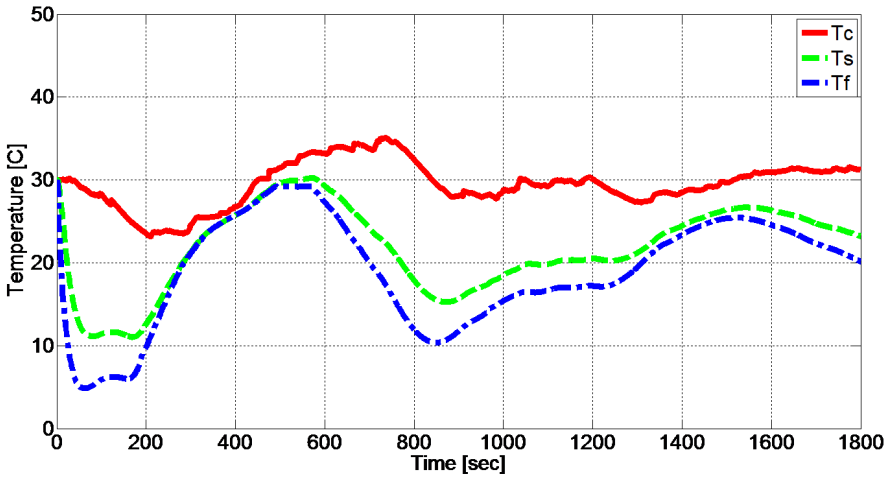

Figure 3.10: Test 3.8 - Battery Core, Battery Surface, and Cooling Air Temperatures Verse Time with Classical Controller

3.5 Summary

In hybrid power vehicles, Li-ion batteries are widely used for energy storage. With high rate current load applied on the batteries, the heat generated from Joule losses easily leads to battery system failure due to unsteady temperature control. To improve the battery core temperature stabilization, an electric-thermal model of the cylindrical Li-ion battery is developed for air-cooling battery thermal management systems. A nonlinear back-stepping controller and a linear optimal controller are proposed for ideal cooling air temperature calculations. Cooling air mass flow rate is obtained based on the heat generating rate from the battery thermal model to keep the temperature distribution uniform across the battery bank. The numerical results show that the battery internal temperature can be stabilized by controlling the optimal cooling air temperature with tracking errors smaller than 2.43 $^{\circ}C$. The improvements in cooling power conservation are observed by optimal controlling the cooling air temperature in comparison to a classical PI controller.

Chapter 4

Hybrid Electric Vehicle Battery Pack Thermal Management System - Modeling and Control

The lithium-ion battery pack in hybrid electric vehicles is an important energy storage device that requires proper thermal management. A considerable amount of heat is generated by the battery cells due to their internal resistance during charging and discharging, especially for peak vehicle loads. This study focuses on developing a smart controlled thermal management solution integrating a vapour compression system. A lumped parameter cylindrical battery thermal model is developed with a Kalman observer to estimates the transit temperature changes of the battery surface, battery core, and cooling air flowing around the cells. For the first time, the optimal battery cooling air temperature is investigated using optimal control theory. A model predictive controller is then introduced to regulate the refrigerant compressor and track the ideal cooling air temperature. In a case study, the power consumption of the thermal management system and the battery internal temperature behaviours

are investigated under an urban assault cycle. For various operation configurations and conditions, the numerical results demonstrate that peak error of the battery core temperature can be tracked within 0.25 $^{\circ}C$ of the target value and the cooling system energy consumption can be reduced by up to 58%.

4.1 Introduction

Battery performance is of great importance in electric and hybrid electric vehicle (HEV) operation. Battery cells generate a high amount of heat during charging and discharging, mainly due to internal resistance. This heat generation leads to a temperature rise inside the battery pack. The thermal behaviour of the batteries influences their chemistry and electrical reactions. In general, the battery capacity will be reduced if the temperature regularly exceeds the normal operating range. Consequently, batteries must be controlled within a certain desired working temperature level to ensure stable performance and long life. Much attention is now being focused on developing reliable thermal management systems for the battery package in ground vehicles.

A Li-ion battery with generally larger heat generation rate for given volume, is considered the most attractive electrical energy storage solution for its better power density than either lead-acid or NiMH batteries (Pollet et al., 2012). To realize higher HEV mileage and power output requirements, various topics on Li-ion battery thermal management system design have been studied. A large amount of research work has been completed on electric vehicle battery modeling (Fang et al., 2010)(Hu et al., 2011b). Peck *et al.* (Peck et al., 2012) developed a battery model to estimate current density, voltage distribution, and local heating on the electrodes. Gross and Clark (Gross and Clark, 2011) introduced a battery life aging model and applied it to

real world environmental conditions, which permitted optimization of battery thermal management strategies. Sun *et al.* (Sun et al., 2011) discussed the effect of different cooling structures on the heat rejection from battery packs. Teng and Yeow (Teng, 2012)(Teng and Yeow, 2012) developed a series of battery thermal models using a finite element analysis approach. Lastly, a systematic approach for Li-ion battery thermal management was proposed by Jayaraman *et al.* (Jayaraman et al., 2011).

This dissertation investigates a computer controlled battery thermal management system (BTMS) to stabilize the internal temperature of battery cells by tracking a prescribed cooling air temperature applying a vapor compression air conditioning (AC) system. A cylindrical battery cell applied in the standard commercial A123 system (Pistoia, 2014) was chosen as the object of this study. The AC system is modeled in AMESim. A battery electric-thermal model is created to estimate the transit temperature change of the battery surface, battery core, and the coolant flowing through the battery bank. The battery model also simulates the electrical output voltage and the state of charge (SOC). The model-based battery cooling controller has been designed to determine the optimal inlet cooling air temperature. Next, a model predictive controller is applied to the air condition system to track the desired cooling air temperature as determined by the battery cooling controller. The overall thermal management system structure is shown in Fig. 4.1. This chapter also investigates how different cooling structures affect the cooling air temperature tracking and their influences on heat removal efficiency to provide insights into battery thermal management design and manufacture process.

The reminder of the chapter is organized as follows. In Section 4.2, an AHR32113 cylindrical battery cell model is mathematically described. The procedures to calculate the ideal cooling air temperature using a Kalman filter and a linear optimal controller are outlined in Section 4.3. Section 4.4 introduces a model predictive con-

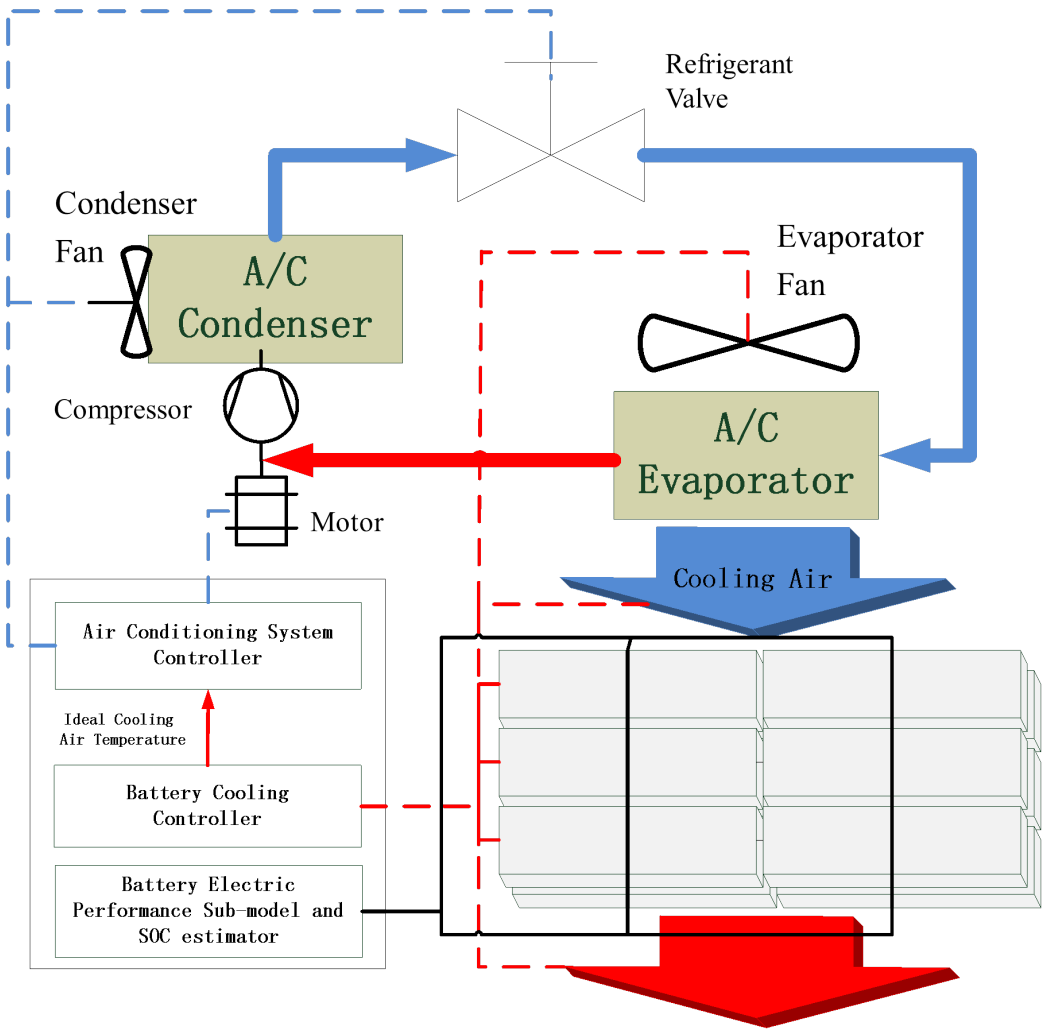

Figure 4.1: Battery Thermal Management System Structure

troller designed to regulate the refrigerant compressor speed in the AC system and provide the ideal cooling air temperature. Section 4.5 presents the numerical results for a battery thermal management system performance. The simulation results demonstrate that the proposed control method works as expected and stabilizes the battery temperature around the target value with a small error. Section 4.6 concludes this chapter.

4.2 Battery Pack Model

In this study, the selected battery pack has a nominal power rating of 110 kW powered by 240 AHR32113 cells. The batteries are evenly distributed in 12 modules with 20 cells each. The battery layout in every module is uniformed - 10 columns and 2 rows. Three modules, 6 rows of battery cells in total, are cooled in the same air stream as shown in Fig. 4.1. To identify the ideal temperature of inlet cooling air $T_{core,r}$, and the air mass flow rate necessary to remove the heat load, $\dot{m}_{air}$, the battery pack model considers three factors: electrical dynamics, state of charge (SOC), and thermal behaviour as shown in Fig. 4.2.

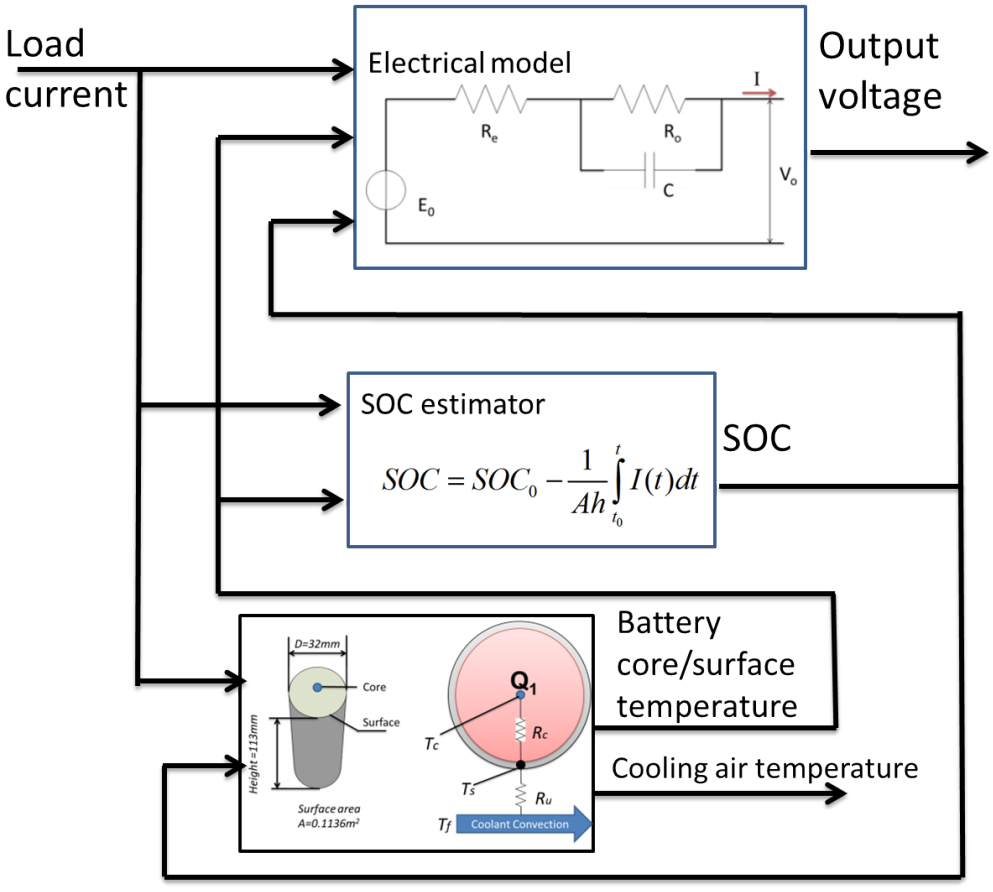

Figure 4.2: Battery Thermal Electric Model Structure

The battery's electrical behavior is represented by the Randles model (Guzzella and Sciarretta, 2007) corresponding to a simplified circuit. The model describes the battery with an ideal power source, an internal resistance, and a RC network. The electric dynamic equation can be expressed as

$$V_b = E_b - R_e I - V_e \tag{4.1}$$

where $I = C\frac{\mathrm{d}V_e}{\mathrm{d}t} + \frac{V_e}{R_e}$, Eq. (4.1) can be rewritten as $R_e I = E_b - V_b - V_{cap}$, so the above relationships becomes

$$R_e C \frac{\mathrm{d}V_{cap}}{\mathrm{d}t} = E_b - V_b - V_{cap}\left(1 + \frac{R_e}{R_b}\right) \tag{4.2}$$

where $I = C\frac{\mathrm{d}V_{cap}}{\mathrm{d}t} + \frac{V_{cap}}{R_{cap}}$. Eq. (4.1) can be rewritten as $R_{cap} I = E_b - V_b - V_{cap}$, so the above relationships becomes

$$C_{core}\frac{\mathrm{d}T_{core}}{\mathrm{d}t} = \left(\frac{T_s - T_{core}}{R_{core}}\right) + Q_b \tag{4.3}$$

where V_{cap} is the voltage applied on the capacitor, and V_b is the battery output voltage. The load current, I , is an input to the battery electric sub-model.

The values of R_e and R_{cap} in the electric model are dependent on the SOC, battery core temperature, T_{core}, and the difference in the charge and discharge phases. The state of charge estimator output includes the open source voltage, the SOC, and the internal resistances R_b and R_{cap}. A detailed online SOC estimation method using a Kalman filter was introduced in (Di Domenico et al., 2008), but the power distribution optimization is not the main topic of interest. In this work, the SOC calculation is simplified to a Coulomb Counting method, $SOC = SOC_0 - \frac{1}{Ah}\int_{t0}^{t} I(t)\,\mathrm{d}t$. The term SOC_0 is the initial battery state of charge, and Ah is the battery's nominal capacity.

The battery thermal sub model is derived based on a two-state, surface temperature, T_s, and core temperature, T_{core}, cylindrical battery thermal model introduced by Forgez *et al.* (Forgez et al., 2010) introduced (refer to Fig. 4.2) with the dynamics

$$C_s \frac{\mathrm{d}T_s}{\mathrm{d}t} = \left(\frac{T_f - T_s}{R_u}\right) - \left(\frac{T_s - T_{core}}{R_{core}}\right) \tag{4.4}$$

The parameters C_{core} and C_s are the heat capacity of the battery core and the battery surface, respectively. The thermal resistance, R_{core}, between the battery core and the battery surface, was assumed to be a constant value (A4). And the thermal resistance between the battery surface and the cooling air, R_u , is decided by the convective heat transfer coefficient, h, on the battery surface and convective transfer area. Lin *et al.* (Lin et al., 2011) proposed a parameterization method to estimate , C_{core}, C_s, R_{core} and R_e. The heat generation rate, Q_b, is approximately equal to the concentrated Joule loss as

$$Q_b = I^2 R_e + I_{Rb}^2 R_b \tag{4.5}$$

The relationship between the cooling air flow rate requirement and the heat generation rate in the battery pack was established in (Damodaran et al., 2011). The cooling air flow rate is determined to maintain a uniform temperature distribution across the battery bank and effectively expel the heat. The air temperature change should be controlled under 5 $^{\circ}C$. The battery surface convective heat transfer coefficient, h, varies with the cooling air mass flow rate and the average convective heat transfer coefficient for the entire batteries bundle is derived by the average Nusselt number for air flow across the tube bundles composed of 10 rows

$$Re_D = \rho_{air} V_{max} D/\mu \tag{4.6}$$

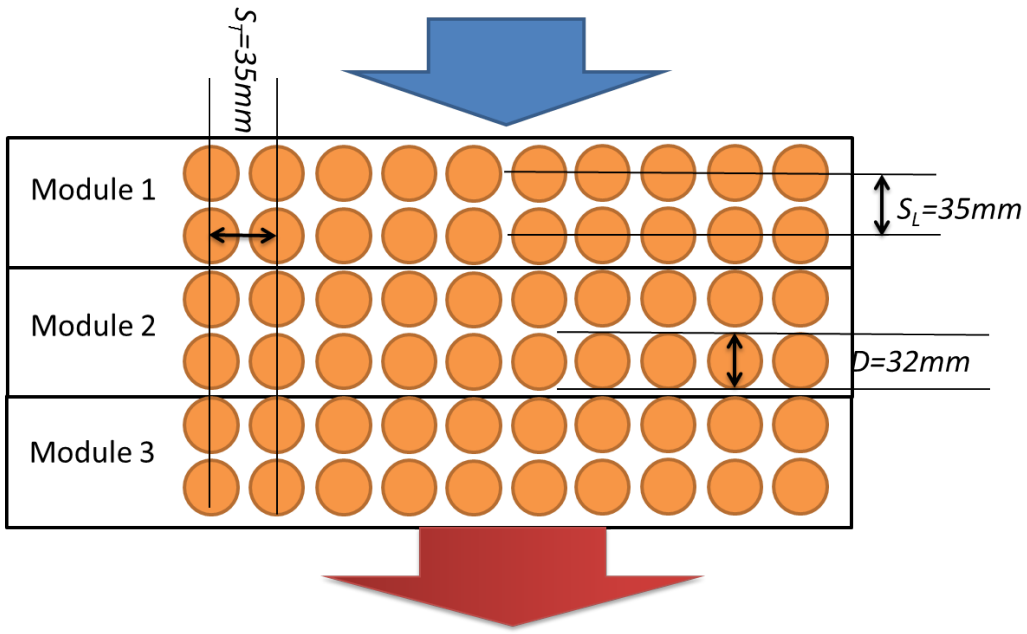

Figure 4.3: Battery Layout Configuration in Three Modules (Top View)

$$Nu_D = 0.262 Re_D^m Pr^c \left(\frac{Pr}{Pr_s}^{1/4} \right) \tag{4.7}$$

where c and m are factors determined by the distance between each cell, the number of battery rows and Re_D. When $Re > 2000$, as it is in this case, the heat transfer coefficient, h_b, is given as

$$h_b = Nu_D \, (k_{air}/D) \tag{4.8}$$

The configuration parameters of the battery cells inside the module can be described by the battery distances, SL and ST, as shown in Fig. 4.3 per top view of three lined up battery modules.

The variable V_{max} in Eq. (4.6) denotes the maximum air flow velocity inside the battery pack. Since the batteries are placed in lines, the maximum flow velocity

can be calculated as

$$V_{max} = \left(\frac{\dot{m}_{air}}{\rho_{air} A_{cross}}\right)\left(\frac{S_T}{S_T - D}\right) \tag{4.9}$$

The air density, ρ_{air}, the dynamic viscosity, μ, and the air thermal conductivity k_{air}, are considered constant. The values of A_{cross}, D, S_L, and S_T are also fixed. Substituting the thermal characteristics of air in Table 4.1 into Eq. (4.6) through Eq. (4.9), allows the estimated relationship between the cooling air mass flow rate and the battery surface convective heat transfer coefficient to be expressed in a simplified form as

$$h_b = 617.04 \dot{m}_{air}^{0.6} \tag{4.10}$$

Using the convective heat transfer coefficient, the differential equation describing the cooling air transit temperature change flows across the battery bank is written as

$$C_f \frac{\mathrm{d}T_{f,k}}{\mathrm{d}t} = \frac{T_s - T_{f,k}}{R_u} \dot{m}_{air} c_{p,air} \left(T_{f,k-1} - T_{f,k}\right) \tag{4.11}$$

where $R_u = 1/(h_b A_b)$ is the thermal resistance at the battery surface and A_b is the battery cooling surface area. The parameter C_f is the heat capacity of the air surrounding one battery column, $c_{p,air}$is the specific heat of air under atmosphere pressure, and the subscript k is the column index. A larger k means that the column is positioned further away from the air inlet port. The cooling air temperature, $T_{f,k}$, denotes the air temperature at the $k-th$ column's outlet position. This thermal model of cooling air reflects its temperature change at different battery columns, and estimates the resulting uneven temperature distribution inside the battery bank.

4.3 Optimal Control and Kalman Filter for Battery Core Temperature

Traditional battery thermal management system designs often consider the cooling air mass flow rate, but do not select the cooling air temperature as a control variable. Constant inlet air temperature may not achieve the target battery core temperature stabilization regardless of the applied cooling air mass flow rate., especially when the heat generation rate exceeds a critical value (for instance, if the $Q_b > (T_{core,r} - T_f)/R_{core}$, the target temperature will not be reached) (Teng et al., 2011). This section will introduce an observer to estimate the battery core temperature, and an optimal controller to calculate the ideal inlet cooling air temperature.

The lumped parameter thermal model for the cylindrical battery and cooling system establish a basis for the controller design. Given a constant cooling air mass flow rate, the cooling surface heat transfer coefficient is time invariant too. Considering the battery heat generated, Q_b, in Eq. (4.3), and the inlet cooling air temperature, $T_{f,0}$, in Eq. (4.11) as the system inputs, the thermal model of the battery cell in first column can be expressed in a linear state space form as

$$\begin{bmatrix} \frac{\mathrm{d}T_{core}}{\mathrm{d}t} \\ \frac{\mathrm{d}T_s}{\mathrm{d}t} \\ \frac{\mathrm{d}T_f}{\mathrm{d}t} \end{bmatrix} = \begin{bmatrix} \frac{-1}{R_{core}C_{core}} & \frac{1}{R_{core}C_{core}} & 0 \\ \frac{1}{R_{core}C_s} & \left(\frac{-1}{R_{core}C_s} + \frac{-1}{R_uC_s}\right) & \frac{1}{R_uC_s} \\ 0 & \frac{1}{R_uC_f} & \frac{\left(-\dot{m}_{air}c_{p,air}-1\right)}{R_uC_f} \end{bmatrix} \begin{bmatrix} T_{core} \\ T_s \\ T_f \end{bmatrix} + \begin{bmatrix} \frac{1}{C_{core}} & 0 \\ 0 & 0 \\ 0 & \dot{m}_{air}c_{p,air} \end{bmatrix} \begin{bmatrix} Q_b \\ T_{f,in} \end{bmatrix} \tag{4.12}$$

The battery surface and cooling air temperature, T_s and T_f , can be directly

measured, but the battery core temperature, T_{core} , cannot be measured by sensors. The error in the battery core temperature estimation exists due to heat generation calculation uncertainties, and the lack of core temperature feedback. The model output is defined as

$$\hat{Y} = \begin{bmatrix} T_s \\ T_f \end{bmatrix} = \begin{bmatrix} 0 & 1 & 0 \\ 0 & 0 & 1 \end{bmatrix} \begin{bmatrix} T_{core} \\ T_s \\ T_f \end{bmatrix} \tag{4.13}$$

The battery core temperature stabilization problem can be solved by using linear optimal control theory. This system can be shown to be both observable and controllable. From a controller design stand point, the battery heat generation is not a controllable input but rather considered to be a disturbance as it's not determined by the cooling system. To find the optimal inlet cooling air temperature, $T_{f,d}$, to remove the generated heat, the battery core temperature must be estimated.

An observer is required to correct the battery core temperature. The observer is built using Kalman filter theory, to estimate the unmeasured temperature states, based on measured states, T_s and T_f. Several assumptions are applied in the observer design process. (A1), Battery cells located in same column share a uniform cooling condition; (A2), Only battery surface and the cooling air temperatures, T_s and T_f, can be measured with sensors; (A3), Constant and uniform cooling fluid (air) flow rate, $\dot{m}_{air}$ (constant thermal resistance R_u at battery surface) across all batteries; and (A4), Battery inner thermal resistance, R_{core}, is constant.

The observer is constructed in the following form

$$\begin{cases} \dot{\hat{X}}_b = \mathbf{A}_b \hat{X}_b + \mathbf{B}_b U_b + L\left(y - \mathbf{C}_b \hat{X}_b\right) \\ Y = \mathbf{C}_b \hat{X}_b \end{cases} \tag{4.14}$$

where $\mathbf{A}_b$ and $\mathbf{B}_b$ are the system matrices defined in the Eq. (4.12) The feedback gain matrix, L, is designed to minimize the cost function that may be defined as $\int_{t_0}^{t_1} \left[e^T(t) W e(t)\right] \mathrm{d}t$ where $e = X_b - \hat{X}_b$ and W is the weighting matrix.

$$L = QC^T \left(ww^T\right)^{-1} \tag{4.15}$$

The mean measurement error vector maybe defined as $w = [w_1; w_2]$, where w_1 is mean error magnitude of the battery surface temperature sensors, and w_2 is the mean error magnitude of the cooling air temperature sensors. In Eq. (4.15), Q is obtained by finding the nonnegative definite symmetric solution of a corresponding algebraic Riccati equation, and the gain matrices L can be solved off-line, given that the system matrices and the measurement noise magnitude vector are time invariant.

With the corrected estimation of the battery core temperature, the optimal temperature of the inlet cooling air, $T_{f,d}$, can be determined by applying the optimal controller design technique. The control law is designed to minimize the selected function

$$\int_{t_0}^{t_1} \left\{ \left[X_{b,r}(t) - \hat{X}_b(t)\right]^T R_1 \left[X_{b,r}(t) - \hat{X}_b(t)\right] + \tilde{U}^T R_2 \tilde{U} \right\} \mathrm{d}t \tag{4.16}$$

where R_1 and R_2 are positive symmetric weighting matrices. In this study, $R_1 = [1,0,0;0,0,0;0,0,0]$ and $R_2 = [1,0;0.001,0]$ were selected to stabilize the battery core temperature, T_{core} , to its reference value, $T_{core,r}$ .The variable $\tilde{U} = \left[Q_b, T_{f,d} - U_0\right]^T$ is

the input magnitude vector from Eq. (4.12). The first element is the heat generation rate, and the second element is the range of the target inlet cooling air temperature.

The optimal control law is obtained by solving the feedback and feed forward gain matrices with the set point . The linear optimal controller is constructed as

$$\begin{cases} H_c = \left(R_1 \left(\mathbf{A}_b - \mathbf{B}_b F_0\right)^{-1} \mathbf{B}_b \right. \\ F_0 = R_2^{-1} \mathbf{B}_b^T P; U_0 = H_c^{-1} X_{b,r} \\ U_b = -F_0 \hat{X}_b + U_0 \end{cases} \tag{4.17}$$

in which P is solved as the non-negative definite solution of the corresponding algebraic Riccati equation. The term is an adjusting parameter. The controller obtains the ideal inlet cooling air temperature, $T_{f,d}$, as the second element in the optimal input

$$T_{f,d} = U_b(2) \tag{4.18}$$

The ideal inlet cooling air temperature to minimize the cost function in Eq. (4.16) is identified in Eq. (4.18).

4.4 Model Predictive Controller for AC System

In this section, a controller will be constructed to track the ideal cooling air temperature by regulating the air conditioning (AC) refrigerant compressor speed using model predictive control theory. The AC system typically consists of a compressor, a condenser, an expansion valve, an evaporator, and an accumulator. These components are connected by a set of tubes and pipes. A big dynamic modeling challenge lies in accurately addressing the phase changing (liquid, two phase or superheated vapor) of the refrigerant. In previous work (McKinley and Alleyne, 2008)(Li et al.,

2011)(Li and Alleyne, 2010), a moving boundary method was introduced to model a transient heat exchanger with a large set of states. However, highly nonlinear models are too sophisticated for real time controller design. In this study, a model predictive controller based on a step response model will be utilized to regulate the battery cooling air temperature at the battery pack's air inlet.

Model predictive control treats the condition air temperature tracking problem as an infinite horizon optimal control strategy design with a quadratic performance criterion (Rawlings, 1999). The controller design procedure includes reference specification, output prediction, control action sequence computation, and error feedback. The system uses the ideal cooling air temperature, $T_{f,d}$, as the reference. With application of a reduced order step response model, the controller is built in following steps. First, apply a step signal to the compressor speed, from 100 RPM to 1,000 RPM at $t = t_0$. Then record the output conditioned air temperature every one second to generate the model array $A_{step} = [a1, a2, a3, \ldots, a70]$. The total sample time is chosen as 70 seconds (70 elements in the model array), which is sufficient for the system to reach steady state. The element ai denotes the conditioned air temperature at the $i-th$ second after the step input change has been applied. The sampling time constant is 1 second which is small enough to accurately describe the transit response of the system.

Define $u_{(i)}$ as the normalized compressor speed at the $i-th$ time instant so that the actual compressor speed may be obtained as

$$\omega_{(i)} = \beta_1 u_{(i)} + \beta_2 \tag{4.19}$$

The compressor speed change at $i-th$ instant becomes

$$\delta\omega_{(i)} = \beta_1 \left(u_{(i)} - u_{(i-1)} \right) \tag{4.20}$$

where $\beta_1$and β_2 are constant controller parameters, correspond to the step input of the compressor speed. With the normalized input $u_{(i)}$, define the past input array as

$$U_{(i-1)} = \left[u_{(i-70)}, u_{(i-69)}, u_{(i-68)} ... u_{(i-1)} \right]^T \tag{4.21}$$

The prediction horizon is an adjustment parameter. In this case, a five second prediction is applied considering both tracking accuracy and computation cost. The input change in the future five seconds may be constructed as

$$\begin{cases} \Delta u_{(i)} = u_{(i)} - u_{(i-1)} \\ \Delta U_{(i)} = \left[\Delta u_{(i)}, \Delta u_{(i+1)}, ... \Delta u_{(i+4)} \right]^T \end{cases} \tag{4.22}$$

Applying the convolution theorem, the predicted conditioned air temperature vector at the $i+1-th$ instant after the pump speed change would be

$$\hat{T}_{air}\,(i+1) = T_{ss} H - S_{(i)} \Delta U_{(i)} - S_0 U_{(i-1)} \tag{4.23}$$

where $H \in \mathscr{R}^{5\times 1}$ is a vector with all elements are 1. To maintain the positive relationship between the input and the output, it is convenient to define a new array S as Eq. (4.24), whose element $s_i = T_{ss} - a_i$. The variable T_{ss} is the steady state output air temperature under 100 RPM pump speed. S and S_0 are both the step response

sample model system matrices constructed as:

$$S = \begin{bmatrix} s_1 & 0 & 0 & 0 & 0 \\ s_2 & s_1 & 0 & 0 & 0 \\ s_3 & s_2 & s_1 & 0 & 0 \\ s_4 & s_3 & s_2 & s_1 & 0 \\ s_5 & s_4 & s_3 & s_2 & s_1 \end{bmatrix} \tag{4.24}$$

$$S_0 = \begin{bmatrix} s_{70} - s_{69} & \dots & s_4 - s_3 & s_3 - s_2 & s_2 \\ 0 & s_{70} - s_{69} & \dots & s_4 - s_3 & s_3 \\ 0 & 0 & s_{70} - s_{69} & \dots & s_4 \\ 0 & 0 & 0 & \dots & s_5 \\ 0 & 0 & \dots & s_7 - s_6 & s_6 \end{bmatrix} \tag{4.25}$$

To implement a recirculation cooling air flow configuration, Eq. (4.23) needs to be modified for the model predictive controller. The reference MPC output should now be the difference between the target cooling air temperature and the air temperature at the battery package outlet, $T_{f,out}$, rather than the constant value of the ambient air temperature. The predicted cooling air temperature vector becomes

$$\hat{T}_{air}\,(i+1) = T_{f,out}H - S_{(i)}\Delta U_{(i)} - S_0 U_{(i-1)} \tag{4.26}$$

In this study, a five-second predictive horizon control is robust enough to offer accurate cooling air temperature tracking performance. Let the prediction vector be

expressed as following equations.

$$\begin{cases} \hat{Y}_{(i+1)} = [\hat{y}(i+1), \hat{y}(i+2)...\hat{y}(i+5)]^T \\ \hat{Y}^0_{(i+1)} = \left[y(i+1)^0, y(i+2)^0...y(i+5)^0\right]^T \end{cases} \tag{4.27}$$

where $\hat{y}_{(i)}$ is the prediction of the conditioned air temperature decreased in the evaporator. The element $y^0_{(i+5)}$ is the prediction of the conditioned air temperature decreased at i-th time instant if the compressor speed maintains current value. The prediction of the output conditioned air temperature under varying input is obtained by substituting the future inputs change defined in Eq. (4.22) into the step response model so that

$$\begin{cases} \hat{Y}_{(i+1)} = S\Delta U_{(i)} + \hat{Y}^0_{(i+1)} \\ \hat{Y}^0_{(i+1)} = S_0 U_{(i-1)} \end{cases} \tag{4.28}$$

Feedback updates are implemented to correct the predicted output due to inaccurate predictions. Applying the latest measurement of the conditioned air temperature at the evaporator outlet, $T_f\,(i)$. The measured output is the air temperature decreased, $y_{(i)} = T_{f,out} - T_f\,(i)$. The corrected prediction of the step response becomes

$$\tilde{Y}_{(i+1)} = S\Delta U_{(i)} + \hat{Y}^0_{(i+1)} + H\left(y_{(i)} - \hat{y}_{(i)}\right) \tag{4.29}$$

where $\tilde{Y} \in \mathscr{R}^{5\times 1}$,$U_{(i-1)} \in \mathscr{R}^{70\times 1}$,$S \in \mathscr{R}^{5\times 5}$ and $S_0 \in \mathscr{R}^{5\times 70}$

Fig. 4.4 shows a comparison of the simulated conditioned air temperatures generated by the step response model and the AMESim simulation for a same compressor speed profile. It can be observed that the step response agrees favourably with AMESim. Thus, the step response model can be applied in the model predictive controller design.

The controller calculates the compressor speed derivatives for the future time instants as an input vector as

$$\Delta U_{(i)} = \left[\Delta u_{(i)}, \Delta u_{(i+1)} ... \Delta u_{(i+4)}\right]^T \tag{4.30}$$

The optimized ΔU is calculated to minimize a selected quadratic performance criterion of the error between the predicted system output and the desired output over the prediction horizon. The selected quadratic performance cost function, $J_{(i)}$, may be stated as

$$J_{(i)} = \left(Y_r - \tilde{Y}_{(i+1)}\right)^T M_1 \left(Y_r - \tilde{Y}_{(i+1)}\right) + \Delta U_{(i)} M_2 \Delta U_{(i)} \tag{4.31}$$

where the M_1 and M_2 are the weighting matrices, and $Y_r = \left[y_{r(i+1)}, y_{r(i+2)}, ... y_{r(i+5)}\right]^T$ is the reference trajectory matrices obtained from ideal cooling air signal sent from battery cooling controller. The variable Y_r may be obtained from Eq. (4.18) so that

$$y_{r(i)} = T_{f,out(i-5)} - T_{f,d(i-5)} \tag{4.32}$$

To minimize the quadratic performance function, $J_{(i)}$. Set $\partial J_{(i)} / \partial \Delta U_{(i)} = 0$. The control law can be derived based on the Eq. (4.29) to Eq. (4.31) so that

$$\begin{cases} E^0_{(i+1)} = Y_{r(i)} - S_0 U_{(i-1)} \\ K_e = \left(S^T M_1 S + M_2\right)^{-1} S^T M_1 \\ \Delta U(i) = K_e E^0_{(i+1)} \end{cases} \tag{4.33}$$

Given that the cooling air mass flow rate and refrigerant valve position are fixed in this context, the system is SISO. The error feedback gain, K_e , can be evaluated

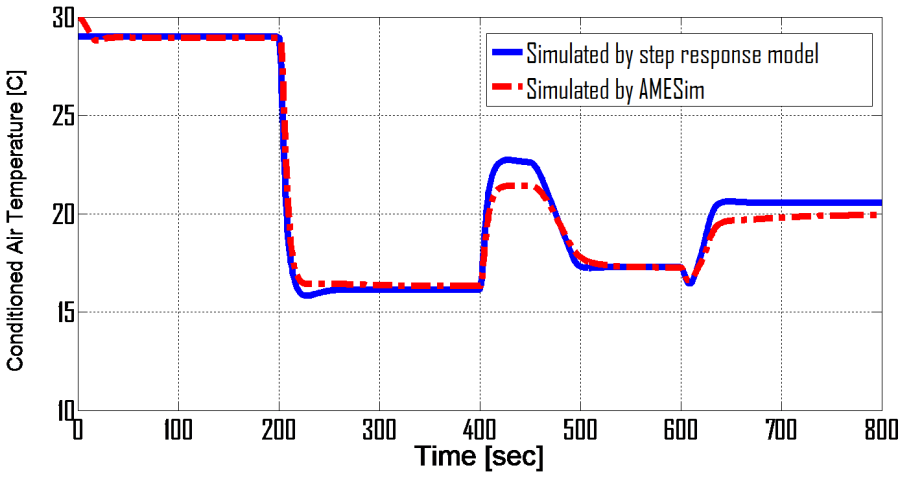

Figure 4.4: Simulated Conditioned Air Temperatures in Step Response Model and AMESim

off line, which is favourable for real time control. Fig. 4.4 shows that the conditioned air temperature simulated by the step response model agrees with the results from AMESim model very well.

4.5 Case Study - Battery Thermal Management

To evaluate the thermal management system controller design, the electric current profile for an urban assault cycle (refer to Fig. 4.5) will be considered in the case study. The variables of interest include the battery core temperature,E_{comp}, and the cooling system compressor energy consumption, . The evaporator fan power consumption is not discussed since a constant cooling air mass flow rate has been imposed. The AHR32113 battery pack and the mathematical model parameters for this case study are listed in Table 4.1.

Eight tests will be conducted with two different surrounding temperatures, two air circulation configurations, and two different control strategies as listed in Table 4.5. The reference battery core temperature, $T_{core,r}$, is 30 $^{\circ}C$ for all tests. The

Table 4.1: AHR32113 Module and Model Parameter

Cell cooling area	0.1136	m^2
Cell Diameter	32	mm
Cell height	110	mm
Cell Capacity	4.5/4.3	Ah
Energy Content	14.6	Wh
Discharge Power	550	W
Voltage	3.3	V
Operating Temp	-30 to 55	$^{\circ}C$
Storage Temp	-40 to 60	$^{\circ}C$
A_{cross}	0.0455	m^2
c	0.36	None
C_{core}	268	JK^{-1}
C_f	0.708	JK^{-1}
C_s	18.8	JK^{-1}
k_{air}	0.0258	$W/m/K$
m	0.63	None
$\dot{m}_{air}$	0.18	kg/sec
Pr	0.71	None
R_{core}	1	K/W
S_L	35	mm
S_T	35	mm
ρ_{air}	1.16	kg/m^3
μ	1.864e-5	Ns/m^3

control strategies are the optimal model predictive control and the traditional on/off control. The air circulation structures include single path and recirculation. In the former one, cooling air is sourced from the surroundings; thus, the air temperature at the evaporator inlet is the same as the ambient temperature. The cooling air is then completely exhausted to the ambient from the battery pack once the cell heat removal process has occurred. The latter approach recirculates the cooling air from the battery pack outlet back into the evaporator which is expected to reduce the energy consumption and increase the efficiency (Wang et al., 2011) in comparison to the first design, especially for high ambient temperatures.

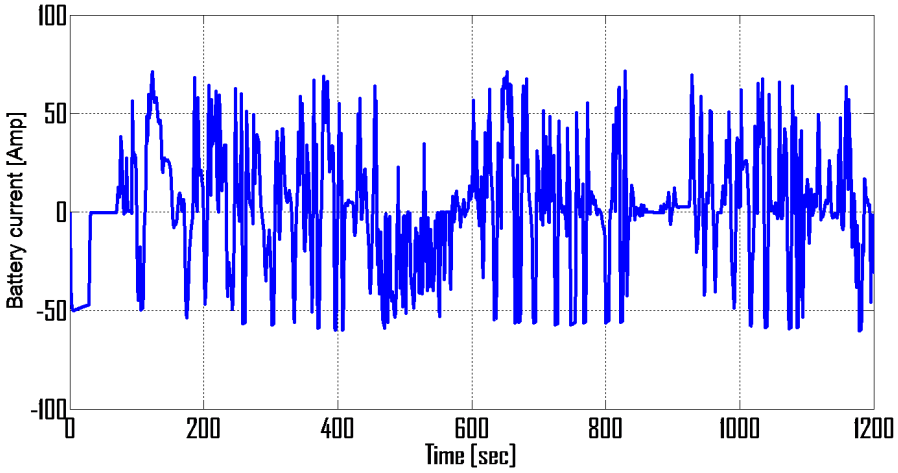

Figure 4.5: Battery Current Profile Verses Time for The Urban Assault Cycle

In the study, two sets of battery package models are integrated into the system. The plant model is created with both an electric submodel and a thermal model for heat generation input. The controller model is designed with the Kalman observer using the cooling air temperature and battery surface temperature feedback from the plant model sensors. The overall controller structure for the battery cooling system is shown in Fig. 4.6.

For Test 4.1, the optimal controller and MPC controller are applied. The cooling air is drawn directly from the surroundings and then exhausted to the ambient environment from the battery pack outlet, per the single path configuration. The initial battery core temperature is set as 30 $^{\circ}C$ in the plant model while the initial value of the battery core temperature in the controller model is set as 35 $^{\circ}C$. Fig. 4.7 shows the observer performance, in which the dotted line is the estimated battery core temperature in the controller model and the solid line denotes the simulated battery core temperature from the plant model. These graphical results indicate that the estimated and measured battery core temperature error converges to zero within 30 seconds.

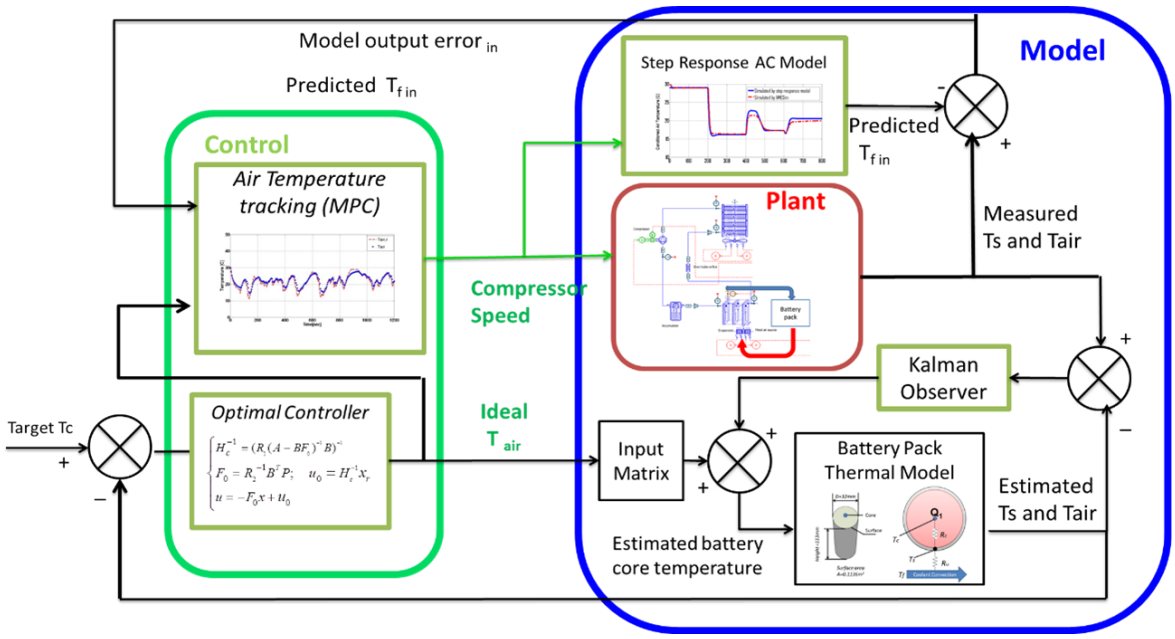

Figure 4.6: Battery Thermal Management Controller Structure

Fig. 4.8 displays the reference ideal inlet cooling air temperature, $T_{f,d}$, calculated by the optimal controller. The model predictive controller regulates the compressor speed in the vapor compression system to adjust the cooling air temperature, T_f, at the evaporator outlet. The measured cooling air temperature tracks the reference trajectory with an average error of 1.71 $^{\circ}C$.

The corresponding battery pack and cooling air temperatures are displayed in Fig. 4.9. The battery core temperature is maintained to a small neighbourhood of the reference value with an average error of 0.24 $^{\circ}C$. If needed, the error can be further reduced by adjusting the weighting matrix R_2 in the cost function and the matrix M_2 in the quadratic performance index per Eq. (4.16) and Eq. (4.31). However, in practice, a decrease in the weighting matrices R_2, may cause the ideal cooling air temperature to exceed the normal output range which will require intense speed changes in the refrigerant pump operation.

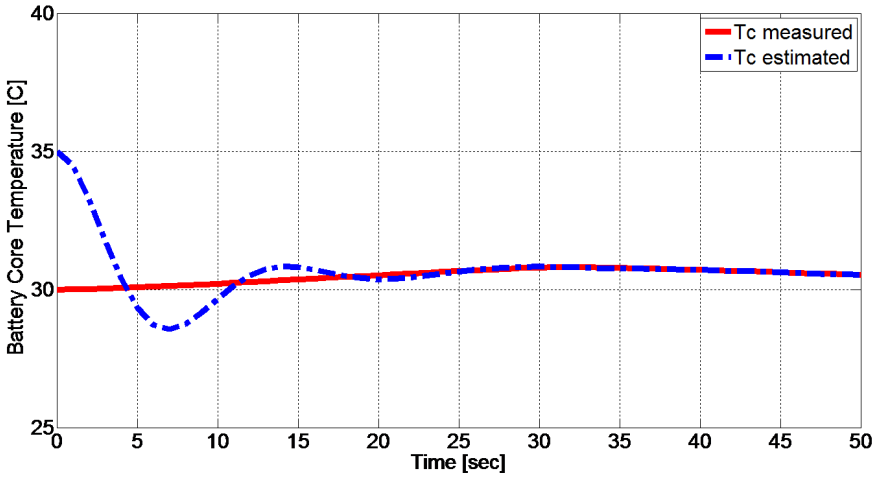

Figure 4.7: Test 4.1 - Estimated and Actual Battery Core Temperature with Optimal Observer

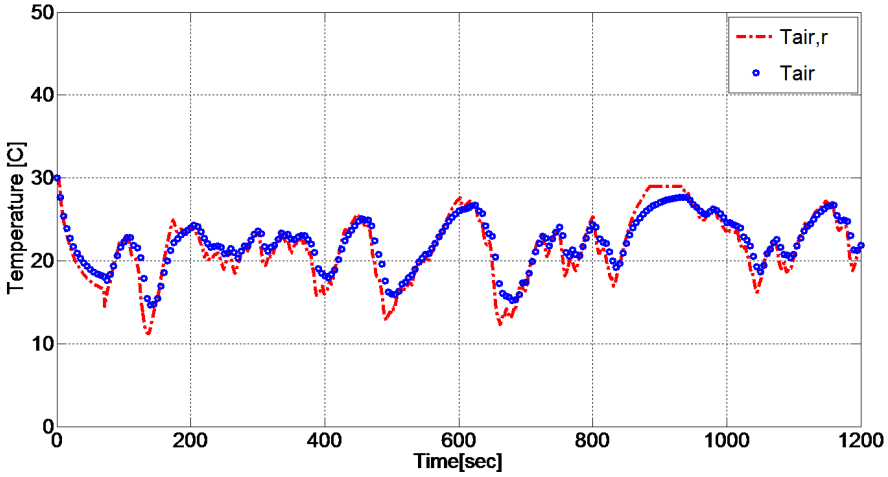

Figure 4.8: Test 4.1 - Model Predictive Control (MPC) Cooling Air Temperature Tracking Performance (Solid) for Optimal Control Reference Signal (Dash)

Table 4.2: Cooling Scenarios for Tests 4.1 - 4.8 in Numerical Study

Test No.	T_{amb}, $[^{\circ}C]$	Cooling Air Circulation Configuration	Control Strategy	Cooling Air Temp Tracking Error, $T_f - T_{f,d}$,$[^{\circ}C]$	Battery Core Temp Tracking Error, $T_{core} - T_{core,r}$ $[^{\circ}C]$	Heat Removal, Q_o $[kJ]$	Compressor Energy Consumption E_{comp} $[kJ]$
4.1	30	Single,path	Optimal/MPC	1.71	0.24	1,068	526
4.2			On/Off	N/A	0.61	1,079	801
4.3		Recirculated	Optimal/MPC	1.83	0.25	1,070	224
4.4			On/Off	N/A	0.57	1,126	542
4.5	40	Single,path	Optimal/MPC	15.83	>5.6	1,808	5,517
4.6			On/Off	N/A	>5.6	1,813	5,577
4.7		Recirculated	Optimal/MPC	1.56	0.22	1,959	1,439
4.8			On/Off	N/A	0.38	2,091	1,848

The single path cooling air flow configuration can typically remove heat at a larger magnitude than the heat generated by the battery cells. The cooling air at the battery pack outlet is generally only increased by 3 $^{\circ}C$ to 6 $^{\circ}C$ and still cooler than the surrounding temperature. By recycling the cooling air from the battery package outlet back to the evaporator, the heat load in the evaporator will be reduced. In Test 4.3, the recirculated cooling air flow structure with the modified MPC provides good cooling air and the battery core temperature tracking per Table 4.5. However, the energy consumption of the compressor in the 1,200 second simulation is significantly reduced when compare with Test 4.1 by 58%.

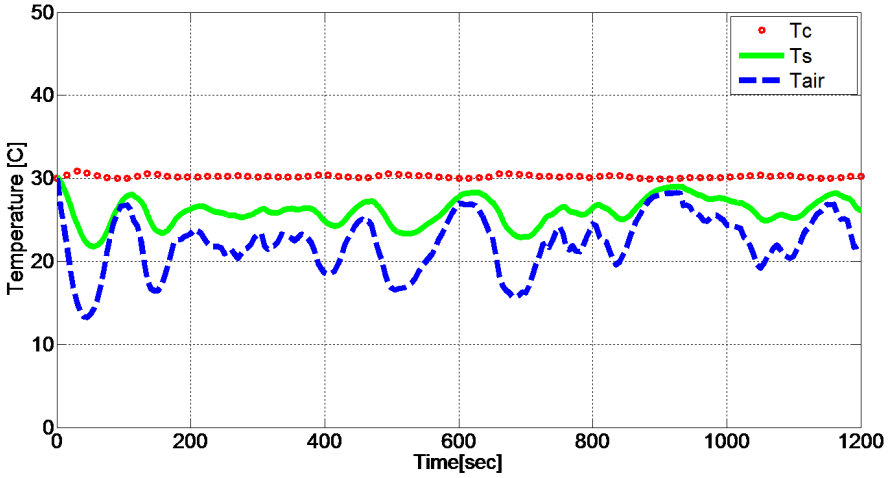

Figure 4.9: Test 4.1 - Simulated Battery Core, Surface plus the Cooling Air Temperatures

In Tests 4.5 to 4.8, the surrounding temperature is set at 40 $^{\circ}C$. Test 4.5 uses the single path cooling air configuration. When the ambient temperature is higher than the desired battery core temperature, the reference cooling air temperature is very difficult to achieve with this air flow structure. Applied with maximum compressor speed, the cooling air temperature is still higher than target value. Consequently, the battery core was not driven to target temperature within the simulation time and

the total energy cost of the compressor is as high as E_{comp} =5517 kJ.

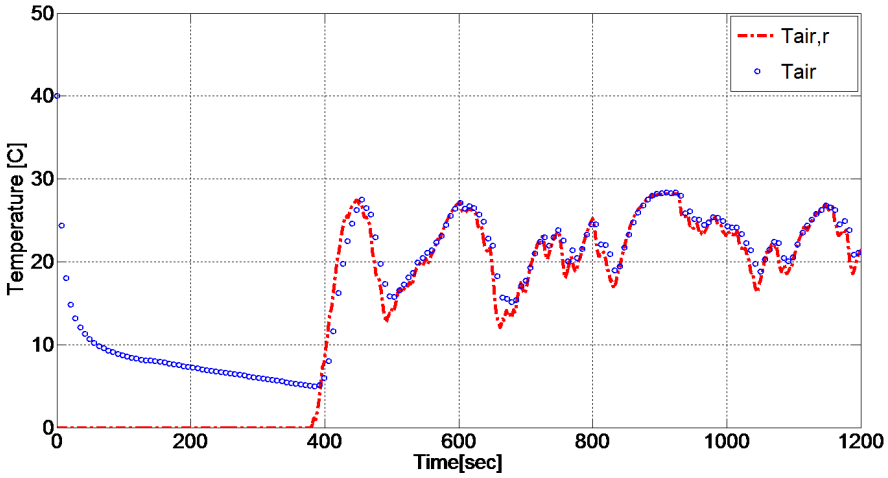

Figure 4.10: Test 4.7 - Model Predictive Control (MPC) Cooling Air Temperature Tracking Performance (Solid) for Optimal Control Reference Signal (Dash)

For the Test 4.7, the recirculated cooling air flow reduces the heat load so that the cooling system can successfully track the battery core temperature. The ideal cooling air temperature, $T_{f,d}$, calculated by the optimal controller is displayed in Fig. 4.10 with the actual cooling air temperature as tracked by the model predictive controller. The average error in the cooling temperature is 1.56 $°C$ with a compressor energy usage of 1,439 kJ per Table 4.5. Fig. 4.11 displays the simulation results of Test 4.7. The battery core temperature is cooled down to 30 $°C$ from the initial surrounding temperature within a relatively short time and was maintained at this temperature with an average error of 0.25 $°C$. The results indicate that the proposed MPC method using a step response model can satisfactorily track the desired cooling air temperature, although the vapour compression system is highly nonlinear.

To investigate the advantage of the optimal control strategy in power conservation, Tests 4.2, 4.4, 4.6, and Test 4.8 were conducted with a conventional switched on/off control strategy. In these four tests, the compressor operates with its maxi-

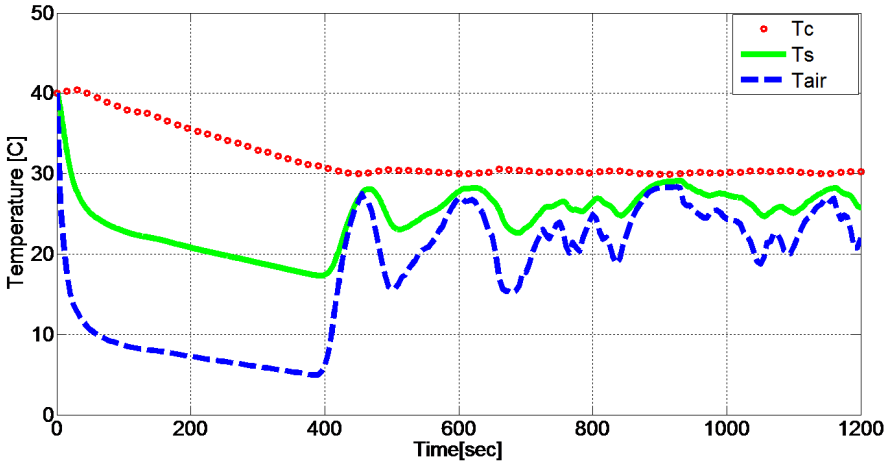

Figure 4.11: Test 4.7 - Simulated Battery Core, Surface plus the Cooling Air Temperatures

mum speed when the battery core temperature reaches 30.5 $°C$. When the battery core is cooled to 29 $°C$, the compressor speed is reduced to 150 rpm to avoid potential local hot spots. In Test 4.2 (single path), the compressor energy consumption is 801 kJ, which is higher than Test 4.1. The compressor energy consumption in Test 4.4 (recirculation path) is 542 kJ, and it is 1.4 times higher than Test 4.3. In Test 4.6, simulation results are similar to Test 4.5 with the compressor operating at maxim speed during the whole simulation due to the single path cooling air configuration. With recirculation cooling air configuration, the proposed optimal/MPC control strategy provides the advantages of a 23% to 58% power conservation in comparison to conventional on/off strategy.

4.6 Summary

A hybrid electrical vehicle battery thermal management control system using a model predictive controller has been proposed. The air conditioning system is integrated into the battery thermal management system (BTMS) to effectively remove

the heat generated by the battery cells during high load charging/ discharging operations. A traditional battery cooling system only controls the flow rate rather than the temperature of the coolant, which limits the heat removal rate. This study investigated the cooling air temperature control problem for the first time. The proposed BTMS applies a Kalman filter to correct the immeasurable battery core temperature estimation and calculates the ideal cooling air temperature by optimal control theory. The identified ideal cooling air temperature is sent to the AC control system as a reference input signal. Model predictive control (MPC) theory is then applied to regulate the AC refrigerant compressor speed. Simulation results demonstrate that the MPC controller is able to handle the conditioned air temperature tracking with a small error and delay. The batteries' core temperature can be stabilized around the target for various cooling conditions while minimizing the power consumption.

Chapter 5

An Electric Motor Thermal Management System for Hybrid Vehicles - Modeling and Control

The permanent magnet electric motor (e-motor) is widely seen in the hybrid electric vehicles (HEV) powertrains. The motor internal temperature tolerance limits its torque/power capabilities. The dominant heat sources inside the e-motors locate near the machine windings in the stator, thus the local temperatures of different positions inside the machine are not uniformly distributed. To keep the electric motor functioning properly without exceeding the temperature limits, an robust thermal management system is introduced. This study proposes a new concept of thermal management system for permanent magnet electric motors with a reduced order thermal model, which is utilized for real-time peak temperature control. A linear quadratic optimal regulator is built to calculate the ideal (target) heat removal rate at the e-motor cooling surface. Then a nonlinear tracking controller is designed to govern the air-liquid cooling system operation and achieve the target heat removal

rate tracking. In a urban assault driving cycle simulation with the proposed cooling control strategy, the motor stator hot spot is stabilized with an average error of 0.13 $^{\circ}C$, and a 81% power consumption reduction is achieved comparing to the classical controller to maintaining a same level of temperature tracking. In the convoy escort driving cycle, the proposed cooling system energy consumption can be reduced by 71%.

5.1 Introduction

The continuous developments in electric (EV) and hybrid-electric vehicle (HEV) propulsion systems require highly efficient and powerful electric motors (e-motors). The temperature limitations of permanent magnet electric motors are rather strict due to the thermal impact on the torque and power capabilities. Therefore, a reliable electric motor thermal management strategy is required to maintain the machine's thermal stabilization. Meanwhile, the power consumption of the cooling system should be minimized to promote fuel efficiency. Recently, increased attention has been focused on the development of advanced HEV powertrain thermal management systems (Park et al., 2013)(Shams-Zahraei et al., 2012).

A brief literature survey will be presented. Li *et al.* (Li et al., 2006) investigated a cooling system for e-motors applying both numerical simulation and experimental tests under various fan hub configurations. Salah *et al.* (Salah et al., 2010) applied nonlinear control theory to an advanced thermal management system design for the internal combustion engine (ICE) cooling fan and demonstrated the improvements in temperature tracking and power efficiency. For the cooling system design purposes, the thermal behaviour of the electric motors has been described by lumped parameter thermal models (Bellettre et al., 1997), (Mellor et al., 1991). Soparat and

Benyajati (Soparat and Benyajati, 2013) introduced a thermal management system designed for motors using liquid coolant. Tao *et al.* proposed a model based controller design for HEV battery pack thermal management systems to achieve battery core temperature stabilization (Tao and Wagner, 2016). Based on previous work (Tao et al., 2015) (Salah et al., 2008), the e-motor's thermal management system efficiency can be largely improved with optimized cooling actuator operation which utilize advanced control theories. This approach should lead to enhanced temperature tracking performance while minimizing power consumption for the subsystem components.

In this paper, a new HEV e-motor thermal management system concept using optimal and nonlinear back-stepping control theories will be investigated. The proposed cooling system control algorithm tracks the prescribed heat removal rate with the help of a reduced-order e-motor thermal model. The thermal model is derived from a full order three dimensional (3D) finite element analysis (FEA) model whose order is reduced for fast temperature prediction and real time control purposes. The simplified thermal model can accurately predict the machine internal temperature with a high computational efficiency. A cooling cycle with a counter flow air-liquid heat exchanger is also modelled. The coolant pump and fan rotational speeds are regulated by a nonlinear back-stepping controller. A numerical study will be conducted with different cooling scenarios and control strategies. The simulation results should demonstrate that the proposed e-motor thermal management system can stabilize the machine's highest internal temperature within the desired range, while reducing the cooling system auxiliary power consumption.

The rest of the paper is organized as follows. Section 5.2 offers a brief introduction of the reduced-order e-motor thermal model. In Section 5.3, the cooling system model is mathematically described. Section 5.4 introduces the optimal regulator which is designed to calculate the ideal cooling surface heat removal rate. Next, the

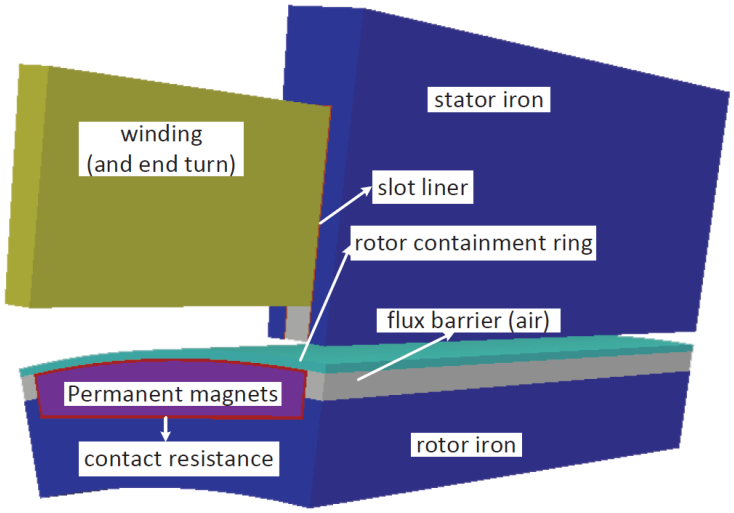

Figure 5.1: Geometry of an Interior Permanent Magnet (IPM) Machine

back-stepping controller is created for the heat removal rate tracking. The numerical study and accompanying discussion are presented in Section 5.5 to demonstrate the performance of the proposed e-motor thermal management system. The last section concludes the paper.

5.2 Reduced Order Electric Motor Thermal Model

The proposed thermal management system aims to regulate the highest temperature inside the electric motor mechanical housing. To accomplish this goal, a thermal model for the electric motor must be available to monitor the machine's dynamic temperature changes. 3D finite element analysis (FEA) is frequently used to describe thermal behaviour. A full-ordered FEA model is capable of providing accurate temperature estimation inside the electric machine, but may have large computational requirements and therefore not suitable for real time controller design.

A UQM PowerPhase 145 machine (UQM, 2015) is considered with the physical

Table 5.1: PowerPhase 145 Machine Parameters

Parameters	Value	Unit
Continuous power	85	kW
Continuous torque	250	Nm
Diameter	280	mm
Length	279	mm
Maximum speed	8000	RPM
Maximum efficiency	94%	-
Peak power	145	kW
Peak torque	400	Nm
Power density	2.9	kW/kg
Weight	50	kg

dimensions and the performance parameters listed in Table 5.1. The structure of the e-motor, shown in Fig. 5.1, includes a stator and a rotor. The windings, which are the dominant heat source, are located in the stator. The stator is generally hotter than the rotor. The coolant flows across the stator outer surface and removes heat from the cooling surface. A reduced-order 3D finite-element based dynamic thermal model of the electric machine, with high computational efficiency, will be derived using an orthogonal decomposition method to maintain the temperature prediction accuracy.

The process followed to derive the reduced-order thermal model will be briefly reviewed. The partial differential equation associated with thermal conduction in the electric motor is given as

$$d\frac{\mathrm{d}T}{\mathrm{d}t} - k\nabla^2 T = q \tag{5.1}$$

where T is the continuum temperature. The parameters d and k are the specific heat and the thermal conductivity, respectively. The heat flux, q, is the system input. The conduction Eq. (5.1) can be written in discretized form by meshing the model using the standard FEA method as

$$\mathbf{D}\,\dot{\overrightarrow{t}} + \mathbf{K}\,\overrightarrow{t} = \overrightarrow{q} \tag{5.2}$$

In this expression, $\overrightarrow{t}$ is the nodal temperature vector of the finite element mesh, $\mathbf{K}$ is the finite element matrix corresponding to the material thermal conductivity, and $\mathbf{D}$ is the finite element matrix corresponding to the specific heat. The terms $\mathbf{K}$ and $\mathbf{D}$ are both symmetric matrices. The vector $\overrightarrow{q}$ denotes the excitation of the thermal model, including losses and the convection heat transfer on the boundaries of the machine.

The full order finite element model is too computationally demanding, and consequently, will execute too slowly. Thus, the model order must be reduced for real time control purposes. Considering Eq. (5.2), the system eigenvector matrix, $\mathbf{V}$ can be obtained by solving $(\mathbf{K} - \lambda_i \mathbf{D})\, \overrightarrow{v}_i = 0$. Next, the model may be reformed by changing the basis, $\overrightarrow{t} = \mathbf{V}\, \overrightarrow{x}$, so that Eq. (5.2) becomes

$$\mathbf{V}^T \mathbf{D} \mathbf{V}\, \dot{\overrightarrow{x}} + \mathbf{V}^T \mathbf{K} \mathbf{V}\, \overrightarrow{x} = \mathbf{V}^T\, \overrightarrow{q} \tag{5.3}$$

The eigenmodes may be separated into "dynamic" and "static" modes so that $\mathbf{V} = [\mathbf{V}_d; \mathbf{V}_s]$ (Donaldson, 2006) . The most significant excited eigenstates are considered to be the dynamic modes. These elements may be selected by evaluating the extent of excitation of the $i-th$ eigenmode for a given input vector $\overrightarrow{q}$ so that

$$E_i = \tau_i\, \overrightarrow{v}_i^T\, \overrightarrow{q} \tag{5.4}$$

where τ_i is the time constant of the $i-th$ eigenmode. The system response of interest is governed by the eigenmodes with the slowest time constant. Consequently, the

following variables may be defined as

$$\begin{cases} \mathbf{V}_d^T \mathbf{D} \mathbf{V}_d = \mathbf{d}_d \\ \mathbf{V}_s^T \mathbf{D} \mathbf{V}_s = \mathbf{d}_s \\ \mathbf{V}_d^T \mathbf{K} \mathbf{V}_d = \mathbf{k}_d \\ \mathbf{V}_s^T \mathbf{K} \mathbf{V}_s = \mathbf{k}_s \end{cases} \tag{5.5}$$

where $\mathbf{d}_d$, $\mathbf{d}_s$, $\mathbf{k}_d$, and $\mathbf{k}_s$ are all diagonal matrices.

Assuming that the static modes instantaneously converge to their quasi-steady-state values, the nodal temperatures become

$$\overrightarrow{t} = \mathbf{V}_d \overrightarrow{x}_d + \left(\mathbf{K}^{-1} - \mathbf{V}_d \mathbf{k}_d^{-1} \mathbf{V}_d^T \right) \overrightarrow{q} \tag{5.6}$$

Substituting Eq. (5.6) into Eq. (5.2), the dynamic eigenmodes can be decoupled and simulated separately as

$$\mathbf{d}_d \dot{\overrightarrow{x}}_d + \mathbf{k}_d \overrightarrow{x}_d = \mathbf{V}_d^T \overrightarrow{q} \tag{5.7}$$

Applying the proposed order-reduction method to both the original stator and rotor FEA models, the model order can be reduced to a reasonable number for real time prediction of the machine temperature with a small simulation error. In the current study, the orders of the stator and rotor thermal models are chosen as 40 and 20, respectively. The maximum relative errors of this reduced order model are 1.15% and 0.07% when compared to the full order FEA model, whose states are 120K for the stator, and 97K for the rotor. The detailed derivation and experimental validation of this task has been reported in a previous work (Zhou et al., 2013).

5.3 Cooling System Model

The cooling system consists of an electrically controlled pump, a counter flow radiator, and a variable speed air fan. The coolant, driven by the electric pump, flows through the radiator and dissipates the heat transported from the motors. The heat transfer rate inside the radiator, and the heat removal rate on the electric motors' cooling surfaces are critical for accurate temperature tracking. In this section, the air-liquid cooling system will be modeled. The model simulates the heat removal rate under varying coolant and air flow rates, plus it predicts the transit temperature changes in the fluids. The power consumption of the pump and radiator fan will also be estimated.

5.3.1 Heat Exchanger Model

The flow paths of the coolant and the air outside the radiator are evenly divided into small control volumes. The cooling system thermal structure is displayed in Fig. 5.2. The overall heat transfer coefficient of the radiator, U_{rad}, is a function of the mass flow rates of the coolant and cooling air. This coefficient can be derived by applying empirical relations, the NTU method (Iu et al., 2007), experimental measurements, and/or computational fluid dynamics. The radiator heat transfer coefficient may be empirically described as

$$h_{rad} = \frac{1}{\frac{1}{k_{wall}} + \frac{1}{a_w \dot{m}_w^{b_w}} + \frac{1}{a_{air} \dot{m}_{air}^{b_{air}}}} \tag{5.8}$$

where k_{wall} is the tube wall material conductivity, and a_{air}, a_w, b_{air} and b_w are constant parameters associated with the heat exchanger structure. The subscript "air" and "w" indicate air and coolant sides respectively. Assuming that the radiator

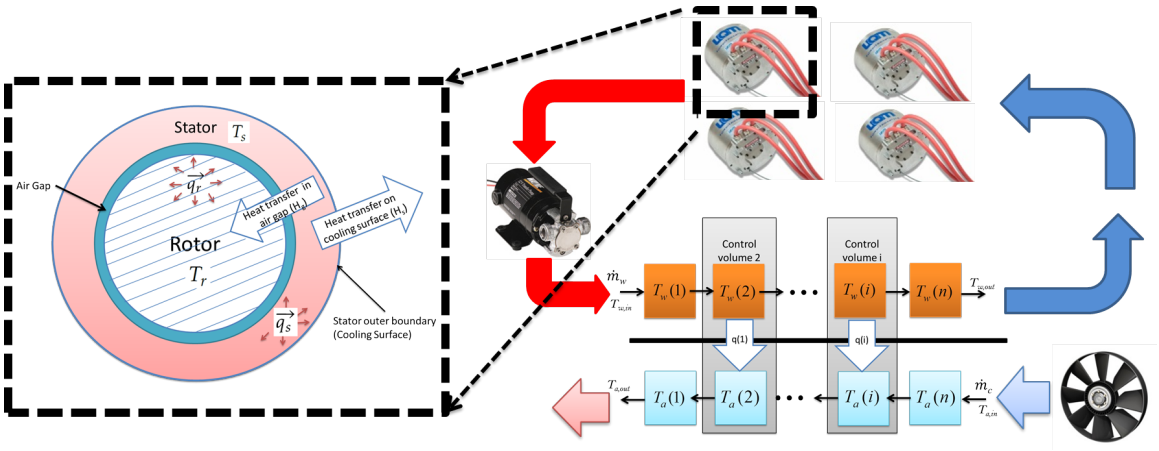

Figure 5.2: E-motor Cooling System Model Structure.

is divided into n control volumes, and that the heat exchange surface area of the radiator is A_{rad}, then the equivalent heat transfer coefficient for each control volume may be determined to be $h_{rad}A_{rad}/n$.

The heat transfer rate from the hot to the cold fluids in the $i-th$ control volume may be calculated based on the local fluid temperature difference at the control volume inlet so that

$$\Delta T_{rad}(i) = T_w(i) - T_{air}(i) \tag{5.9a}$$

$$q_{rad}(i) = \min\left\{\frac{\Delta T_{rad}(i)A_{rad}U_{rad}}{n}; \frac{\Delta T_{rad}(i)\dot{m}_{air}c_{p,air}\dot{m}_w c_{p,w}}{\dot{m}_{air}c_{p,air} + \dot{m}_w c_{p,w}}\right\} \tag{5.9b}$$

The subscript "i" is the control volume index. The variables $\dot{m}_{air}$ and $\dot{m}_w$ denote the mass flow rates of air and coolant, $c_{p,air}$ and $c_{p,w}$ are the specific heat of air and coolant, and $\Delta T_{rad}(i)$ is the temperature difference between the two fluids at the inlet of the $i-th$ control volume. Based on heat transfer principles, the heat transfer

rate inside each control volume cannot be larger than $\Delta T_{rad}(i)\frac{\dot{m}_{air}c_{p,air}\dot{m}_w c_{p,w}}{\dot{m}_{air}c_{p,air}+\dot{m}_w c_{p,w}}$. This is the maximum possible heat transfer rate which will make the temperatures of the two fluids converge at the outlet of this control volume.

The change in control volume temperatures is determined by the mass flow rates of the coolant and cooling air. The fluid temperature inside the $i-th$ control volume may be expressed as

$$\frac{\mathrm{d}T_w(i)}{\mathrm{d}t} = \left(T_w(i) - T_w(i+1)\right)\frac{n\dot{m}_w}{M_{w,rad}} - \frac{nq_{rad}(i)}{M_{w,rad}c_{p,w}} \tag{5.10}$$

The first term on the right side of Eq. (5.10) describes the temperature change due to coolant flow. The second term accounts for the heat transfer from the other fluids. The parameter $M_{w,rad}$ represents the mass of the coolant located inside the radiator. Similarly, the transit temperature change of air inside the $i-th$ control volume may be described as

$$\frac{\mathrm{d}T_{air}(i)}{\mathrm{d}t} = \left(T_{air}(i) - T_{air}(i+1)\right)\frac{n\dot{m}_{air}}{M_{air}} + \frac{nq_{rad}(i)}{M_{air}c_{p,air}} \tag{5.11}$$

The parameter M_{air} denotes the mass of radiator cooling air. By connecting the flow path segments representing hot coolant and cold air flows in a reversed direction, the overall counter flow structure can be simulated.

The total radiator heat removal rate is the sum of the heat transfer inside all the control volumes such that

$$Q_{rad} = \sum_{i=1}^{n} q_{rad}(i) \tag{5.12}$$

5.3.2 Estimation of Cooling System Power Consumption

The cooling system power consumption is an important index to evaluate overall efficiency. The energy cost associated with the cooling cycle, mainly attributed to the radiator fan and the coolant pump, can be mathematically described as

$$\begin{cases} \dot{m}_w = \frac{N_{pump} Dis \rho_w}{60} \\ dP_w = (\frac{N_{pump} Dis}{60 A_{flow}})^2 \rho_w C_{p,rad} + \dot{m}_w^2 C_{p,pipe} \\ E_{pump} = \frac{N_{pump} D_{is} dP_w}{60} \end{cases} \tag{5.13}$$

where the variable $\dot{m}_w$ denotes the coolant mass flow rate, and E_{pump} represents the estimated pump power. The term N_{pump} is the pump rotating speed. The parameter Dis is the maximum pump displacement, $\dot{m}_w$ is the estimated coolant mass flow rate, $C_{p,rad}$ and $C_{p,pipe}$ are the pressure rise coefficients in the radiator and in the pipes, and A_{flow} is the cross section area of the internal coolant flow path in the radiator. The term dP_w is the total coolant pressure increased due to the pump.

In a similar manner, the performance and power consumption of the radiator cooling fan may be stated as

$$\begin{cases} \dot{m}_{air} = \frac{D_{fan}^3 C_{flow} N_{fan} \rho_{air}}{60} \\ dP_a = D_{fan}^2 C_{pres} (\frac{N_{fan}}{60})^2 \rho_{air} \\ E_{fan} = \frac{D_{fan}^3 C_{flow} N_{fan} dP_a}{60} \end{cases} \tag{5.14}$$

where the variable N_{fan} is the fan speed and $\dot{m}_{air}$ is the air mass flow rate. The parameters C_{flow} and C_{pres} denote the flow rate coefficient and the pressure drop coefficient, respectively. The parameter D_{fan} is the fan diameter, dP_{fan} is the total pressure increased due to the fan, and E_{fan} is the total power consumption rate of

the radiator fan in watts.

The values of A_{flow}, $C_{p,rad}$, C_{flow}, $C_{p,pipe}$, C_{pres}, Dis, ρ_{air} and ρ_w, are all considered to be constant. Thus, the estimation of power consumption of coolant pump and cooling air fan can be related directly to the mass flow rate of the fluids through the heat exchanger. It can be shown that the power consumption of the coolant pump and fan are proportional to the cubed flow rates.

5.3.3 Heat Removal on Motor Cooling Surface

A series hybrid electric vehicle (HEV) configuration with four electric motors, which are located at each wheel is under study. The cooling system must simultaneously handle the heat removal task for all motors. It is assumed that the motor torque and speed, as well as their heat generation rates, are uniform. To maintain proper machine temperature, the coolant exiting the radiator is evenly divided into four streams and delivered to each motor. After cooling the electric motors, the coolant streams merge and recirculate through the pump and radiator.

To integrate together the cooling and e-motor thermal models, the stator external cooling surface heat transfer must be considered. The governing equation for the coolant temperature in each motor becomes

$$\frac{\mathrm{d}T_{w,o}}{\mathrm{d}t} = (T_{w,in} - T_{w,o})\frac{\dot{m}_{w,m}}{M_m} + \frac{Q_m}{M_m c_{p,w}} \tag{5.15}$$

where $T_{w,in}$ and $T_{w,o}$ are the coolant temperatures at motor inlet and outlet. The variable $\dot{m}_{w,m}$ is the mass flow rate of the coolant inside the electric motor. For an HEV with four motors, $\dot{m}_{w,m} = 0.25\dot{m}_w$. The coolant mass in one electric motor, M_m, is assumed to be constant since the mass flow rates at motor inlet and outlet are equal. The first term of the right side of Eq. (5.15) is the coolant temperature

change due to the heat transferred by the coolant flow rate. The second term is the temperature change resulting from the motor heat transfer.

The heat transfer on the motor cooling surface, q_m is given by

$$Q_m = \Delta T_m h_u A_u \tag{5.16}$$

In this expression, ΔT_m is the log mean temperature difference between the stator outer surface and the coolant temperature such that

$$\Delta T_m = \frac{T_{w,in} - T_{w,o}}{\ln[(T_{so} - T_{w,o})/(T_{so} - T_{w,in})]} \tag{5.17}$$

where T_{so} is the temperature of the stator's outer cooling surface with an effective cooling area, A_u. The effective convection coefficient at the machine cooling surface, h_u, is derived analytically (Bergman et al., 2011).

The coolant travels across the motor surface as turbulent flow inside a circular tube, and the heat transfer coefficient is estimated as follows,

$$\begin{cases} Nu_D = \frac{(f/8)(\mathrm{Re}_D - 1000)Pr}{1+12.7(f/8)^{1/2}(Pr^{2/3}-1)} \\ \mathrm{Re}_D = 4\dot{m}_{w,m}/D_h/\mu_w \\ f = (0.79\log\mathrm{Re}_D - 1.64)^{-2} \\ h_u = k_w Nu_D/D_h \end{cases} \tag{5.18}$$

The heat flux, $\overrightarrow{q}_s$, on the cooling surface, is the only element of the thermal model input vector,that can be regulated by the cooling system. It may be defined as the heat transfer rate on a unit area of the motor cooling surface so that

$$\overrightarrow{q}_s = \frac{Q_m}{A_u} \tag{5.19}$$

5.4 Design of Controllers

A series of two controllers will be designed to adjust the operations of the coolant pump and radiator fan for stator peak internal temperature tracking and power minimization. The prescribed e-motor thermal model can be rewritten in state space form as

$$\begin{cases} \dot{\overrightarrow{x}}_s = \mathbf{A}_s \overrightarrow{x}_s + \mathbf{B}_s \overrightarrow{q}_{(s)} \\ \overrightarrow{T}_s = \mathbf{V}_{ds} \overrightarrow{x} + \mathbf{D}_s \overrightarrow{q}_{(s)} \end{cases} \tag{5.20}$$

$$\begin{cases} \dot{\overrightarrow{x}}_r = \mathbf{A}_r \overrightarrow{x}_r + \mathbf{B}_r \overrightarrow{q}_{(r)} \\ \overrightarrow{T}_r = \mathbf{V}_{dr} \overrightarrow{x}_r + \mathbf{D}_r \overrightarrow{q}_{(r)} \end{cases} \tag{5.21}$$

where $\overrightarrow{x}_s$ and $\overrightarrow{x}_r$ are the stator and rotor eigenmodes respectively. The state space system matrices, derived using Eq. (5.7) may be expressed as

$$\begin{cases} \mathbf{A}_s = -\mathbf{k}_{d,s}\mathbf{d}_{d,s}^{-1} \\ \mathbf{B}_s = \mathbf{V}_{d,s}\mathbf{d}_{d,s}^{-1} \\ \mathbf{D}_s = \left(\mathbf{K}_{d,s}^{-1} - \mathbf{V}_{d,s}\mathbf{k}_{d,s}^{-1}\mathbf{V}_{d,s}^{T}\right)\mathbf{d}_{d,s}^{-1} \\ \mathbf{A}_r = -\mathbf{k}_{d,r}\mathbf{d}_{d,r}^{-1} \\ \mathbf{B}_r = \mathbf{V}_{d,r}\mathbf{d}_{d,r}^{-1} \\ \mathbf{D}_r = \left(\mathbf{K}_{d,r}^{-1} - \mathbf{V}_{d,r}\mathbf{k}_{d,r}^{-1}\mathbf{V}_{d,r}^{T}\right)\mathbf{d}_{d,r}^{-1} \end{cases} \tag{5.22}$$

The conduction heat transfer in the air gap between the stator inner surface and the rotor external surface can be calculated using the boundary temperatures as well as the effective conduction heat transfer coefficient in the air gap. Thus, the stator and rotor thermal models can be derived separately and then joined by the air gap heat transfer shared by both parts.

The stator's state-space thermal model in Eq. (5.20) is employed to design a linear regulator for calculating the ideal heat flux, $\overrightarrow{q}_{s,d}$. As the only controllable input is the convective heat flux at the motor's cooling surface, the controller will consider just the stator portion of the e-motor.

5.4.1 Ideal Heat Removal Rate

The e-motor hot spots generally correspond to positions inside the windings. With this observation, the control objectives can be reduced to only a few elements in the thermal model output vector by properly designing the weighting matrix. To design an optimal controller to calculate the ideal heat removal requirement, define the cost function as

$$J_m = \int_{t0}^{t1} \left\{ [\overrightarrow{T}_s - \overrightarrow{T}_{s,r}]^T R_2 [\overrightarrow{T}_s - \overrightarrow{T}_{s,r}] + \widetilde{u}^T R_3 \widetilde{u} \right\} \mathrm{d}t \tag{5.23}$$

where $R_2 \in \mathcal{R}_{ns \times ns}$ and $R_3 \in \mathcal{R}_{5\times 5}$ are positive symmetric weighting matrix. The parameter $_{ns}$ represents the number of stator model output vector elements. The variable $\widetilde{u} = \overrightarrow{q}_{s,d} - u_0$ denotes the magnitude of the system inputs, while $T_{s,r}$ is the reference stator peak temperature.

In this study, R_2 is designed to only stabilize the stator's peak internal temperature.(e.g., the 2^{nd} to 12^{th} output vector elements). So R_2 is constructed such that only the 2^{nd} to 12^{th} elements on its diagonal are non-zero

$$R_2(ij) = \begin{cases} P_{R2}; i = j \text{ and } 1 < i < 13 \\ 0; \text{ otherwise} \end{cases} \tag{5.24}$$

The linear optimal controller may be expressed as

$$\begin{cases} H_c^{-1} = \left(R_2 \left(\mathbf{A}_s - \mathbf{B}_s F_0\right) \mathbf{B}_s\right)^{-1} \\ u_0 = \mathbf{V}_{ds} H_c^{-1} \overrightarrow{T}_{s,r} \\ F_0 = R_3^{-1} \mathbf{B}_s^T P \\ \overrightarrow{q}_{s,d} = -F_0 T_s + u_0 \end{cases} \tag{5.25}$$

where P is solved as the non-negative definite solution of the corresponding Algebraic Riccati equation.

The ideal heat removal rate at the machine cooling surface is identified by the corresponding element in the ideal stator heat flux, $\overrightarrow{q}_{s,d}$, to minimize the cost function Eq. (5.23). To emphasize the limitation that only the convection heat transfer input of this model, which is the third element in this case, is controllable, the weighting matrix, R_3, is designed such that

$$R_3(ij) = \begin{cases} P_{R3}; i = j = 1, 2, 4, 5 \\ 1; i = j = 3; \\ 0; i \neq j; \end{cases} \tag{5.26}$$

Thus the weighting coefficient of the third input is much smaller than the rest of the four uncontrolled inputs.

To minimize the prescribed cost function, the regulator impacts the feedback gain mainly on the third input. The large weighting coefficients of the other inputs reduce the allowed magnitude of these uncontrollable heat flux. The ideal heat removal rate at the motor cooling surface may be calculated as

$$Q_{m,d} = \overrightarrow{q}_{so,d} A_u \tag{5.27}$$

where $\overrightarrow{q}_{so,d}$ is the corresponding element of the target input vector, $\overrightarrow{q}_{s,d}$ calculated in Eq. (5.25). This target heat removal rate is supplied to the cooling system controller as a reference signal.

5.4.2 Nonlinear Controller Design for Heat Removal Rate Tracking

A nonlinear tracking controller will be designed to regulate the coolant pump and radiator fan for ideal heat removal rate tracking. The control objective is to eliminate the heat removal rate tracking error, e_Q, which is defined as

$$e_Q = Q_{m,d} - Q_m \tag{5.28}$$

The controller is designed to achieve the tracking error's asymptotically stability so that

$$e_Q < \varepsilon_e \text{ as } \rightarrow \infty \tag{5.29}$$

where ε_e is a small positive constant. This stability can be realized if the tracking error changes can be constructed in the following form

$$\frac{\mathrm{d}e_Q}{\mathrm{d}t} = -k_e e_Q \tag{5.30}$$

where the variable k_e should be a positive constant. To formulate the state equation, the time derivative of the tracking error in Eq. (5.28) becomes

$$\frac{\mathrm{d}e_Q}{\mathrm{d}t} = \frac{\mathrm{d}Q_{m,d}}{\mathrm{d}t} - \frac{\mathrm{d}Q_m}{\mathrm{d}t} \tag{5.31}$$

Substituting Eq. (5.30) and Eq. (5.31) into (5.28) yields the cooling surface

heat removal rate needed

$$\frac{\mathrm{d}Q_m}{\mathrm{d}t} = \frac{\mathrm{d}Q_{m,d}}{\mathrm{d}t} + k_e e_Q \tag{5.32}$$

The relationship between the coolant mass flow rate and the heat removal rate in Eq. (5.16) to Eq. (5.18) allow the time derivative of the heat removal rate to be defined as

$$\frac{\mathrm{d}Q_m}{\mathrm{d}t} = A_u \Delta T_m \frac{\partial h_u}{\partial \dot{m}_w} \frac{\mathrm{d}\dot{m}_w}{\mathrm{d}t} + A_u h_u \frac{\mathrm{d}\Delta T_m}{\mathrm{d}t} \tag{5.33}$$

The time derivative of the log mean temperature difference, $\frac{\mathrm{d}\Delta T_m}{\mathrm{d}t}$, is obtained as

$$\frac{\mathrm{d}\Delta T_m}{\mathrm{d}t} = \frac{\partial \Delta T_m}{\partial T_{w,m}} \frac{\mathrm{d}T_{w,m}}{\mathrm{d}t} + \frac{\partial \Delta T_m}{\partial T_{w,r}} \frac{\mathrm{d}T_{w,r}}{\mathrm{d}t} \tag{5.34}$$

We substitute Eq. (5.33) into (5.32) so that the control law of the coolant mass flow rate can be written as

$$\dot{m}_{w,m} = \int \frac{\frac{\mathrm{d}Q_{m,d}}{\mathrm{d}t} + e_Q - A_u h_u \frac{\mathrm{d}\Delta T_m}{\mathrm{d}t}}{(A_u \Delta T_m \frac{\partial h_u}{\partial \dot{m}_w})} \mathrm{d}t \tag{5.35}$$

In the above expression, $\frac{\partial h_u}{\partial \dot{m}_w}$ can be obtained from Eq. (5.18) and the $\frac{\mathrm{d}Q_{m,d}}{\mathrm{d}t}$ term may be eliminated using integration by parts. The proposed coolant mass flow rate $\dot{m}_w$ in each motor to track the ideal heat removal rate, $Q_{m,d}$, is given as

$$\begin{aligned} \dot{m}_{w,m} = & \frac{1}{A_u \frac{\partial h_u}{\partial \dot{m}_w}} \left(\frac{Q_{m,d}}{\Delta T_m} + \int Q_{m,d} \frac{\frac{\mathrm{d}\Delta T_m}{\mathrm{d}t}}{\Delta T_m^2} \right) \mathrm{d}t \\ & + \frac{1}{\frac{\partial h_u}{\partial \dot{m}_w}} \int \frac{e_Q - h_u \frac{\mathrm{d}\Delta T_m}{\mathrm{d}t}}{\Delta T_m} \mathrm{d}t \end{aligned} \tag{5.36}$$

It is assumed that the coolant mass flow rate is proportional to the pump speed.

Similarly, the air mass flow rate is proportional to the fan speed. The air mass flow rate will be set to be proportional to the coolant mass flow rate as $\dot{m}_{air} = 16\dot{m}_{w,m}$. The operation speed of pump and fan can be immediately obtained from Eq. (5.13) and Eq. (5.14). However, the actual heat removal rate, q_m is not a measurable feedback so an observer must be constructed.

5.4.3 Heat Transfer Rate Estimation

Practically, the heat removal rate in each motor cannot be directly measured. In the coolant temperature governing Eq. (5.15), the second term on the right hand side contains the cooling surface heat transfer rate, q_m. This heat removal rate is estimated using an observer constructed with measurable parameters that include the coolant temperatures at motor inlet and outlet, as well as the coolant mass flow rate, $\dot{m}_w$.

The exit coolant temperature observer may be designed as follows.

$$\begin{aligned}\frac{\mathrm{d}\hat{T}_{w(out)}}{\mathrm{d}t} =& (T_{w,in} - T_{w,o})\frac{\dot{m}_w}{M_m} + \\ & K_1\left(T_{w,o} - \hat{T}_{w(out)}\right) + K_2\int\left(T_{w,o} - \hat{T}_{w(out)}\right)\mathrm{d}t\end{aligned} \tag{5.37}$$

Applying Laplace transforms on both equations (5.15) and (5.37), it can be shown that the estimation of the heat transfer rate $\hat{q}_m$ becomes

$$\begin{aligned}\hat{Q}_m =& M_{w,m}c_{p,w}\times \\ & \left[K_1\left(T_{w,o} - \hat{T}_{w(out)}\right) + K_2\int\left(T_{w,o} - \hat{T}_{w(out)}\right)\mathrm{d}t\right]\end{aligned} \tag{5.38}$$

The unmeasurable coolant mass flow rate term e_Q term in Eq. (5.36) can be replaced by $\hat{e}_Q$ where $\hat{e}_Q = Q_{m,d} - \hat{Q}_m$.

The proposed thermal management control strategy structure is demonstrated in Fig. 5.3.

5.5 Case Study - Urban Assault and Convoy Escort Driving Cycles

To validate the proposed control strategy, a representative series of numerical simulation will be conducted for different operating scenarios and thermal management control methods. All the studies correspond to real life driving cycles with the total simulation time set to $t = 1,800$ *sec*. A summary of the case numbers and driving cycles, as well as cooling methods, is listed in Table 5.3. For the first three cases, the simulations correspond to the urban assault driving cycle while the last three cases simulate the convoy escort driving cycle. The ambient temperature is 48 $^{\circ}C$. and the target stator internal peak temperature is set at $T_{s,r}$ =90 $^{\circ}C$. Table 5.2 lists the constant parameters in the prescribed cooling system model and the controller designs.

Table 5.2: Cooling System Parameter Data

Parameters	Value	Unit	Parameters	Value	Unit
A_u	0.113	m^2	K_P	4	-
A_{flow}	1	cm^2	M_h	2	kg
$c_{p,air}$	1000	$J/kg/^{\circ}C$	M_c	0.5	kg
$c_{p,w}$	4090	$J/kg/^{\circ}C$	Mw	0.5	kg
$Cp, pipe$	0.8	-	P_{R2}	3×10^5	-
$Cpres$	0.7	-	P_{R3}	5×10^5	-
$Cflow$	0.348	-	T_B	0.5	$^{\circ}C$
Dis	25	cm^3	$T_{s,r}$	90	$^{\circ}C$
D_{fan}	0.35	m	ρ_{air}	1.099	kg/m^3
D_h	2	cm	ρ_w	0.001	kg/cm^3
k_w	0.6	$W/m^{\circ}C$	μ_w	0.0014	N
K_I	150	-			

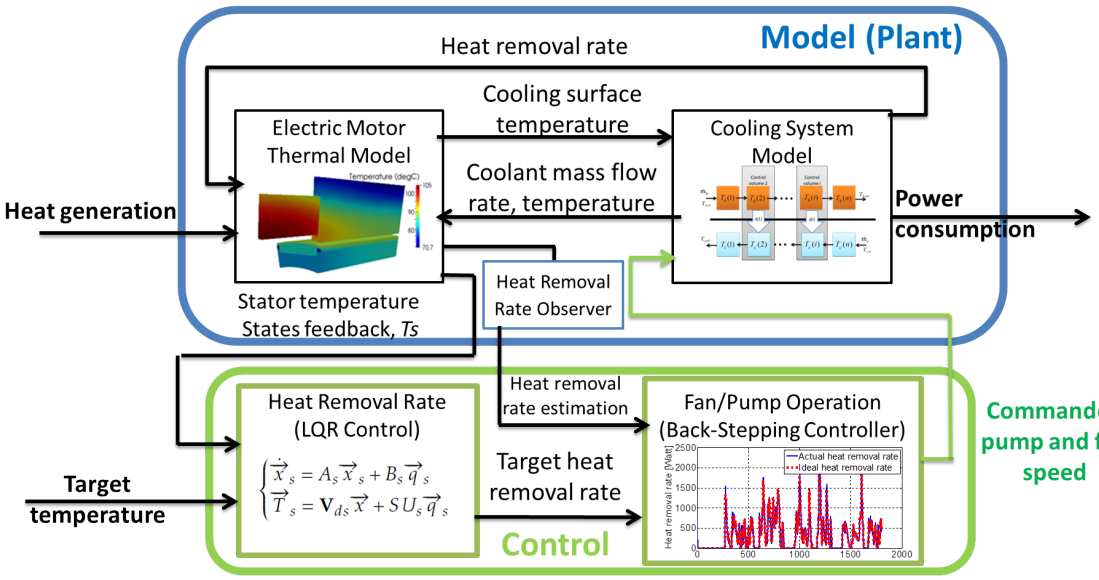

Figure 5.3: E-motor Thermal Management System Controller Design

For comparison purposes, a proportional-integral (PI) and a bang-bang (switch On/Off) controller are also considered. The classical PI control may be stated as

$$\dot{m}_w = K_P e_{hot} + K_I \int e_{hot} \mathrm{d}t \tag{5.39}$$

where K_P and K_I are the selected positive proportional and integral controller gains. The error signal, e_{hot}, represents the error between the hot spot temperature and the target value.

The conventional bang-bang control, or switch on/off controller is used in vehicle thermal management systems. When the stator peak internal temperature reaches upper limit $T_{max} = T_{s,r} + T_B$, the pump and radiator fan are switched on and operate at the maximum speed. When the stator peak internal temperature drops down to $T_{max} = T_{s,r} - T_B$, the coolant pump and radiator fan are switched off, where $T_B = 0.5\ ^\circ C$.

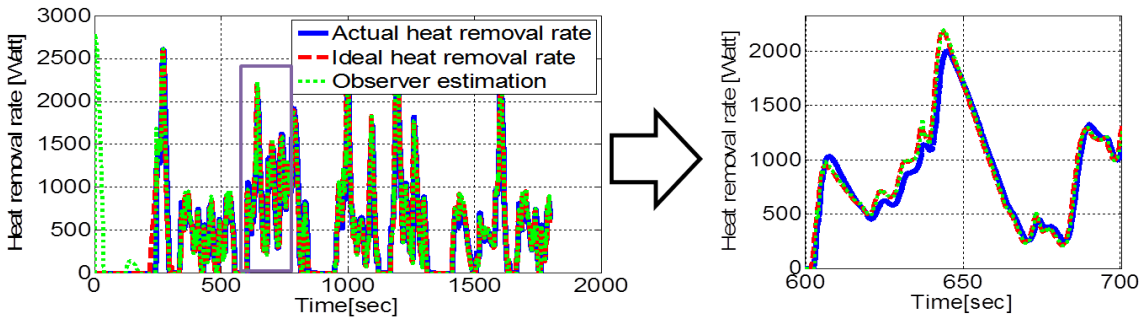

Figure 5.4: Test 5.1 - Heat Removal Rate Tracking with Observer and Optimal-Tracking Control: Actual Heat Removal Rate, Q_m, Desired Heat Removal Rate, $Q_{m,d}$, and Estimated Heat Removal Rate, $\hat{Q}_m$

The cooling system performances for Tests 5.1 to 5.6 are summarized in Table 5.3. The heat removed, stator peak internal temperature performance, and the cooling system power consumption are listed. For Tests 5.1 and 5.4, the nonlinear controllers designed in Section 5.4 are applied. The optimal regulator calculates the ideal heat removal rate per unit area on the stator surface, $H_{m,d}$. The tracking controller regulates fan and pump speeds to track the prescribed ideal heat removal rate. For Tests 5.2 and 5.5, the cooling system is operated by the classical PI controller. A conventional bang-bang control is applied in Tests 5.3 and 5.6.

The numerical results for Test 5.1 are displayed in Fig. 5.4 with the heat removal rate versus time. The blue solid line is the actual heat removal rate, q_m. The red dash line is the ideal heat removal rate that is calculated by the optimal regulator, q_{md}, and the green dot line is the heat removal rate estimated by the observer, $\hat{q}_m$ based on the measurements of coolant temperature change and its mass flow rate. The observer achieves an accurate estimation of heat removal rate and enables the nonlinear controller tracking heat removal rate to the target value with fast response and small error.

Fig. 5.5 displays the e-motor rotor and stator temperatures for Test 5.1. The

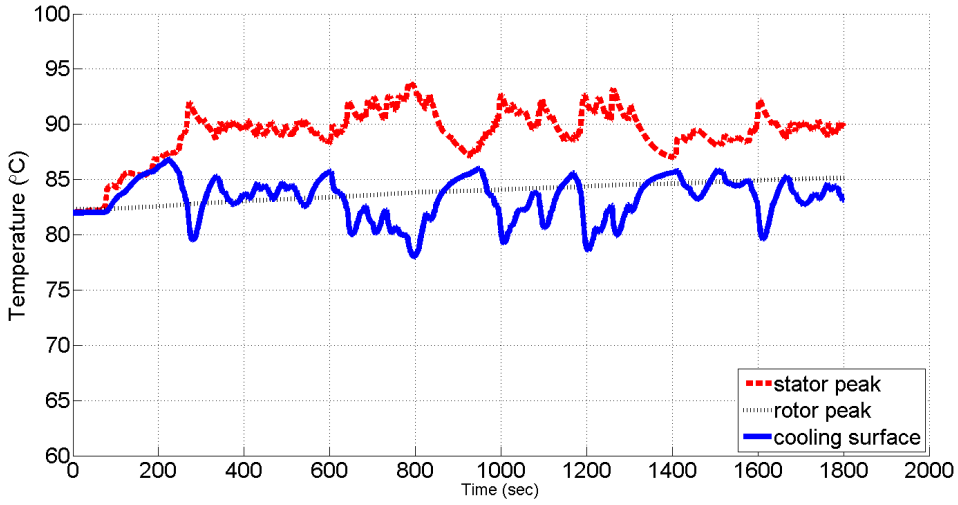

Figure 5.5: Test 5.1 - Simulated E-motor Temperatures of Stator, T_s, Rotor, T_r, and Cooling Surface, T_{so}, under Urban Assault Driving Cycle with Optimal-Tracking Control.

graph shows that the peak temperature inside the machine housing can be stabilized around the reference value with maximum error of 3.85 $^{\circ}C$. The stator internal peak temperature is tacked with an average error of $\overline{e}_{hot}$ =0.13 $^{\circ}C$. The temperature gradient across the stator is maintained below 12 $^{\circ}C$.

The e-motor temperatures simulated in Test 5.2 are presented in Fig. 5.6. By applying the classic PI controller, the stator peak internal temperature is stabilized around the target value of 90 $^{\circ}C$. However, without considering the thermal resistance of the stator and the heat generation rate, the average tracking error is $\overline{e}_{hot}$ =1.98 $^{\circ}C$ which obviously exceeds Test 5.1.

The driving cycle simulation results for Test 5.3 are shown in Fig. 5.7. The bang-bang controller offers acceptable hot spot temperature tracking around the target with the average tracking error $\overline{e}_{hot}$ =1.68 $^{\circ}C$. A drawback of this control method is that the cooling surface temperature is much lower than the peak internal temperature, which indicates a large temperature gradient from the internal to the external

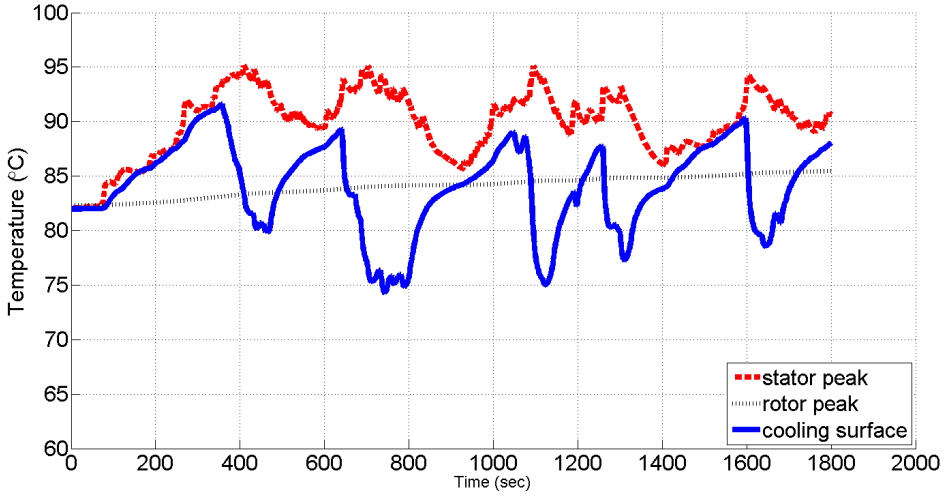

Figure 5.6: Test 5.2 - Simulated E-motor Temperatures of Stator, T_s, Rotor, T_r, and Cooling Surface, T_{so}, under Urban Assault Driving Cycle Hot Spot Temperature with PI Control.

Table 5.3: Numerical Study: Control Scenarios and Simulation Results

Test No.	Driving Cycle	Control Strategy	Heat Removal $[kJ]$	Hot Spot Temp Tracking Error $[°C]$		Energy Cost $[kJ]$	
				Maximum	Average	Pump	Fan
5.1	Urban Assault	Optimal Tracking	8.44×10^2	3.85	0.13	0.63	33.7
5.2		Hot Spot PI	8.05×10^2	5.16	1.98	1.94	1.05×10^2
5.3		Switch On/Off	8.5×10^2	3.82	1.68	0.68	36
5.4	Convoy Escort	Optimal Tracking	1.26×10^3	7.84	0.32	3.2	1.75×10^2
5.5		Hot Spot PI	1.28×10^3	8.45	1.25	4.62	2.46×10^2
5.6		Switch On/Off	1.25	8.13	1.85	4.05	2.16×10^2

motor surface. The unnecessary cooling and the large coolant flow rate together require a greater cooling system power consumption.

The simulation results of the electric motor temperature for Test 5.4 are displayed in Fig. 5.8. It can be observed that, during most of the driving cycle, the peak stator inner temperature was stabilized around the reference value of 90 $°C$. However, when the heat generation rate is higher than the heat removal capability of the cooling cycle, the stator hot-spot temperature reaches a peak value of 98 $°C$. This situation occurs even though the cooling system operates with maximum fan/pump

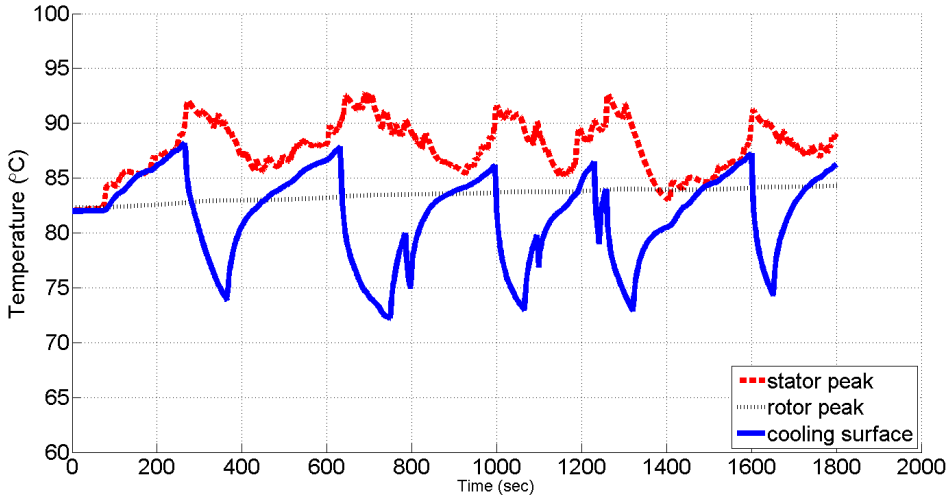

Figure 5.7: Test 5.3 - Simulated E-motor Temperatures of the Stator, T_s, Rotor, T_r, and Cooling Surface, T_{so} under the Urban Assault Driving Cycle with Switch On/Off Control

speed due to the demanding driving cycle. The optimal-tracking controller offers an average tracking error of $\overline{e}_{hot} = 0.32\ ^{\circ}C$.

The simulation results for Test 5.6 are demonstrated in Fig. 5.9. The stator peak internal temperature is stabilized by the bang-bang controller with an average tracking error of $\overline{e}_{hot}$ =1.85 $^{\circ}C$. The bang-bang control runs the coolant pump and fan at full speed. The machine suffers a large temperature fluctuation in this test. In contrast, the classic PI controller offers smaller tracking error of $\overline{e}_{hot}$ =1.25 $^{\circ}C$ in Test 5.5.

The power consumption and the total heat removal for each test are also listed in Table 5.3. The proposed thermal management system (Tests 5.1, 5.4) offers advantages in power consumption. For the urban assault driving cycle, the classical PI controller requires about 210% more cooling system power consumption when compared to the proposed optimal-tracking control strategy. In Test 5.3, the fan and coolant pump consumed only 106% of the energy cost in Test 5.1, but with

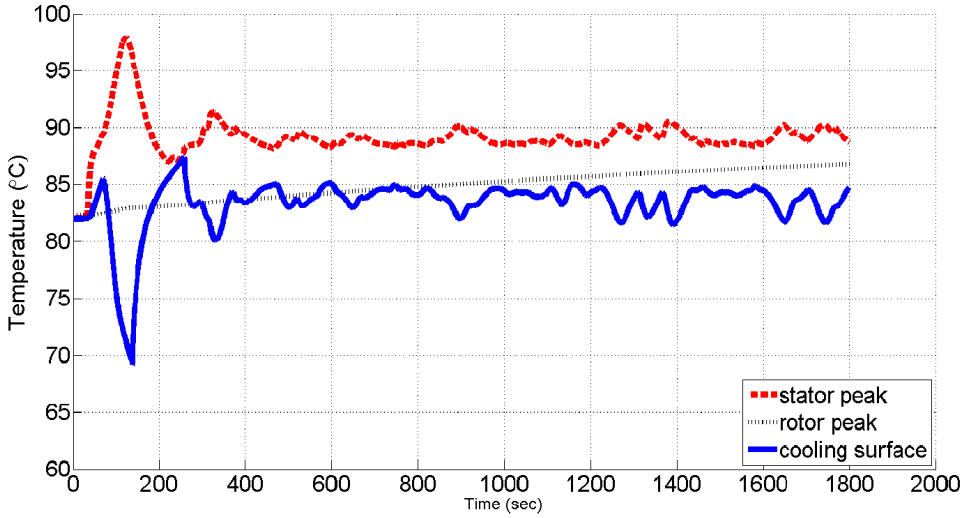

Figure 5.8: Test 5.4 - Simulated E-motor Temperatures of Stator, T_s, Rotor, T_r, and Cooling Surface, T_{so}, under Convoy Escort Driving Cycle with Optimal-Tracking Control.

larger average hot spot temperature tracking error. For the convoy escort driving cycle, the proposed control strategy also shows advantages in cooling actuator's power conservation. The energy lost in Test 5.4 is 178.2 kJ while in Test 5.5 the classic PI controller took 40% higher power consumption.

The optimal-tracking controller takes advantage of the temperature gradient and the conductive heat transfer between the heat source and the cooling surface using the reduced-order thermal model. This control method effectively tracks the heat generation inside the machine and balance the heat removal rate to it, and consequently reduces the energy waste from unnecessary over-cooling. Tests 5.1 and 5.4 provide better performance in both hot spots temperature stabilization and power consumption conservation. Furthermore, the controller is suitable in practical cooling systems designed for various kinds of electric machines with minimized cooling system power costs.

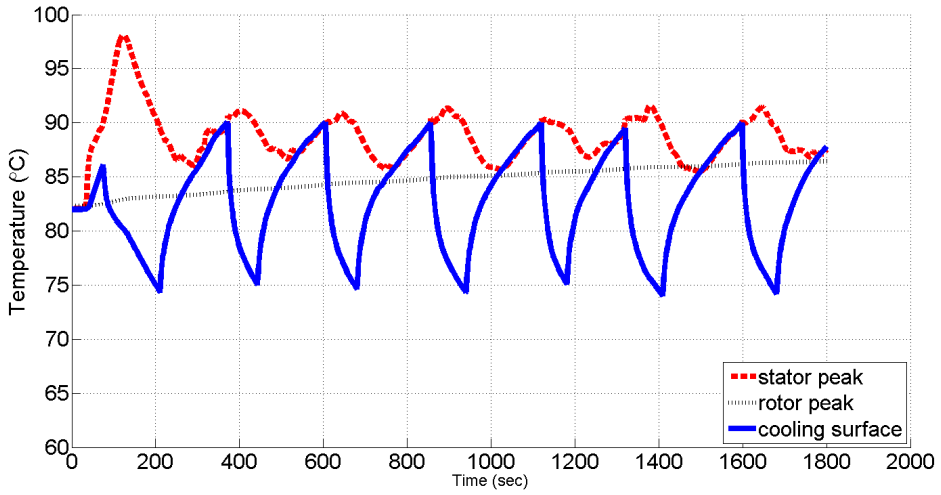

Figure 5.9: Test 5.6 - Simulated E-motor Temperatures of the Stator, T_s, Rotor, T_r, and Cooling Surface, T_{so} under the Convoy Escort Driving Cycle with Switch On/Off Control.

5.6 Summary

A reduced-order electric motor thermal model, derived from a three-dimensional finite element analysis simulation, offers high accuracy and computational efficiency. The e-motor model serves as the basis for a thermal management system which stabilizes the peak temperature inside the machine under driving cycles with large torque loads. A linear regulator, based on optimal control theory, calculates the optimal heat removal rate on the motor's interior cooling surface. This ideal heat removal rate serves as the reference in a nonlinear tracking controller. Two numerical case studies have demonstrated that the proposed thermal management system can stabilize the hot spot temperatures inside the electric motor at the target value with small tracking error and reduced cooling system power consumption.

Chapter 6

An Engine Thermal Management System Design for Military Ground Vehicle – Simultaneous Fan, Pump and Valve Control

The pursuit of greater fuel economy in internal combustion engines requires the optimization of all subsystems including thermal management. The reduction of cooling power required by the electro-mechanical coolant pump, radiator fan(s), and thermal valve demands real time control strategies. To maintain the engine temperature within prescribed limits for different operating conditions, the continual estimation of the heat removal needs and the synergistic operation of the cooling system components must be accomplished. The reductions in thermal management power consumption can be achieved by avoiding unnecessary over-cooling efforts which are often accommodated by extreme thermostat valve positions. In this paper, an optimal nonlinear controller for a military M-ATV engine cooling system will be pre-

sented. The prescribed engine coolant temperature will be tracked while minimizing the pump, fan(s), and valve power usage. A case study investigates the proposed control strategy's performance in comparison to other methods for temperature tracking and energy conservation. The optimal nonlinear controller offered satisfactory coolant temperature tracking with an average error of 0.35 $^{\circ}C$ and at least 13% reduction in total cooling power.

6.1 Introduction

Modern ground vehicles apply a variety of electronic sensors, on-board controller systems, and electric driven actuators to regulate the powertrain's operation for improved fuel economy and reduced tailpipe emissions. Advanced control algorithms have been introduced for precise fuel injection, spark delivery, air flow management, and transmission shifting to name a few process to satisfy federal regulations while meeting consumer demands. Applying model-based control strategies for accurate thermal management system operation is a promising approach as vehicle cooling has not yet received thoughtful widespread attention from the automotive engineering community.

In an engine cooling system, the actuators (pump, fans) operate at full rotational speed to reach their maximum heat removal capabilities when the engine load and ambient temperature are high. In this instance, the thermostat valve will be fully open. In contrast, the actuator speeds can be reduced and thermostat valve predominately closed when the thermal load and ambient temperatures are low which promotes passive convective cooling. However, in between these extremes, the thermal management system's operation needs to be optimized for variable heat rejection to achieve temperature tracking with minimal power usage. A medium thermal load

under a moderate surrounding temperature provides a space for advanced thermal management controller designs as shown in Fig. 6.1.

An efficient thermal management system design is essential for powertrain reliability, fuel economy, and performance (Park et al., 2013). In a study by Park and Jung (Park and Jung, 2010), various powertrain cooling system architectures and the accompanying effect on the power consumption has been investigated. The upgrade of mechanical actuators in cooling systems by real time controlled electro-mechanical components facilitates improved efficiency under most operating conditions. A variety of control strategies, applied to advanced vehicle powertrain thermal management systems, have been studied (Badekar et al., 2006)(Tao and Wagner, 2014). The integration of an electric pump and smart valve for faster engine coolant warm up time and reduced temperature fluctuation has been reported in (Wagner et al., 2002). Cho *et al.* (Cho et al., 2007) explored the benefit of a controllable electric pump for truck engine cooling which offers a significant reduction in power consumption and possible heat exchanger downsize. Page *et al.* (Page and Kozierowski, 2005) investigated a classical PID controller for the cooling system featuring with multiple electric radiator fans and heat controlled thermostats. A suite of nonlinear control strategies was developed by Salah *et al.* (Salah et al., 2010) to adjust the smart valve position and the coolant flow rate to track the desired engine temperature. A differential flatness nonlinear controller has demonstrated improved temperature trajectory tracking performance (Aschemann et al., 2011).

The radiator fan(s) has been identified to consume that greater power within engine cooling systems when compared to the other components (pump, smart valve) (Moyle et al., 2006). Recently, attention has focused on optimizing the fan(s) speed to minimize power usage while rejecting sufficient heat. Wang *et al.* (Wang et al., 2015) conducted a detailed experimental analysis of multiple electric radiator fan

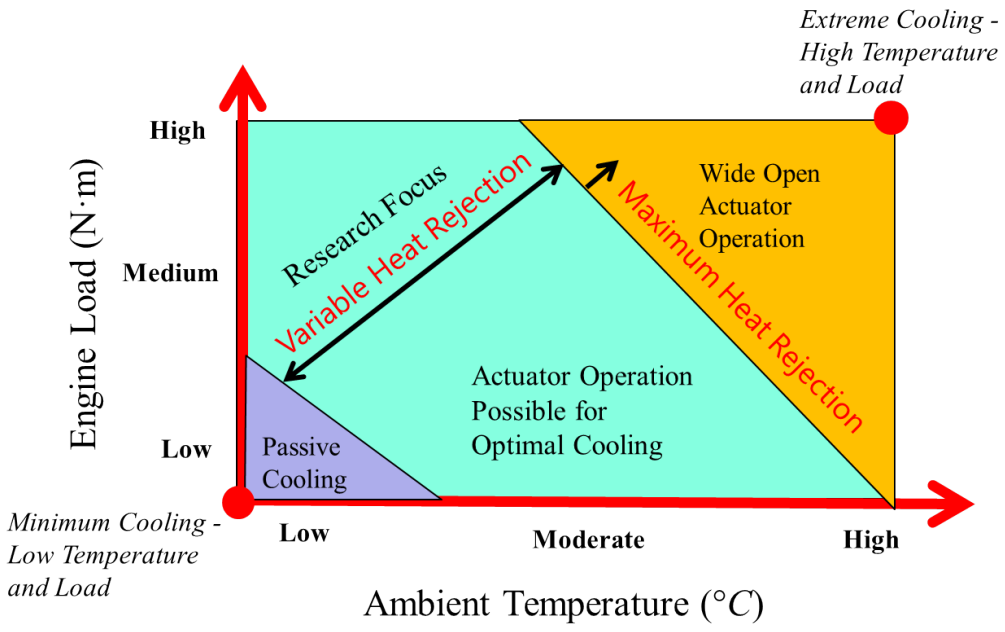

Figure 6.1: Engine Cooling System Optimization Control Space for Power Cost Reduction: Variable Heat Rejection for Medium Thermal Load under Moderate Ambient Temperature

configurations. A rule of thumb and optimization control strategy for total fan array power minimization based on thermal load was proposed (Wang and Wagner, 2015a). Within the area of hybrid electric vehicles (HEV), Tao *et al.* (Tao and Wagner, 2016) developed a model predictive controller to regulate the compressor speed in vapour compression systems to track cooling air temperature and stabilize core battery temperatures within battery packs. A high fidelity electric motor thermal model was implemented in a heavy-duty HEV cooling system controller which tracked the motor's inner peak temperature (Tao et al., 2015).

This research study will examine an engine thermal management system for military ground vehicles, specifically an M-ATV, as shown in Fig. 6.2. The proposed control strategy will synchronously regulate the radiator fan, coolant pump, and smart valve operations to track the prescribed reference temperature with con-

Figure 6.2: Notional MRAP All-Terrain Vehicle (M-ATV).

sideration power consumption. The remainder of this paper is arranged as follows. In Section 6.2, a lumped parameter thermal model is presented that describes the engine cooling system's thermal behaviour. In addition, a suite of actuator models will be developed to estimate the power consumption. In Section 6.3, an optimal nonlinear controller, with two supplemental controllers, will be designed. A case study with numerical results will be presented and discussed to explore the performance and power consumption for different control strategies in Section 6.4. Section 6.5 concludes this work.

6.2 Library of Mathematical Models

An engine thermal management system, featuring electric driven actuators, will be mathematically modeled to establish a basis for controller designs. The M-ATV proposed cooling system configuration consists of an internal combustion engine (ICE), electric coolant pump, smart valve, variable speed fan, and radiator (refer to

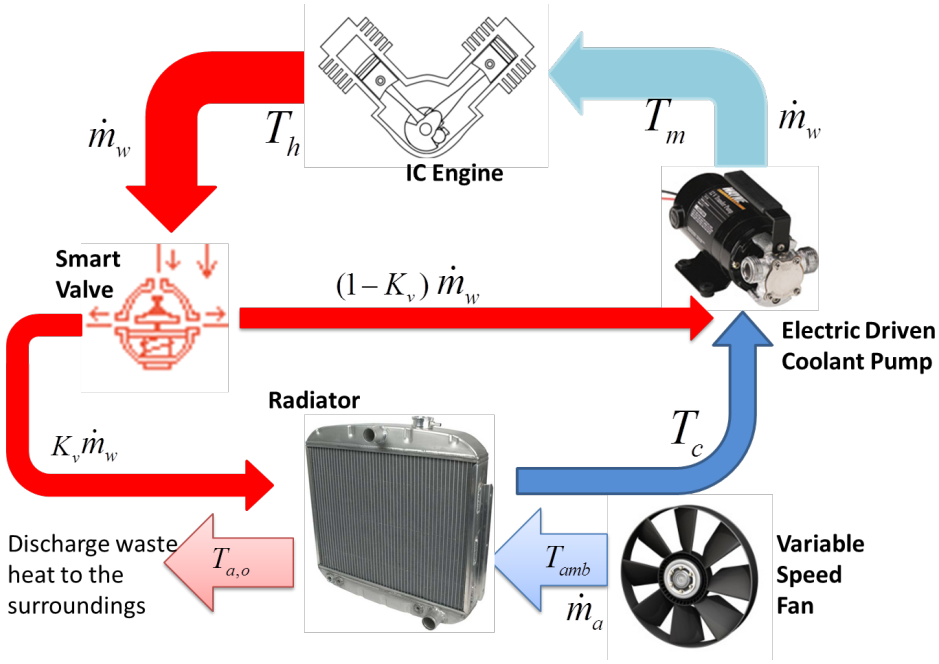

Figure 6.3: Engine Cooling System Configuration.

Fig. 6.3). A lumped parameter approach will be pursued to develop the differential and algebraic equations.

6.2.1 Thermal Dynamics of the Engine and Heat Exchanger

The coolant is circulated by the electric pump through the cooling system as shown in Fig.6.3. The smart valve allows a temperature dependent portion of the total coolant flow through the radiator and the remainders goes back to engine directly. The coolant discharges the combustion heat in the radiator via forced convective heat transfer. The governing thermal equation for the coolant temperature change at the engine outlet, T_h, may be expressed as

$$M_{w,e}c_{p,w}\frac{\mathrm{d}T_h}{\mathrm{d}t} = h_e\left(T_e - T_c\right) + \dot{m}_w c_{p,w}\left(T_c - T_h\right) \tag{6.1}$$

where $M_{w,e}$ is the coolant mass inside the engine. The parameter $c_{p,w}$ is the specific heat of water. The term Q_e represents the engine waste heat from combustion. The second term on the right side of Eq. (6.1) is the heat removal attributed to the coolant mass flow rate, $\dot{m}_w$.

The coolant at the pump's outlet, or engine inlet, is a mixture of the cold and hot coolant streams. The smart valve regulates the coolant mass flow through the radiator and bypass. A portion of the coolant will flow into the radiator and discharge the waste heat to the ambient surroundings. The bypass circuit directs the remaining fluid flow right to pump. In this study, the valve is electrically driven and linearly controlled such that $0 \leq K_v \leq 100\%$. When $K_v = 100\%$, the valve is fully open and all the coolant will be directed into the radiator. In contrast, $K_v = 0\%$ means that the valve is closed and all the coolant is routed through the bypass to the pump.

The the coolant temperature at the pump's outlet, T_{pump}, is a linear combination of the hot, T_h, and cold, T_c, coolant temperatures defined as

$$T_{pump} = (1 - K_v)T_h + K_v T_c \tag{6.2}$$

The differential equation for cold coolant temperature at the radiator outlet, Tc, may be written as

$$M_{w,r} c_{p,w} \frac{\mathrm{d}T_c}{\mathrm{d}t} = K_v \dot{m}_w c_{p,w} (T_h - T_c) - Q_{rad} \tag{6.3}$$

where $M_{w,r}$ is the coolant masses inside the radiator, the variable Q_{rad} on the right side is the heat transfer from the coolant to the cooling air in the radiator. The term $K_v \dot{m}_w c_{p,w} (T_h - T_c)$ denotes the heat transferred by the coolant flow itself due to temperature differences.

Finally, the dynamic change in the cooling air temperature at the radiator outlet, $T_{air,o}$, is modelled as

$$M_{air,r}c_{p,air}\frac{\mathrm{d}T_{air,o}}{\mathrm{d}t} = Q_{rad} + \dot{m}_{air}c_{p,air}\left(T_{amb} - T_{air,o}\right) \tag{6.4}$$

In this expression, the parameter $M_{air,r}$ is the air mass inside the radiator control volume, and denotes the specific heat of air. The term T_{amb} represents the temperature of the ambient air, which will be delivered through the radiator by the variable speed fan at mass flow rate, $\dot{m}_{air}$.

6.2.2 Cooling Actuators: Radiator Fan and Pump

The total power consumption of the cooling system should be reduced to help satisfy the legislated fuel and emissions requirements. Only the power consumed by the radiator fan and the coolant pump will be analysed, given that the power used by the smart valve is negligible. The radiator heat transfer is directly affected by the cooling air mass flow rate provided by the fan which may be written as

$$\dot{m}_{air} = D_{fan}^3 C_{flow}\rho_{air}\left(\frac{N_{fan}}{60}\right) \tag{6.5}$$

where N_{fan} is the fan speed, and C_{flow} is the flow rate coefficient. The parameters D_{fan} and ρ denote the equivalent fan diameter and the cooling air density.

The total air pressure increase due to the fan, dP_{fan} may be calculated as

$$dP_{fan} = D_{fan}^2 C_{press}\rho_{air}\left(\frac{N_{fan}}{60}\right)^2 \tag{6.6}$$

where the parameter C_{press} is defined as the pressure drop coefficient across the

radiator. The fan power consumption rate, E_{fan} , is given as

$$E_{fan} = D_{fan}^3 C_{flow} dP_{fan} \left(\frac{N_{fan}}{60} \right) \tag{6.7}$$

For a given cooling system, the values of C_{flow}, C_{press}, D_{fan}, and ρ_w are constant. Thus, the estimation of the radiator fan power consumption can be characterized as a function of the air mass flow rate so that

$$E_{fan} = k_{fan} \dot{m}_{air}^3 \tag{6.8}$$

where $k_{fan} = D_{fan}^{-4} C_{press} \rho_{air}^{-1} C_{flow}^{-2}$, The coolant mass flow rate. $\dot{m}_w$, driven by the electric pump, is dependent on the pump rotation speed, N_{pump}, such that

$$\dot{m}_w = \rho_w \left(\frac{N_{pump}}{60} \right) Dis \tag{6.9}$$

where the term Dis is the maximum pump displacement. The parameter ρ_w denotes the water density while the variable N_{pump} is the pump speed.

The total pressure drop across the radiator and the pipe in the coolant flow is calculate as

$$dP_w = \rho_w C_{p,rad} \left(\frac{N_{pump} Dis}{60 A_{flow}} \right)^2 + \dot{m}_w^2 C_{p,pipe} \tag{6.10}$$

where $C_{p,rad}$ and $C_{p,pipe}$ denote the pressure rise coefficients in the radiator and pipe, respectively. The parameter A_{flow} is the coolant flow cross section area in the radiator. The pump power consumption rate, E_{pump}, is defined as

$$E_{pump} = dP_w \left(\frac{N_{pump}}{60} \right) Dis \tag{6.11}$$

The pump's power consumption can be summarized as a function of the coolant mass flow rate given the parameters A_{flow}, $C_{p,rad}$, C_{pipe}, Dis, and ρ_w for a given cooling system as

$$E_{pump} = k_{pump}\dot{m}_w^3 \tag{6.12}$$

where $k_{pump} = \rho_w^{-1}C_{p,pipe} + A_{flow}^{-2}\rho_w^{-2}C_{p,rad}$,

Note that the power consumption of the water pump and radiator fan are both proportional to the cube of the given fluid flow rate.

6.3 Controller Designs

An optimal nonlinear controller, based on the thermal model, will be designed to minimize the total power consumption of the prescribed ICE cooling system. For comparison purposes, two other control strategies will also be introduced including a state flow controller, and a classical PI controller.

6.3.1 Optimal Nonlinear Control

An optimal nonlinear controller will simultaneously regulate the operation of the coolant pump, radiator fan, and smart valve to track the desired engine temperature while using the theoretically minimum total power. The primary control objective is to stabilize the coolant temperature, T_h, to the prescribed target value, $T_{h,d}$.

6.3.1.1 Pump Speed Control

The coolant pump electric motor shaft speed will be controlled by an adaptive nonlinear controller. Define the coolant temperature tracking error as

$$e_h = T_h - T_{h,d} \tag{6.13}$$

The T_{pump} term in Eq. (6.1) may be replaced by Eq. (6.2), and divide both side of the equation by M_w,$e_c p, w$, the coolant temperature change at the engine outlet can be simplified as

$$\frac{\mathrm{d}T_h}{\mathrm{d}t} = \frac{1}{M_{w,e}}\left[\frac{Q_e}{c_{p,w}} - K_v \dot{m}_w (T_h - T_c)\right] \tag{6.14}$$

Considering that the waste heat of combustion, Q_e, is not measurable, an estimation of engine heat generation, $\hat{Q}_e$, is applied in the controller design. So, define the heat generation estimation error as

$$\tilde{Q} = \hat{Q}_e - Q_e \tag{6.15}$$

The desired target coolant temperature, $T_{h,d}$, is constant. The tracking error dynamic change may be evaluated by computing the time derivative of Eq. (6.13) so that

$$\dot{e}_h = \dot{T}_h - \dot{T}_{h,d} = \frac{\mathrm{d}T_h}{\mathrm{d}t} \tag{6.16}$$

To stabilize the coolant temperature, the control objective can be stated as

$$e_h \leq \xi \text{ as } t \to \infty \tag{6.17}$$

To realize this control purpose, a Lyapunov based backstepping adaptive controller may be developed to regulate the pump speed by determining the coolant mass flow rate, . First, define the second term in Eq. (6.3) as

$$u_1 = \frac{K_v \dot{m}_w}{M_{w,e}}(T_h - T_c) \tag{6.18}$$

A Lyapunov function, V, can be selected as

$$V = \frac{1}{2}\left(e_h^2 + \tilde{Q}_e^2\right) \tag{6.19}$$

The Lyapunov function must be positive definite. If its time derivative is negative definite, the coolant temperature tracking error and the heat generation estimation error converges to zero eventually (De Queiroz et al., 2012). Assuming that the change of Q_e is slow, then the Lyapunov function time derivative can be written as

$$\dot{V} = e_h \dot{e}_h + \tilde{Q}_e + \dot{\tilde{Q}}_e \tag{6.20}$$

A control law, u_1, may be proposed with the form

$$u_1 = k_e e_h + \frac{\hat{Q}_e}{M_{w,e} c_{p,w}} \tag{6.21}$$

Replace the second term in Eq. (6.14) by Eq. (6.21), so that the dynamic change of the coolant temperature tracking error becomes

$$\dot{e}_h = -k_e e_h - \frac{\tilde{Q}_e}{M_{w,e} c_{p,w}} \tag{6.22}$$

Now design the heat generation estimation as

$$\dot{\hat{Q}}_e = \frac{e_h}{M_{w,e} c_{p,w}} \tag{6.23}$$

In the next step, substitute Eq. (6.22) and Eq. (6.23) into Eq. (6.20), the derivative of the Lyapunov function can be written as

$$\dot{V} = -k_e e_h^2 + \tilde{Q}_e \left(\dot{\hat{Q}}_e - \frac{e_h}{M_{w,e} c_{p,w}} \right) = -k_e e_h^2 \tag{6.24}$$

The Lyapunov function converges to zero with a negative definite time derivative. This indicates that the coolant tracking error, e_h, can be stabilized by applying the proposed input U_1 in Eq. (6.21). The desired coolant mass flow rate in the engine can be solved with Eqs. (6.19) and (6.22) as

$$\dot{M}_{w,d} = \frac{M_{w,e} \left[k_e e_h + \frac{\int e_h \mathrm{d}t}{(M_{w,e} c_{p,w})^2} \right]}{K_v (T_h - T_c)} \tag{6.25}$$

6.3.1.2 Fan Speed Control for Total Power Minimization

The overall objective of the optimal nonlinear controller design is to minimize the total cooling system power consumption. Thus, the operation of the radiator fan must be optimized as it represents the largest electrical power consumption. The cooling air mass flow rate control law is developed by tracking the cold coolant temperature, T_c, to a desired value, $T_{c,d}$, such that the total power consumption of the pump and fan is minimized with any arbitrary thermal load. Consider the system model in a static condition. It can be observed from Eqs. (6.3) and (6.4) that when the time derivatives of the cooling fluids temperatures are zero, the heat transfer rate

inside the radiator is proportional to the coolant and air mass flow rates as

$$Q_{rad} = K_v \dot{m}_w c_{p,w}(T_h - T_c) \tag{6.26}$$

$$Q_{rad} = \dot{m}_{air} c_{p,air}(T_{a,o} - T_{amb}) \tag{6.27}$$

To facilitate the optimization process, assume that the radiator size is large enough to satisfy the heat removal rate and the heat transfer can be fully developed inside the radiator. Consequently, the cooling air and the coolant temperatures are considered very close to each other at the radiator outlet. An optimization variable, T_x, to be defined as

$$T_x = T_{air,o} = T_c \tag{6.28}$$

Substituting Eqs. (6.26) and (6.27) into Eqs. (6.8) and (6.12), allows the total power consumption rate, E, of coolant pump, E_{pump} , and the radiator fan, E_{fan}, to be derived as

$$E = k_{fan}\left(\frac{Q_{rad}}{K_v c_{p,w}(T_h - T_x)}\right)^3 + k_{pump}\left(\frac{Q_{rad}}{c_{p,air}(T_x - T_{amb})}\right)^3 \tag{6.29}$$

To minimize the total power consumption rate with respect to the fluids temperature at the radiator outlet, T_x, a desired value of T_x can be solved by

$$\frac{\partial E}{\partial T_x} = 0 \tag{6.30}$$

which leads to the result

$$\left(\frac{T_x - T_{amb}}{T_h - T_x}\right) = \left(\frac{k_{pump}}{k_{fan}}\right)^{\frac{1}{4}}\left(\frac{c_{p,air}}{c_{p,w}K_v}\right)^{\frac{3}{4}} = X \tag{6.31}$$

Given that the hot coolant temperature is tracked to $T_{h,d}$, and the ambient air temperature, T_{amb}, is constant, the desired cooling air temperature at the radiator outlet can be derived by solving Eq. (6.30) and Eq. (6.31) so that

$$T_{air,o,d} = T_{h,d} - \frac{T_{h,d} - T_{amb}}{1 + X} \tag{6.32}$$

When the coolant and air flow exiting the radiator converges to the desired temperature per Eq. (6.31), the total power consumption of the pump and fan, E, reaches a minimum point. The radiator fan speed is regulated to track this outlet cooling air temperature, $T_{air,o,d}$. A nonlinear adaptive controller can be developed in a similar manner as the coolant mass flow rate controller. Define the radiator outlet air temperature tracking error, $e_{a,o}$, as

$$e_{a,o} = T_{air,o} - T_{air,o,d} \tag{6.33}$$

To track the coolant temperature, the control objective can be stated as

$$e_{a,o} \leq \xi \text{ as } t \to \infty \tag{6.34}$$

Comparing Eqs. (6.1) and (6.4), it may be observed that the procedure to construct the cooling air mass flow rate control law will be similar to the coolant mass flow rate control law. Hence, the desired cooling air mass flow rate in the radiator is finally given as

$$\dot{m}_{air,d} = \frac{M_{air,rad}\left[k_e e_{air,o} + \frac{\int e_{air,o}\mathrm{d}t}{\left(M_{air,rad}c_{p,air}\right)^2}\right]}{(T_{air,o} - T_{amb})} \tag{6.35}$$

Note that in the above expression, there's no K_v term involved in the denominator, since the smart valve operation does not affect the radiator air flow.

6.3.1.3 Smart Valve Position Control

To avoid the potential of localized peak temperatures that exceed established limits inside the engine block, the minimum coolant mass flow rate is established as When the target coolant mass flow rate derived from Eq.(6.25) is smaller than $\dot{m}_{w,min}$, the smart thermal valve is closed to reduce the coolant flow through the radiator and achieve the target u_1. The valve opening, K_v, may be calculated as

$$K_v = \frac{\left[k_e + e_h + \frac{\in e_h \mathrm{d}t}{(M_{w,e}c_{p,w})^2}\right] M_{w,e}}{(T_h - T_c)\dot{m}_{w,min}} \tag{6.36}$$

The fan and pump speed can be easily achieved by solving N_{fan} and N_{pump} in Eqs. (6.5) and (6.8) using the target mass flow rates of the cooling fluids, $\dot{m}_{air,d}$ and $\dot{m}_{w,d}$, from Eqs. (6.25) and (6.35), respectively. The control diagram of the proposed optimal nonlinear control system is displayed in Fig. 6.4.

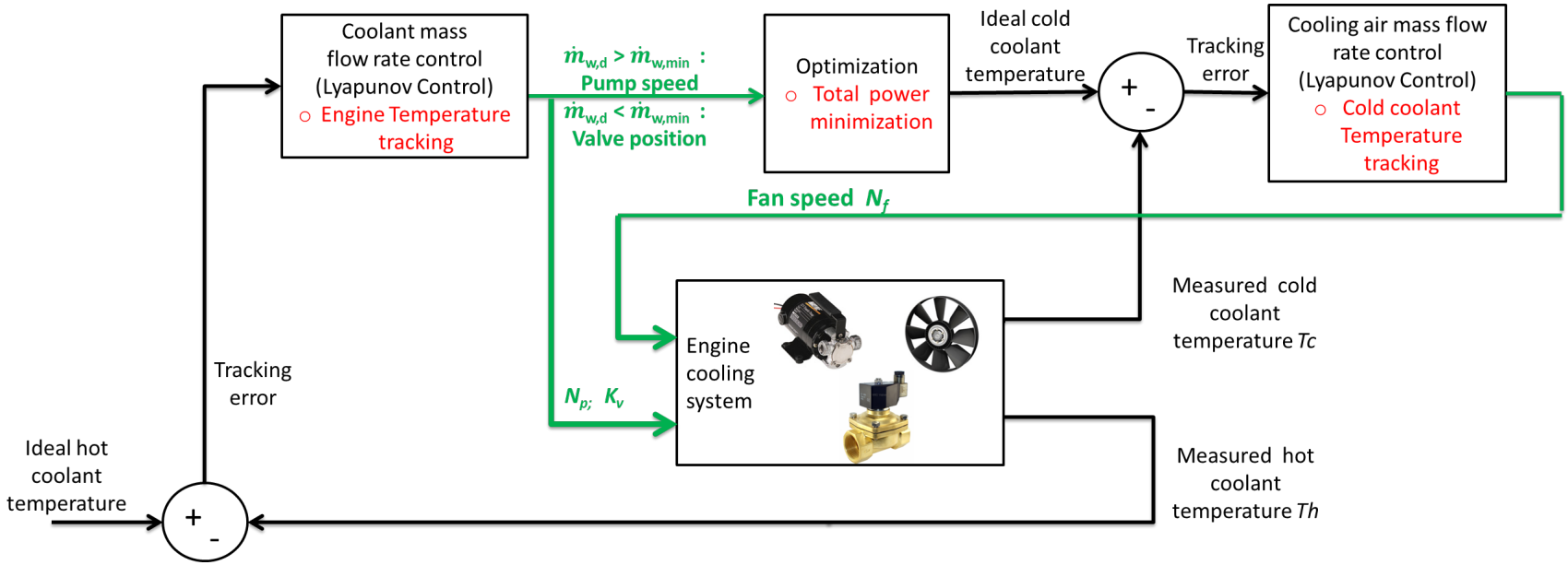

Figure 6.4: Engine Cooling Optimal Nonlinear Control System

6.3.1.4 Derivation of Desired Cooling Air Temperature at the Radiator Outlet

As discussed in Section 6.3.1.2, the cooling air temperature at the radiator outlet can be treated as design variable for the optimized fan speed controller design. To minimize the total power consumption rate with respect to the fluids temperature at the radiator outlet, $T_{x,a}$ desired value of T_x can be solved by

$$\frac{\partial E}{\partial T_x} = 0 \tag{6.37}$$

where $E = k_{fan}\left(\frac{Q_{rad}}{K_v c_{p,w}(T_h - T_x)}\right)^3 + k_{pump}\left(\frac{Q_{rad}}{c_{p,air}(T_x - T_{amb})}\right)^3$. Now, Eq. (6.37) can be written after taking the partial derivative as

$$\begin{aligned} &3k_{fan}\left(\frac{Q_{rad}}{K_v c_{p,w}(T_h - T_x)}\right)^2\left(\frac{-K_v c_{p,w}}{[K_v c_{p,w}(T_h - T_x)]^2}\right) \\ &+ 3k_{pump}\left(\frac{Q_{rad}}{c_{p,air}(T_x - T_{amb})}\right)^2\left(\frac{c_{p,air}}{[c_{p,air}(T_x - T_{amb})]^2}\right) = 0 \end{aligned} \tag{6.38}$$

Now divide both sides of this expression by $3{Q_{rad}}^2$, and then move the second term on the left side to the right side so that

$$\left(\frac{k_{fan}K_v c_{p,w}}{[K_v c_{p,w}(T_h - T_x)]^4}\right) = \left(\frac{k_{pump}c_{p,air}}{[c_{p,air}(T_x - T_{amb})]^4}\right) \tag{6.39}$$

This expression may be re-arranged to express temperature on one side as

$$\left(\frac{(T_x - T_{amb})^4}{T_h - Tx}\right) = \left(\frac{k_{pump}c_{p,air}^3}{k_{fan}K_v^3 c_{p,w}^3}\right) \tag{6.40}$$

Thus, the design variable T_x may be defined such that

$$\left(\frac{T_x - T_{amb}}{T_h - T_x}\right) = \left(\frac{k_{pump}}{k_{fan}}\right)^{\frac{1}{4}}\left(\frac{c_{p,air}}{c_{p,w}K_v}\right)^{\frac{3}{4}} \tag{6.41}$$

which is same as Eq. (6.31). Based on this analysis, the ideal temperature for the air and coolant at the radiator outlet is not influenced by the radiator heat removal rate, Q_{rad}. Consequently, the proposed desired temperature, T_x, per Eq. (6.31) is a function of the valve position, K_v, that minimizes the total power consumption, E.

6.3.2 State Flow Control

A state flow control strategy has been investigated to simultaneously regulate the radiator fan coolant pump and smart valve. According to Wang and Wagner (Wang and Wagner, 2015b), the coolant temperature responds to different cooling actuator combinations with varying magnitudes and time responses. For instance, the smart valve causes the largest coolant temperature change. In contrast, the pump operation provides a faster temperature variation response time with larger fluctuations. Finally, the temperature change due to the radiator fan requires a longer response time when compared to the valve and pump operation. Since the engine fan uses the most power and the smart valve operation consumes a negligible amount, the state flow control strategy can be designed as shown in Fig. 6.5.

In the initial state, the valve is half closed and the coolant flow rate is set to a minimum. The radiator fan is operated on due to the high power cost. To facilitate the implementation of the state flow control algorithm, define a series of threshold values of the engine coolant temperature as

$$T_{h,max} > T_{h,high} > T_{h,d} > T_{h,low} > T_{h,min} \tag{6.42}$$

The parameters $T_{h,max}, T_{h,high}, T_{h,low}$, and $T_{h,min}$ are selected to determine the operation of the cooling system. When the coolant warms up and reaches its desired temperature value, $T_{h,d}$, the valve will fully open to $K_v = 1$. If the coolant

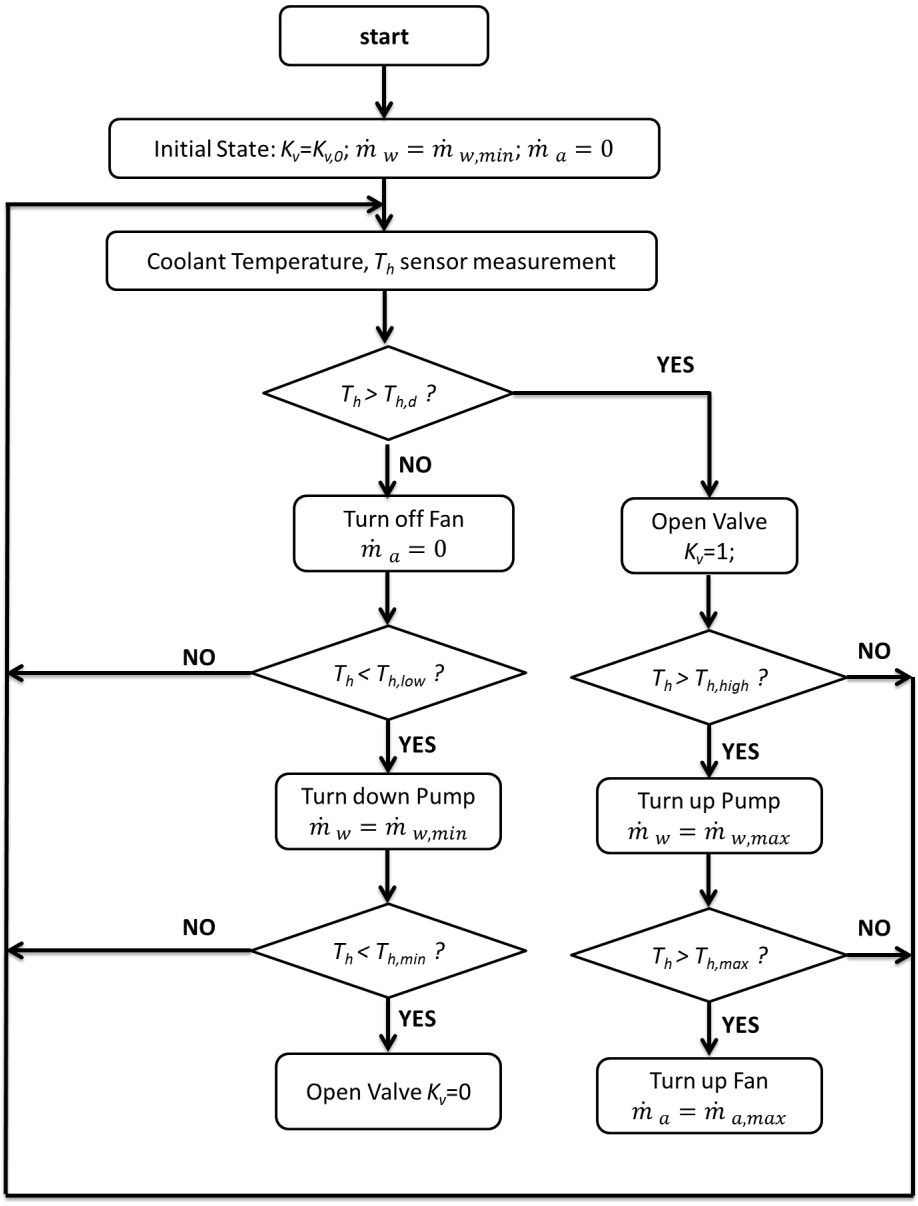

Figure 6.5: State Flow Control System

temperature keeps rising up to $T_{h,high}$, then the coolant pump will be switched to its maximum speed. The radiator fan is only switched on to maximum speed when the sensor measurement T_h reaches the upper band $T_{h,max}$. The radiator fan will then continue operating at its maximum speed until the coolant temperature drops to $T_{h,d}$.

When the coolant temperature starts dropping to $T_{h,d}$, the radiator fan will be switched off first. The coolant pump speed is then decreased to its minimum value when the coolant temperature drops to $T_{h,low}$. The smart valve is placed in a half open state with $K_v = 0.5$ if the coolant temperature continues to drop into the lower band, $T_{h,min}$. By operating the cooling actuators in this synchronized manner, the engine coolant temperature can be regulated around the prescribed value, $T_{h,d}$.

6.3.3 Classic PI Control

A classical proportional integral (PI) controller may be designed to simultaneously regulate the fan, pump, and smart valve operations. The coolant pump and radiator fan speeds, as well as the valve opening position, can be stated in the compact form as

$$\Big[N_{pump}, N_{fan}, K_v\Big] = (K_P + e_h + K_I \int e_h \mathrm{d}t) \left[1, r, \frac{1}{N_{pump,min}}\right] + u_0 \tag{6.43}$$

where $u_0 = (N_{p,0}, N_{fan,0}, K_{v,0})$ is the initial input. The proportional, K_P, and integral, K_I, gains are positive constants. These values are selected such that the cooling air and coolant mass flow rate are proportional per a constant ratio, r, selected by the Calibration Engineer. The initial input u_0 is applied at the beginning of each test. The valve opening position, K_v, has been normalized to an interval of $[0, 1]$ by dividing the pump speed by its minimum value, $N_{pump,min}$

6.4 Case Study - Numerical Results

To evaluate the three control methods designed for an engine cooling system, a case study has been conducted using an engine thermal management system will be modeled in AMESim while the controllers in MATLab/Simulink. The simulation results will be presented and discussed to demonstrate the advantages of the optimal nonlinear controller, in comparison to the conventional state flow and the classical PI controllers. The mean average value of the coolant temperature tracking error, and the total energy consumption of the coolant pump and fan will be reported. The system model and controller parameters have been summarized in Table 6.1.

The military ground vehicle studied is a hybridized mid-size truck equipped with a 7.2 L turbo-diesel engine. Urban assault and convoy escort driving cycles were investigated for cooling performance designs. For each cycle, the engine heat generation rate has been estimated based on the vehicle speed profile, the corresponding fuel consumption rate, and the effective engine propulsion power output. The engine waste heat generation rate, Q_e, for both driving cycles have been displayed in Fig. 6.6.

Six tests were conducted in the Case study as shown in Table 6.2. The target coolant temperature, $T_{h,d}$, is set to be 90 $^{\circ}C$. In the Tests 6.1 to 6.3, the urban assault driving cycle is implemented. While Tests 6.4 to 6.6, feature the convoy escort driving cycle. The coolant temperature tracking and power consumption of the radiator fan and coolant pump were recorded.

Table 6.1: Parameter Values and Simulation Specifications

Parameter	Value	Unit
$c_{p,w}$	4090	$J/(kg°C)$
$c_{p,air}$	994	$J/(kg°C)$
D_{fan}	500	mm
Dis	25	mL
k_{fan}	78.8	-
k_{pump}	86.4	-
k_e	2	-
K_I	10	-
K_P	300	-
$K_{v,0}$	1	-
$M_{air,r}$	0.3	kg
$M_{w,e}$	2	kg
$M_{w,r}$	2	kg
$N_{pump,min}$	1200	RPM
$N_{pump,0}$	1200	RPM
$N_{fan,0}$	2000	RPM
r	1.5	-
T_{amb}	30	$°C$
$T_{h,d}$	90	$°C$
$T_{h,max}$	93	$°C$
$T_{h,high}$	91.5	$°C$
$T_{h,low}$	88.5	$°C$
$T_{h,min}$	87	$°C$
ρ_{air}	1.2	kg/m^3
ρ_w	1000	kg/m^3

Table 6.2: Numerical Study Test Conditions and Simulation Results

Test No.	Driving Cycle	Cooling Control Algorithm	Temperature Tracking Error, e_h $[^\circ C]$		Coolant Pump Energy Cost $[kJ]$	Radiator Fan Energy Cost $[kJ]$	Total Energy Cost $[kJ]$
			Peak	Average			
6.1	Urban Assault	Optimal Nonlinear	3.8	0.35	61.5	162.4	223.9
6.2		State Flow	5.9	1.33	311.4	1478.5	1789.9
6.3		Classical PI	4.2	0.45	36.5	219.6	256..1
6.4	Convoy Escort	Optimal Nonlinear	2.1	0.34	159.6	439.5	599.1
6.5		State Flow	5.3	1.76	636.5	3085.4	3721.9
6.6		Classical PI	5.7	0.79	50.8	643.9	694.7

In Test 6.1, the optimal nonlinear control strategy developed in the Section 6.3.1 was implemented. The coolant temperature responses are displayed in Fig. 6.7, have been stabilized about the target value within an average error of 0.35 $^{\circ}C$. The radiator coolant temperature was tracked to its target value, $T_{air,o,d}$, while minimizing the total actuators energy cost by controlling the radiator fan speed. The mass flow rates of the cooling air and coolant inside the radiator are displayed in Fig. 6.8. The energy costs of the pump and are 61.5 kJ, and 162.4 kJ respectively.

In Test 6.2, the state flow control strategy is applied to regulate the engine cooling system operation. By switching the radiator fan and pump to their maximum speeds whenever the coolant temperature reaches the corresponding threshold, and keeping these actuators operating at the maximum speeds until the coolant temperature is too cold, the coolant temperature suffered frequent fluctuations but remained bounded inside a given range. The average coolant temperature tracking error was 1.33 $^{\circ}C$. In comparison to Test 6.1, the state flow controller requires more actuator energy due to the unnecessary maximum cooling effort.

The coolant temperatures at the engine and radiator outlets and for Test 6.3 have been displayed in Fig. 6.9. Similarly, mass flow rates of the cooling air and coolant inside the radiator have been shown in Fig. 6.10. It may be observed that the classical PI controller stabilizes the coolant temperature to the desired 90 $^{\circ}C$ with a relatively large fluctuation compared to the optimal nonlinear controller in Test 6.1. The average tracking error was 0.45 $^{\circ}C$ with pump and fan power costs of 36.5 kJ and 219.6 kJ. The total energy use was 12% higher than the total cooling energy loss in Test 6.1.

Overall, Tests 6.1 to 6.3 demonstrate that the three control strategies can track the engine coolant to a prescribed desired value with different error magnitudes and cooling energy consumptions. The proposed optimal nonlinear controller and the

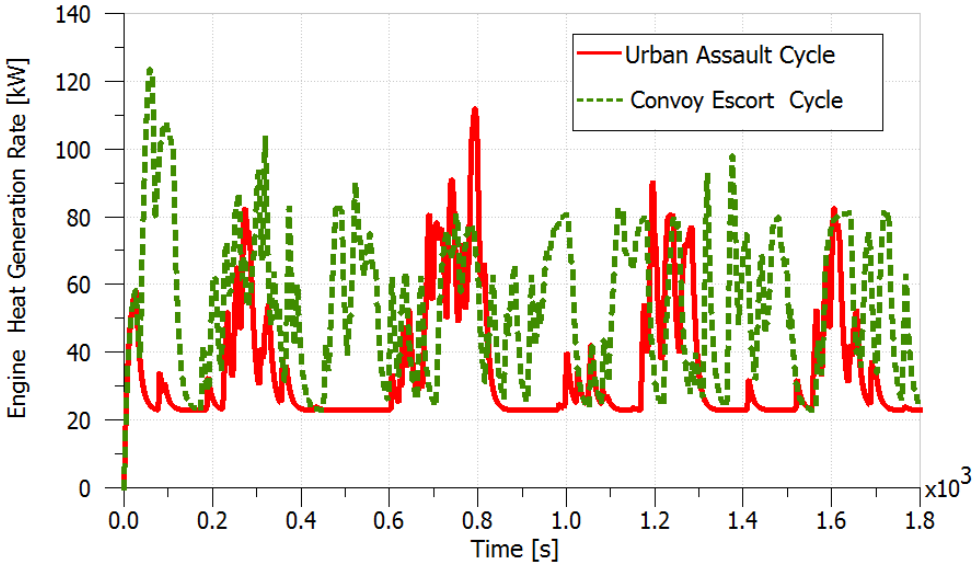

Figure 6.6: Engine Waste Heat Generation Rate in Numerical Study for Urban Assault and Convoy Escort Driving Cycles

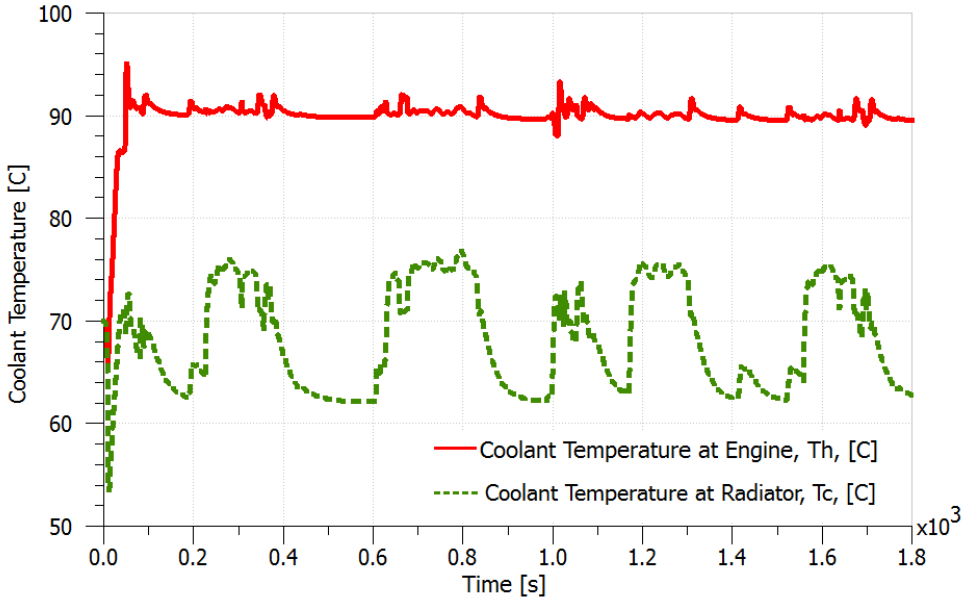

Figure 6.7: Test 6.1 - Engine and Radiator Coolant Temperatures with Urban Assault Driving Cycle and Optimal Nonlinear Controller

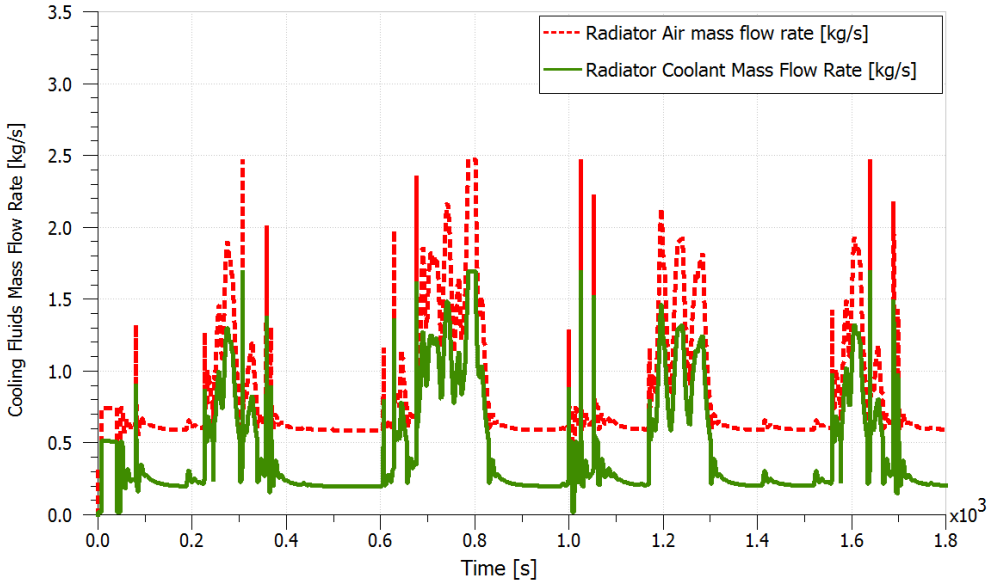

Figure 6.8: Test 6.1 - Coolant and Cooling Air Mass Flow Rates in Radiator with Urban Assault Driving Cycle and Optimal Nonlinear Controller

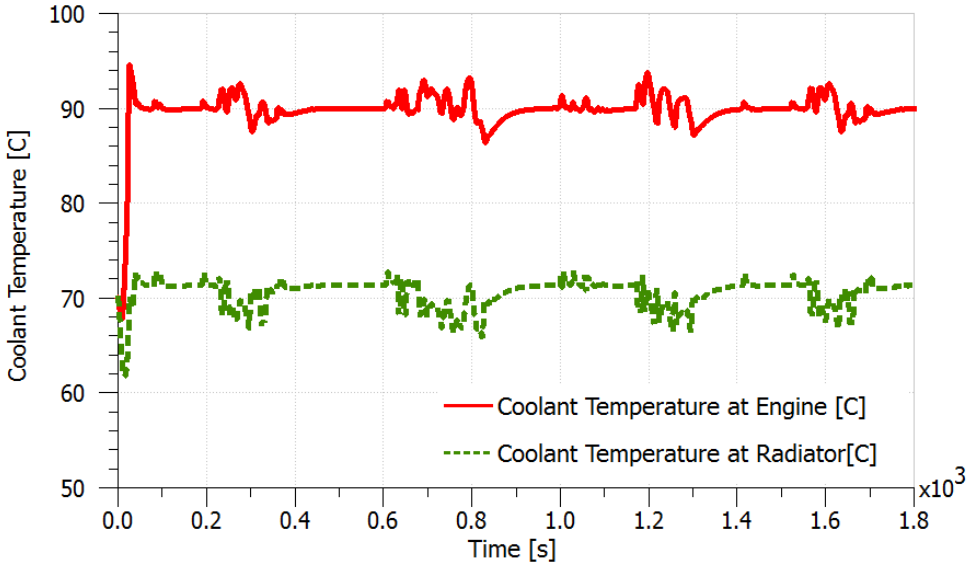

Figure 6.9: Test 6.3 - Engine and Radiator Coolant Temperatures with Urban Assault Driving Cycle and Classical PI Controller

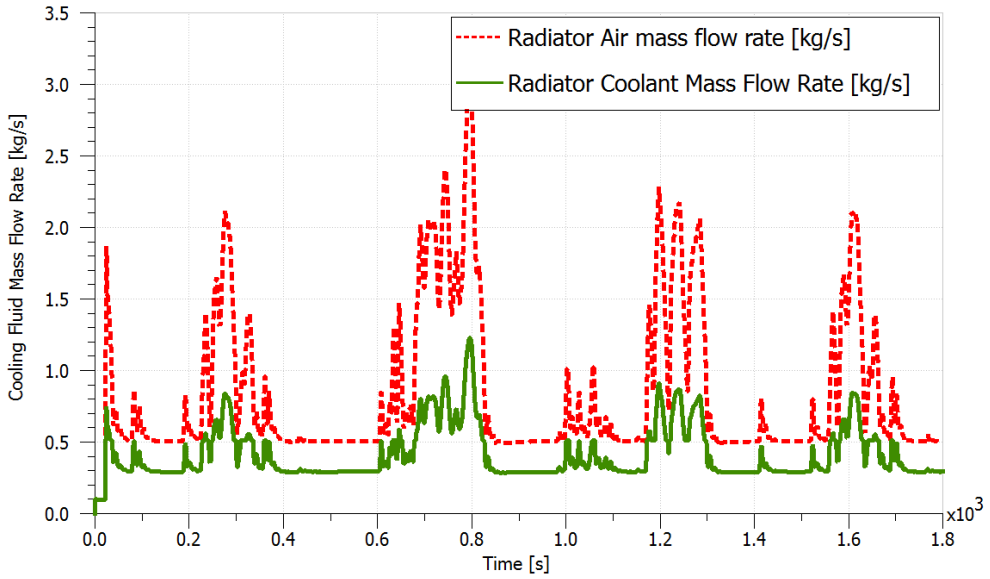

Figure 6.10: Test 6.3 - Coolant and Cooling Air Mass Flow Rates in Radiator with Urban Assault Driving Cycle and Classical PI Controller

classical PI controller provide stable temperature tracking performance when viewed against the state flow controller. The cooling energy use of the optimal nonlinear controller is the smallest for the urban assault driving cycle comparing to the other cooling control algorithms. The engine cooling performance for the different control methods over the convoy escort driving cycle have been investigated in Tests 6.4 to 6.6. The engine coolant temperature in Test 6.4, was tracked favourably to the target value of 90 $^{\circ}C$ with an average tracking error of 0.34 $^{\circ}C$ as shown in Fig. 6.11. The total cooling system power consumption is 599 kJ.

In Test 6.5, the engine coolant temperature is regulated inside the temperature band of $[T_{h,max}, T_{h,min}]$ by the state flow controller. Fig. 6.12 displays the simulated coolant temperature responses with cyclical temperature profile. The control strategy shut down the radiator fan when the coolant temperature drops lower than $T_{h,d}$. This action limited the heat removal capacity of the radiator, and consequently, the

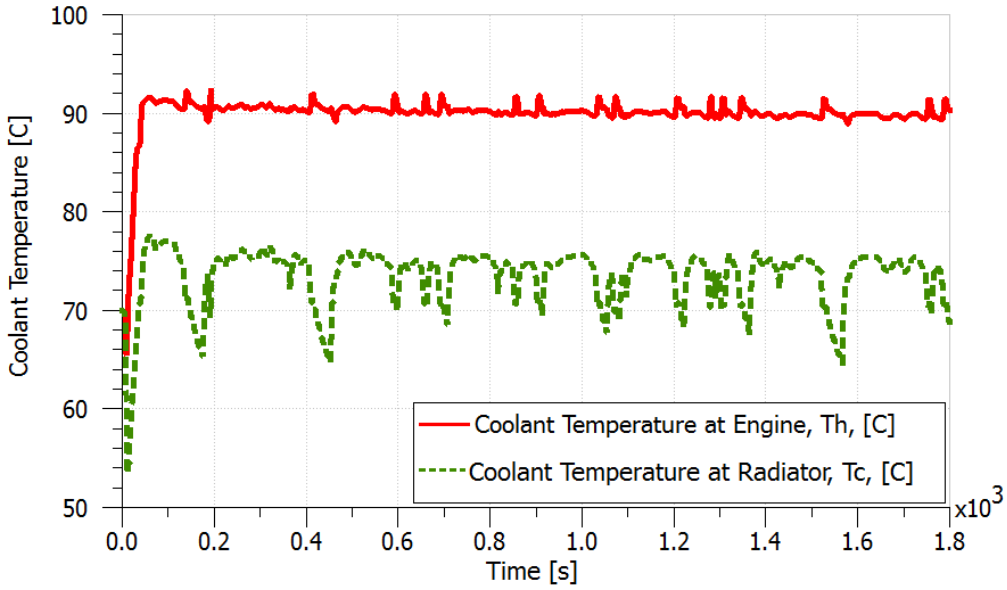

Figure 6.11: Test 6.4 - Engine and Radiator Coolant Temperatures With Convoy Escort Driving Cycle And Optimal Nonlinear Controller.

coolant temperature rose greatly. The temperature tracking error was 1.76 $^{\circ}C$, and significantly exceeded the results from Test 6.4. The maximum speed fan and pump operations, without considering the real time heat removal rate requirement, led to a large waste of energy due to unnecessary cooling the fluids. As a result, the total cooling energy cost was much larger than the proposed nonlinear-optimal method.

Finally, the classical PI controller stabilized the engine coolant temperature with an average error of 0.79 $^{\circ}C$ in Test 6.6 for the convoy escort profile. The total energy consumed by the radiator fan and pump was 694 kJ, and 15% higher than Test 6.4. Overall, the proposed optimal nonlinear control strategy offered better coolant temperature tracking performance and reduced energy consumption for the convoy escort driving cycle.

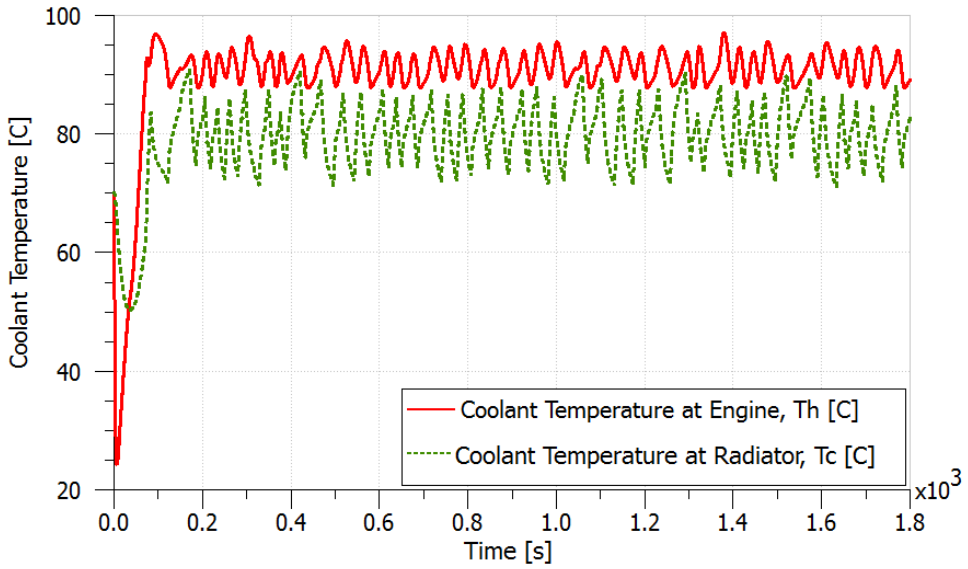

Figure 6.12: Test 6.5 - Engine and Radiator Coolant Temperatures with Convoy Escort Driving Cycle And State Flow Controller.

6.5 Summary

The replacement of the mechanical-based actuators in a conventional engine cooling system with electronic computer controlled elements provides the opportunity to improve the thermal management system performance. In this paper, an optimal nonlinear controller has been proposed for a heavy duty M-ATV engine cooling system to simultaneously control the coolant pump, radiator fan, and smart valve. A numerical case study with two driving cycles demonstrates that the nonlinear cooling control strategy offered smaller temperature tracking error and temperature fluctuation. Further, a 14% reduction in total cooling system power consumption was realized when compared to the conventional state flow controller and the classical PI controller. The proposed engine cooling control strategy provides advantages that merit further study and field testing.

Chapter 7

Conclusions and Recommendations

Cooling remains one of the top challenges for ground vehicles industry. Traditional powertrain thermal management system with mechanical cooling components is hardly capable of meeting the increasingly stringent cooling requirements of the modern vehicle powertrains. This dissertation investigates an advanced powertrain thermal management system for hybrid electrical vehicles to achieve improved temperature tracking performance as well as cooling system power consumption minimization. The study topics included numerical modelling of the HEV power train thermal management system, integration and holistic control of electro-mechanical thermal management actuators. Extensive work has been accomplished on the thermal management systems designed for a lithium-ion battery pack, the electric motors, as well as the internal combustion engine.

In Chapter 3 and Chapter 4, a thermal management system for the HEV battery pack integrating a vapour compression cooling system with real time controller has been developed. A detailed battery pack cooling system has been modeled in an AMESim-Simulink co-simulation to investigate the impact of real life driving cycle electric current profiles on the batteries' thermal behaviours and subsequent smart

cooling system operation. A Kalman filter has been applied to estimate the unmeasurable battery core temperature based on the battery surface and its surrounding cooling air temperature. A model predictive controller (MPC) has been developed using a step response AC system model to regulates the cooling air temperature for accurate internal battery temperature tracking. Numerical results showed that the battery core temperature can be track to the target value within an error of 0.25 $^{\circ}C$ and reduce the compressor power consumption by 50% comparing with conventional control method for an urban assault driving cycle.

In Chapter 5, a new cooling concept has been proposed for the in-hub electric motors for the hotspots temperature tracking. A high-fidelity reduced order electric motor thermal model is applied as the basis for real time controller design. An optimal controller has been formulated to estimate the ideal motor heat removal rate requirements. Then, a nonlinear backstepping controller has been developed to regulate the coolant pump speed for the ideal heat removal rate tracking. The proposed control strategy is suitable for thermal models with different levels of sophistication. Controller concept validation has been conducted under the speed and torque profiles corresponding to real life driving cycles too. the stator hotspot temperature is stabilized with an average error of 0.13 $^{\circ}C$. A 68% and 28.9% total cooling power consumption reduction were observed in the the urban assault cycle and the convoy escort driving cycle, respectively.

An optimal nonlinear control strategy that simutanously regulating the engine cooling pump, fan and coolant valve has been presented in Chapter 6. This engine cooling system optimization has been developed upon the existing thermal management system and heat exchanger models for total cooling power consumption minimization and improved engine coolant temperature tracking. Numerical results demonstrated a significant reduction of the power consumption, and the coolant tem-

perature tracking error is only 0.35 $^{\circ}C$.

In this dissertation, a unified thermal management architecture has been created with proposed controllers for hybrid electric vehicles, to minimize the overall cooling power consumption through the smart management and optimized operation of the distributed cooling system actuators (coolant pumps, refrigerant compressor, cooling air fans), while satisfying the waste heat rejection requirements. A complete mathematical model for a HEV powertrain thermal management system has been developed, which include heat exchangers, coolant pump, cooling air fan, and air conditioning system. A collaborative case study presented at 2015 ARC Annual Review titled "Multi-objective Optimization and Thermal Management of the Vehicle Power System" demonstrated the benefits and influences in between the advanced models for electric machines, holistic approach for thermal management and the vehicle energy management and design optimization on a the whole M-ATV powertrain level.

The accomplished work has established a fundamental basis for improving the vehicle performance through advanced thermal management system control strategies. The research results showed significant advantages in both temperature tracking and energy conservation by introducing the advanced model-based control theory into the HEV powertrain thermal management system. The following works are recommended to be concerned for the future steps of this study.

A. Experimental tests would be valuable for the e-motor cooling concept validation and improvement. In the previous work, the development of the e-motor thermal model has been experimentally validated under the speed and torque profiles corresponding to the real life driving cycles without optimal control of the pump and fan speeds. At this point, the controllers'

performance has only been evaluated within a high fidelity HEV simulation. However, it is recommended to add the experimental validation of the proposed thermal management concept in the future research.

B. Developing new high-fidelity thermal model for the battery pack and internal combustion engine using computational fluid dynamics (CFD) and finite element analysis (FEA) methods will be meaningful. Current lumped parameter thermal model is convenient for controller design while not capable of predicting the hotspots temperature in the system. The application of the reduced ordered FEA based e-motor model with a fast simulation speed has been proven to be a powerful tool for the accurate real-time internal hotspots temperature tracking. Similar high fidelity thermal model should be built for the different versions of battery pack and internal combustion engine, especially the battery pack, for its high sensitivity to the overheated core temperature.

C. Besides continuing exploring the advantages of applying nonlinear controllers to improve the cooling system performance, innovation on the cooling system architecture featuring with new system material could serve great benefits. Optimization of the cooling structure for different powertrain components by introducing thermal bus is expected to offer more compact structure, less cooling actuators, improved overall system safety and higher heat removal efficiency.

Bibliography

Aschemann, H., Prabel, R., Gross, C., and Schindele, D. (2011). Flatness-based control for an internal combustion engine cooling system. In *Mechatronics (ICM), 2011 IEEE International Conference on*, pages pages 140–145. IEEE.

Badekar, R. S., Mahajan, J. S., Kakaye, S. G., Khire, P. N., and Gopalakrishna, K. (2006). Development of control system for electrical radiator fan using dual sensor & microprocessor based electronic unit. In *SAE 2006 World Congress*. SAE Technical Paper 2006-01-1035.

Bellettre, J., Sartre, V., Biaist, F., and Lallemand, A. (1997). Transit state study of electric motor heating and phase change solid-liquid cooling. *Applied Thermal Engineering*, Vol. 17:pages 17–31.

Bergman, T. L., Incropera, F. P., and Lavine, A. S. (2011). *Fundamentals Of Heat and Mass Transfer*. John Wiley & Sons.

Bhatti, M. S. (1997). A critical look at r-744 and r-134a mobile air conditioning systems. *SAE 1997 Transactions - Journal of Passenger Cars*, Vol. 6(6).

Cho, H., Jung, D., Filipi, Z. S., Assanis, D. N., Vanderslice, J., and Bryzik, W. (2007). Application of controllable electric coolant pump for fuel economy and cooling performance improvement. *Journal of engineering for gas turbines and power*, Vol. 129(1):pages 239–244.

Choi, K.-w., Kim, H.-m., Cho, W.-j., and Lee, K.-h. (2007). Investigation of emission reduction effect by controlling cooling system in a diesel engine. In *SAE 2007 World Congress*. SAE Technical Paper2007-01-4064.

Damodaran, V., Murugan, S., Shigarkanthi, V., Nagtilak, S., and Sampath, K. (2011). Thermal management of lead acid battery (pb-a) in electric vehicle. In *SAE 2011 World Congress*. SAE Technical Paper 2011-01-0653.

De Queiroz, M. S., Dawson, D. M., Nagarkatti, S. P., and Zhang, F. (2012). *Lyapunov-Based Control of Mechanical Systems*. Springer Science & Business Media.

Demirdöven, N. and Deutch, J. (2004). Hybrid cars now, fuel cell cars later. *Science*, Vol. 305(5686):pages 974–976.

Di Domenico, D., Fiengo, G., and Stefanopoulou, A. (2008). Lithium-ion battery state of charge estimation with a kalman filter based on a electrochemical model. In *Control Applications, 2008. CCA 2008. IEEE International Conference on*, pages pages 702–707. IEEE.

Donaldson, B. K. (2006). *Introduction to structural dynamics*. Cambridge University Press.

Duan, X. and Naterer, G. (2010). Heat transfer in phase change materials for thermal management of electric vehicle battery modules. *International Journal of Heat and Mass Transfer*, Vol. 53(23):pages 5176–5182.

El-Refaie, A. M., Harris, N. C., Jahns, T. M., and Rahman, K. M. (2004). Thermal analysis of multibarrier interior pm synchronous machine using lumped parameter model. *Energy conversion, IEEE transactions*, Vol. 19(2):pages 303–309.

Fang, W., Kwon, O. J., and Wang, C.-Y. (2010). Electrochemical–thermal modeling of automotive li-ion batteries and experimental validation using a three-electrode cell. *International journal of energy research*, Vol. 34(2):pages 107–115.

Forgez, C., Do, D. V., Friedrich, G., Morcrette, M., and Delacourt, C. (2010). Thermal modeling of a cylindrical lifepo 4/graphite lithium-ion battery. *Journal of Power Sources*, Vol. 195(9):pages 2961–2968.

Gross, O. and Clark, S. (2011). Optimizing electric vehicle battery life through battery thermal management. *SAE International Journal of Engines*, Vol. 4:pages 1928–1943.

Gu, W. and Wang, C.-Y. (2000). Thermal and electrochemical coupled modeling of a lithium-ion cell. *Proc.-Electrochem. Soc*, Vol. 99:pages 748–762.

Guzzella, L. and Sciarretta, A. (2007). *Vehicle Propulsion Systems*, volume Vol. 4. Springer: New York, 2 edition.

Hu, X., Lin, S., Stanton, S., and Lian, W. (2011a). A state space thermal model for hev/ev battery modeling. In *SAE 2011 World Congress*. SAE Technical Paper 2011-01-1364.

Hu, Y., Yurkovich, S., Guezennec, Y., and Yurkovich, B. (2011b). Electro-thermal battery model identification for automotive applications. *Journal of Power Sources*, Vol. 196(1):pages 449–457.

IEA (2014). Co_2 emissions from fuel combustion highlights, 2014 edition. International Energy Agency, `http://www.iea.org/publications/freepublications/publication/CO2EmissionsFromFuelCombustionHighlights2014.pdf`.

Iu, I., Weber, N., Bansal, P., and Fisher, D. (2007). Applying the effectiveness-ntu method to elemental heat exchanger models. *ASHRAE Transactions*, Vol. 113(1):pages 504–513.

Jayaraman, S., Anderson, G., Kaushik, S., and Klaus, P. (2011). Modeling of battery pack thermal system for a plug-in hybrid electric vehicle. In *SAE 2011 World Congress*. SAE Technical Paper 2011-01-0666.

Karimi, G. and Li, X. (2013). Thermal management of lithium-ion batteries for electric vehicles. *International Journal of Energy Research*, Vol. 37(1):pages 13–24.

Lam, L., Newnham, R., Ozgun, H., and Fleming, F. (2000). Advanced design of valve-regulated lead–acid battery for hybrid electric vehicles. *Journal of power sources*, Vol. 88(1):pages 92–97.

Li, B. and Alleyne, A. G. (2010). A dynamic model of a vapor compression cycle with shut-down and start-up operations. *International Journal of refrigeration*, Vol. 33(3):pages 538–552.

Li, B., Peuker, S., Hrnjak, P., and Alleyne, A. (2011). Evaluation of transient refrigerant migration modeling approach on automotive air conditioning systems. *SAE International Journal of Materials and Manufacturing*, Vol. 4(1):pages 864–874.

Li, Z., Savory, E., Ryval, J., Martinuzzi, R., and Blissitt, M. (2006). Effect of fan hub configuration on the cooling airflow through electric motors in engine cooling fan systems. In *SAE 2006 World Congress*. SAE Technical Paper 2006-01-1037.

Lin, X., Perez, H. E., Siegel, J. B., Stefanopoulou, A. G., Ding, Y., and Castanier, M. P. (2011). Parameterization and observability analysis of scalable battery clusters for onboard thermal management. In *International Scientific Conference on Hybrid and Electric Vehicles, Rueil-Malmaison, France*, pages pages RHEVE 2011–1 –11. IFP Energies nouvelless.

Mahamud, R. and Park, C. (2011). Reciprocating air flow for li-ion battery thermal management to improve temperature uniformity. *Journal of Power Sources*, Vol. 196(13):pages 5685–5696.

McKinley, T. L. and Alleyne, A. G. (2008). An advanced nonlinear switched heat exchanger model for vapor compression cycles using the moving-boundary method. *International Journal of Refrigeration*, Vol. 31(7):pages 1253–1264.

Mellor, P., Roberts, D., and Turner, D. (1991). Lumped parameter thermal model for electrical machines of tefc design. In *IEEE Proceedings B (Electric Power Applications)*, volume Vol. 138, pages 205–218. IET.

Moyle, D., Lasecki, M., and Cornish, B. (2006). Thermal kits for truck fleets. In *SAE 2006 World Congress*. SAE Technical Paper 2006-01-3542.

Nairobi and Kenya (2009). Hybrid electric vehicles report, an overview of current technology and its application in developing and transitional countries. Printed by the United Nations Environment Programme, `http://www.unep.org/transport/pcfv/pdf/hev_report.pdf`.

Page, R. W. and Kozierowski, J. (2005). Thermal management for the 21st century-improved thermal control & fuel economy in an army medium tactical vehicle. In *SAE 2005 World Congress*. SAE Technical Paper 2005-01-2068.

Park, H. (2013). A design of air flow configuration for cooling lithium ion battery in hybrid electric vehicles. *Journal of Power Sources*, Vol. 239:pages 30–36.

Park, M., Jung, D., Kim, M., and Min, K. (2013). Study on the improvement in continuously variable transmission efficiency with a thermal management system. *Applied Thermal Engineering*, Vol. 61(2):pages 11–19.

Park, S. and Jung, D. (2008). Numerical modeling and simulation of the vehicle cooling system for a heavy duty series hybrid electric vehicle. SAE Technical Paper 2008-01-2421.

Park, S. and Jung, D. (2010). Design of vehicle cooling system architecture for a heavy duty series-hybrid electric vehicle using numerical system simulations. *Journal of Engineering for Gas Turbines and Power*, Vol. 132(9):pages 092802 1–11.

Peck, S., Olszanski, T., Zanardelli, S., and Pierce, M. (2012). Validation of a thermal-electric li-ion battery model. *SAE International Journal of Passenger Cars-Electronic and Electrical Systems*, Vol. 5(1):pages 154–163.

Pistoia, G. (2014). *Lithium-Ion Batteries: Advances and Applications*. Elsevier, 1 edition.

Policy (2015). Reducing co2 emissions from passenger. `http://ec.europa.eu/clima/policies/transport/vehicles/cars/index_en.htm`.

Pollet, B. G., Staffell, I., and Shang, J. L. (2012). Current status of hybrid, battery and fuel cell electric vehicles: from electrochemistry to market prospects. *Electrochimica Acta*, Vol. 84:pages 235–249.

PricewaterhouseCoopers (2007). An overview of industry data, trends and financial reporting practices. Global Automotive Financial Review. ed. 2007. Price Waterhouse Coopers, https://www.pwc.ru/ru_RU/ru/automotive/assets/pwc_automotive_financial_review2007.pdf.

Rawlings, J. B. (1999). Tutorial: Model predictive control technology. In *American Control Conference, 1999*, volume Vol. 1, pages pages 662–676. IEEE.

Salah, M. H., Mitchell, T. H., Wagner, J. R., and Dawson, D. M. (2008). Nonlinear control strategy for advanced vehicle thermal-management systems. *Vehicular Technology, IEEE Transactions*, Vol. 57(1):pages 127–137.

Salah, M. H., Mitchell, T. H., Wagner, J. R., and Dawson, D. M. (2010). A smart multiple-loop automotive cooling systemâĂŤmodel, control, and experimental study. *Mechatronics, IEEE/ASME Transactions on*, Vol. 15(1):pages 117–124.

Salehi, S. and Shahrokhi, M. (2009). Adaptive fuzzy backstepping approach for temperature control of continuous stirred tank reactors. *Fuzzy Sets and Systems*, Vol. 160(12):pages 1804–1818.

Saxena, A. et al. (2010). Analytical modeling and simulation of auxiliary cooling system of hybrid electric vehicle for improving system performance. In *SAE 2010 World Congress*. SAE Technical Paper 2010-01-1926.

Shams-Zahraei, M., Kouzani, A. Z., Kutter, S., and Bäker, B. (2012). Integrated thermal and energy management of plug-in hybrid electric vehicles. *Journal of power sources*, Vol. 216:pages 237–248.

Soparat, J. and Benyajati, C. (2013). Liquid cooled induction motor: Computational design, heat transfer analysis, parametric study, and performance testing. *SAE International Journal of Alternative Powertrains*, Vol. 2(1):pages 1–6.

Sun, H., Tossan, B., and Brouns, D. (2011). Thermal behavior study on hev air-cooled battery pack. In *SAE 2011 World Congress*. SAE Technical Paper 2011-01-1368.

Tao, X. and Wagner, J. R. (2014). Cooling air temperature and mass flow rate control for hybrid electric vehicle battery thermal management. In *ASME 2014 Dynamic Systems and Control Conference*, pages pages V002T34A002–V002T34A002. American Society of Mechanical Engineers.

Tao, X. and Wagner, J. R. (2016). A thermal management system for the battery pack of a hybrid electric vehicle: Modeling and control. *Proceedings of the Institution of Mechanical Engineers, Part D: Journal of Automobile Engineering*, Vol. 230(2):pages 190–201.

Tao, X., Zhou, K., Andrej, I., Wagner, J. R., Heath, H., and Filipi, Z. (2015). A hybrid electric vehicle thermal management system - nonlinear controller design. In *SAE 2015 World Congress*. SAE Technical Paper 2015-01-1710.

Teng, H. (2012). Thermal analysis of a high-power lithium-ion battery system with indirect air cooling. *SAE International Journal of Alternative Powertrains*, Vol. 1(1):pages 79–88.

Teng, H., Ma, Y., Yeow, K., and Thelliez, M. (2011). An analysis of a lithium-ion battery system with indirect air cooling and warm-up. *SAE International Journal of Passenger Cars-Mechanical Systems*, Vol. 4(3):pages 1343–1357.

Teng, H. and Yeow, K. (2012). Design of direct and indirect liquid cooling systems for high-capacity, high-power lithium-ion battery packs. *SAE International Journal of Alternative Powertrains*, Vol. 1(2):pages 525–536.

Tran, T.-H., Harmand, S., Desmet, B., and Filangi, S. (2014). Experimental investigation on the feasibility of heat pipe cooling for hev/ev lithium-ion battery. *Applied Thermal Engineering*, Vol. 63(2):pages 551–558.

UQM (2015). Uqm powerphase 145 specifics sheet,. `http://www.neweagle.net/support/wiki/docs/Datasheets/UQM/PP145.pdf`.

Wagner, J. R., Paradis, I., Marotta, E., and Dawson, D. (2002). Enhanced automotive engine cooling systems- a mechatronics approach. *International Journal of Vehicle Design*, Vol. 28(1-3):pages 214–240.

Wagner, J. R., Srinivasan, V., Dawson, D. M., and Marotta, E. E. (2003). Smart thermostat and coolant pump control for engine thermal management systems. In *SAE 2003 World Congress*. SAE Technical Paper 2003-01-0272.

Wambsganss, M. W. (1999). Thermal management concepts for higher-efficiency heavy vehicles. In *SAE 1999 World Congress*. SAE Technical Paper1999-01-2240.

Wang, T., Jagarwal, A., Wagner, J. R., and Fadel, G. (2015). Optimization of an automotive radiator fan array operation to reduce power consumption. *Mechatronics, IEEE/ASME Transactions on*, Vol. 20(5):pages 2359–2369.

Wang, T. and Wagner, J. R. (2015a). Advanced automotive thermal management–nonlinear radiator fan matrix control. *Control Engineering Practice*, Vol. 41:pages 113–123.

Wang, T. and Wagner, J. R. (2015b). A smart engine cooling system-experimental study of integrated actuator transient behavior. In *SAE 2015 World Congress*. SAE Technical Paper 2015-01-1604.

Wang, Z., Ukita, T., Nomura, E., and Masuda, Y. (2011). Prediction of air cooling system for ev/hev battery pack. In *SAE 2011 World Congress*. SAE Technical Paper 2011-39-7269.

Whitehouse (2014). Fact sheet: U.s.- china joint announcement on climate change and clean energy cooperation. `https://www.whitehouse.gov/the-press-office/2014/11/11/fact-sheet-us-china-joint-announcement`.

Xu, X. and He, R. (2013). Research on the heat dissipation performance of battery pack based on forced air cooling. *Journal of Power Sources*, Vol. 240:pages 33–41.

Yeow, K., Teng, H., Thelliez, M., and Tan, E. (2012). Thermal analysis of a li-ion battery system with indirect liquid cooling using finite element analysis approach. *SAE International Journal of Alternative Powertrains*, Vol. 1(2012-01-0331):pages 65–78.

Zhang, X., Ivanco, A., Tao, X., Wagner, J. R., and Filipi, Z. (2014a). Optimization of the series-hev control with consideration of the impact of battery cooling auxiliary losses. *SAE International Journal of Alternative Powertrains*, Vol. 3(2):pages 234–243.

Zhang, X., Kong, X., Li, G., and Li, J. (2014b). Thermodynamic assessment of active cooling/heating methods for lithium-ion batteries of electric vehicles in extreme conditions. *Energy*, Vol. 64:pages 1092–1101.

Zhou, K., Pries, J., and Hofmann, H. (2013). Computationally-efficient 3d finite-element-based dynamic thermal models of electric machines. In *Electric Machines & Drives Conference (IEMDC), 2013 IEEE International*, pages 839–846. IEEE.

Zhou, K., Pries, J., Hofmann, H., Kim, Y., Lee, T.-K., and Filipi, Z. (2011). Computationally-efficient finite-element-based thermal models of electric machines. In *Vehicle Power and Propulsion Conference (VPPC), 2011 IEEE*, pages 1–6. IEEE.